ADAMA SCIENCE AND TECHNOLOGY UNIVERSITY

SCHOOL OF ELECTRICAL ENGINEERING AND COMPUTING

DEPARTMENT OF ELECTRICAL AND COMPUTER ENGINEERING

Thesis on

REACTIVE POWER COMPENSATION AND VOLTAGE SUPORT IN WIND FARMS USING PV-STATCOM (case study at Adama-I wind farm)

Submitted to the Department of Electrical and Computer Engineering of Adama Science and Technology University in Partial Fulfillment of the Requirements for the Degree of Master of Science in Electrical Power Engineering

By: Hagos Gebrekidan

Advisor: Milkias Berhanu (PhD Scholar)

May 2017

Adama, Ethiopia

APPROVAL BY BOARD OF EXAMINATION

The following committee members have examined the final copy of this thesis form and content, and recommend that it has to be accepted as a partial fulfillment on the requirements for a degree of Master of Science in Electrical Power Engineering.

Examining committee members

Hinsermu Alemayehu	_____	_____
Chairperson, Department of Electrical and Computer Engineering	Signature	Date
Milkias Berhanu (PhD Scholar)	_____	_____
Advisor	Signature	Date
_____	_____	_____
Internal Examiner	Signature	Date
_____	_____	_____
External Examiner	Signature	Date

CERTIFICATION

I, the undesignated person certify that the thesis entitled “Reactive Power Compensation and Voltage Support in Wind Farms using PV-STACOM” have been read and here by I recommend it for acceptance by Adama Science and Technology University for the partial Fulfillment of the Requirements for the Degree of Master of Science in Electrical Power Engineering .

Milkias Berhanu (PhD Scholar)

Advisor

_____

Signature

DECLARATION

Hagos Gebrekidan Berhe declares that this thesis is my own original work that has never been presented and will not be present by me to any other university for similar or any other degree award.

Hagos Gebrekidan Berhe

_____

Signature

ACKNOWLEDGMENTS

First, I would like to thank Almighty God for all rounded support throughout the process.

Second, I would like to express my genuine gratitude and appreciation to Milkias Berhanu (PhD Scholar) for his continuous help, guidance and support from the start to the end of the thesis work. He directed me to explore and understand the subject matter as well as the way of writing of this thesis. Without his help and sincerity approach, this work would not have been completed. He had supported me many latest books related to my study and even necessary books for my future study. He is honestly responding to all my requests on time even he has great role in writing the comments. Totally, I have not more words to express to his honesty and he is great & active in all of activities of this work. Again, I would like to say thank you Milkias Berhanu (PhD Scholar).

Third, I would like to appreciate Hinsermu Alemayehu, head department of electrical and computer engineering, to his responses all the time actively and politely to all of my requests and a piece of information needed.

Fourth, I will like to thank to all my friends that helps me throughout the whole work next to god.

ABSTRACT

The demand of electrical energy in general and the wind energy specifically is increasing worldwide. The challenges to this energy especially issues related with reactive power compensation and voltage support are increasing. Adama-I Wind Farm (WF) is one of these wind energy systems in Ethiopia. The wind farm mentioned is using non-self-starting, permanent magnet synchronous generators (PMSG) which are liable for the consumption of more active power from the main grid to start their operation. To compensate reactive power, the wind farm is using static capacitor banks and Magnetically Coupled Reactors (MCR) type Static Var Compensators (SVC). However, the capacitor banks are not fast enough to alleviate the problem. In addition, there is no back up supply in the wind farm for the PMSG starting operation. To mitigate the problem of the existing wind farm, photo voltaic-static synchronous compensator (PV-STATCOM) device is proposed in this thesis. The solar inverter is used to act as STATCOM, termed as PV-STATCOM at the main substation or at Point of Common Coupling (PCC) for active power regulation and voltage/reactive power regulations during nighttime and daytime. In this regard, 10 MVAR rated capacity of PV-STATCOM is needed to compensate the given reactive power depending on the capacitive reactive demand of the WF. To show the effect of PV-STATCOM, steady state voltage variation and temporary voltage rise conditions have been analyzed using the total power capacity of the selected WF on its medium voltage connector transmission line. For validation of the system, power world and MATLAB/PowerSim software are used for steady state analysis system and temporary over voltage analysis respectively. Accordingly, results shows with the steady state voltage variation and temporary voltage raise can minimize using PV-STATCOM.

***Key Words**: MATLAB/Simulink, PMSG, PV-STATCOM, Power World, PV-array, solar inverter*

TABLE OF CONTENTS

LIST OF FIGURES

LIST OF TABLES

ACRONYMS AND SYMBOLS

Acronyms

CSA	Canadian Standards Association
DC	Direct Current
DD PMSG	Direct Derive Permanent Magnet Synchronous Generator
FACTS	Flexible AC Transmission System
GTO	Gate Turnoff Thyristor
IEEE	Institute of Electrical and Electronics Engineering
IGBT	Insulated Gate Bipolar Transistor (IGBT)
INC	Incremental Conductance
LVRT	Low Voltage Ride Through
MCR	Magnetically Coupled Reactor
MPPT	Maximum Power Point Tracking
MV	Medium Voltage
NPC	Neutral Point Clamping
NREL	National Renewable Energy Laboratory
OHTL	Overhead Transmission Line
PCC	Point of Common Coupling PV
PLL	Phase locked Loop
PMSG	Permanent Magnet Synchronous Generator
PV	Photovoltaic
PV-STATCOM	Photovoltaic Static Synchronous Compensator
PWM	Pulse Width Modulation

SCADA	Supervisory Control and Data Acquisition
SECS	Solar Energy Conversion Systems
SLGF	Single Line to Ground Fault
SPR	Surface Plasmon resonance
SPWM	Sinusoidal PWM
STATCOM	Static Synchronous Compensator
STC	Standard Test Conditions
SVC	Static Var compensator
SVPWM	State Vector SPWM
TL	Transmission Line
TSP	Tip Speed Ratio
VOC	Voltage Oriented Control
VSC	Voltage Source Converter
VSI	Voltage Source Inverter
WECS	Wind Energy Conversion System
WF	Wind Farm
WHT	Watt Hour time
WRIG	Wound Rotor Induction Generator
WRSG	Wound Rotor Synchronous Generator
WT	Wind Turbine
WTG	Wind Turbine Generators

Symbols

A	Ampere
C	Capacitor
L	Inductor
P	Active Power
Q	Reactive Power
R	Resistor
S	Apparent Power
V	Voltage
X	Reactance

CHAPTER ONE

1. INTRODUCTION

1.1. Background

Over the last twenty years, renewable energy sources were attracting great attention due to the cost increase, limited reserves, and adverse environmental impact of fossil fuels. In the meantime, technological advancements, cost reduction, and governmental incentives have made some renewable energy sources more competitive in the market. Among them, wind energy and solar energy are the fastest growing renewable energy sources [1].

Wind energy have been used for hundreds of years for milling grains, pumping water, and sailing the use of windmills to generate electricity during the late nineteenth century with the development of a 12 kW DC windmill generator [2]. It is, however, only since the 1980s that the technology has become sufficiently mature to produce electricity efficiently and reliably. Over the past two decades, a variety of wind power technologies were developed, which were improved the conversion efficiency and reduced the costs for wind energy production. The size of wind turbines is increasing from a few kilowatts to several megawatts. The capacity of Wind Energy Conversion Systems (WECS) was increasing from time to time. In 2013, more than 35 GW of wind power capacity was added to the global wind generation capacity, which became 318 GW as shown in Fig.1.1 [3].

In addition to the wind energy, the demand to solar energy in the recent years is also increasing worldwide. Due to incentives provided by several governments, small and medium scale PV solar installations were being increasingly installed worldwide [1]. The worldwide installation of PV solar capacity is shown in Fig.1.3 [7].

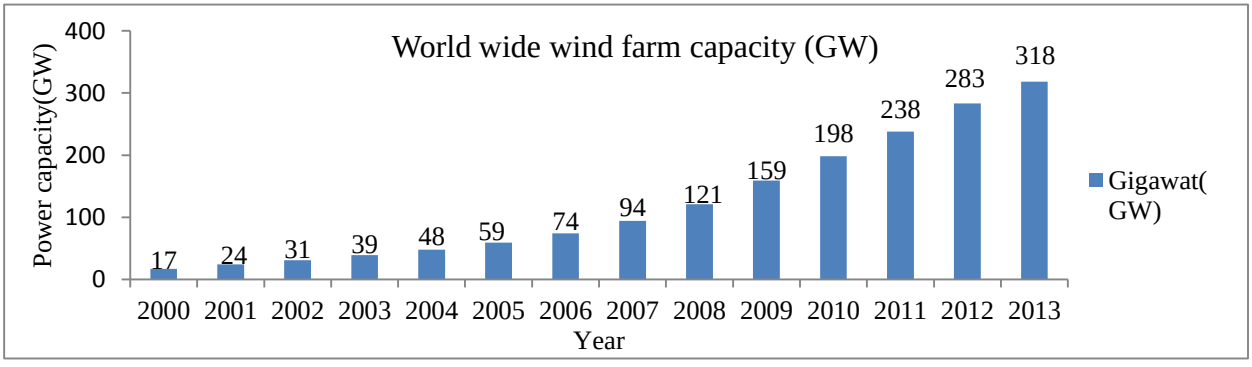

Fig. 1.1. Global wind power capacities (2000-2013)

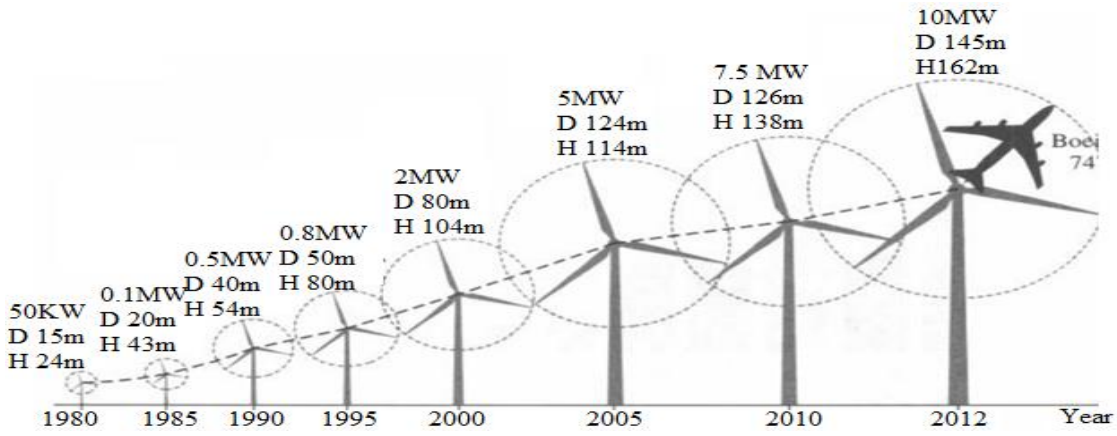

Fig.1.2.Evolution of wind turbine size (D: rotor diameter; H: tower height) and capacity (KW-MW)

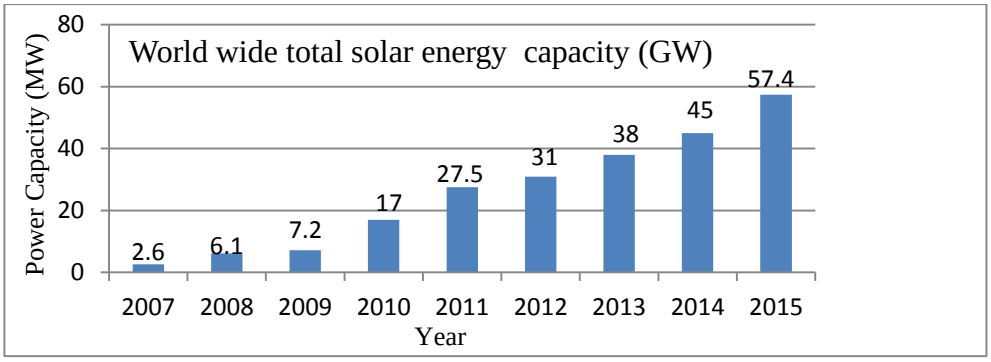

Fig.1.3. Worldwide total solar energy capacity (2007-2015)

According to the master plan report in 2011, wind, and solar energy capacity in the federal democratic republic of Ethiopia is the 153MW Adama-II WF, 95 km southeast of Addis Ababa, 51MW Adama-I WF and the 120 MW Ashegoda WF located 780 km north of Addis Ababa. Projects, which are under study, are the 300 MW Aysha WF, the 42 MW Mesebo-Harena WF, 100 MW Assela WF and the 100 MW Debre Berhan WF [5].

Ethiopia, is situated very close the equator (between 30 and 150 degrees North) with abundant solar energy potential which can be harnessed and put to use in the form of both thermal as well as electrical energy. The average solar radiation is uniform, around 5.20 KWh/m^2. The values vary seasonally, from a minimum of 4.55 KWh/m^2 in July to a maximum of 5.55 KWh/m^2 in February and March. With location, the radiation varies even more widely between 4.25 KWh/ m^2 in extreme western lowlands, 6.25 KWh/ m^2 in Adigrat area (Northern Ethiopia) and 5.098

Kwh/ m^2 /day up to 6.607 Kwh/ m^2/day in Adama (Nazret) city [6]. The following are the recommended solar PV power stations in Ethiopia: Debre Birhan PV power station of 10 MW, Metehara PV power station of 50MW, Awash solar energy PV power station of 20MW, Dera solar energy PV power station of 60 MW, Addis Ababa wind energy and solar energy demonstration base one with a total capacity of 141 MW [5].

1.2. Motivation

Today utilization of solar system to act as conventional STATCOM, termed, as PV-STATCOM is the new technology emerged to replace the dynamic reactive power compensator FACTS devices at wind energy technologies. Since there is a structural and operational similarity between the conventional STATCOM and PV- STATCOM, we can replace the conventional STATCOM. Using these devices at Adama-I WF capacitor and MCR type SVC devices used at the wind farm can be replaced with PV-STATCOM. The voltage variations or reactive power variation impacts of the grid connected wind farm (WF) is increasing and the wind turbine generators' (WTG) connector transmission line capacity is also affected. To solve these impacts different researches shows that reduction of the impacts of the WFs on grid using STATCOM is more beneficial than increasing the number of wind farms and their interconnection transmission lines. However, this device is too expensive. Due to luck of economy devolving countries, such as Ethiopia are using capacitors as reactive power regulators in their wind farms. However, this device is not fast enough in response to the reactive power demand. The PV-STATCOM can be solved the above problems.

1.3. Statement of the Problem

The development of wind energy in the entire world including in our country is increasing. In Ethiopia, most WFs are variable speed WECS (Adama-II and Ashegoda). The Adama-I WF is one of these variable speed WECS which is using a full converter controlled variable speed direct-drive (without gearbox) multi -pole permanent magnet synchronous generators. This variation in power output of the WTGs causes steady voltage variation in the wind farm networks. Towards this, Adama-I wind farm has shunt capacitors and magnetically coupled reactor (MCR) type SVC to act as a reactive power compensators. However, capacitor devices are not fast enough to compensate the reactive power in the wind farm during sudden reactive

current demand requirement in the WF network. Even, the MCR type SVC is an expensive device to use it only as reactive power compensator.

Due to single line to ground fault occurrences at the WF transmission network of Adama-I WTGs, voltage rise is occurred at the WTGs' side. The WTGs' are unable to withstand the voltage rise and disconnect them from the main grid repeatedly at a fault occurrence.

The aforementioned problems can result with the following consequences at the selected wind farm:

- Variable power output of the WTGs' causes steady state voltage variation, power loss and may generally damage of electrical equipment connected to the grid network if the wind turbine generators and the reactive power compensator devices at the WF are unable to meet the required voltage level.
- Disconnection from the main grid and black outs on the WF network in the worst scenario.
- The variation in voltage in the WF networks can reduce the capacity of the WTGs' connector transmission line.

In order to overcome the above problems, dynamic reactive power compensator, FACTS (STATCOM, SVC, etc) devices are widely used now days. STATCOM/SVC devices provide faster and smoother response to changes in voltage due to reactive power variation. However, these devices are expensive when used as only reactive power compensator/voltage regulators. Thus, the PV-STATCOM can solve the above problem with further benefits and that was the main reason for the selection of PV-STATCOM in this thesis. Generally, by installing PV-STATCOM at the PCC of WTGs', we can improve the connectivity of the wind farm to its neighboring grid.

1.4. Objectives

The general and specific objectives of this thesis work are given as follows:

1.4.1. General Objective

The main objective of this thesis is to analyze the reactive power compensation and voltage support in wind farm using PV-STACOM technology.

1.4.2. Specific Objectives

Steady state voltage variations due to wind power output variation and voltage rise due to single line to ground fault (SLGF) are concerns to be reduced using PV-STATCOM at the PCC of the WTGs'. Thus, the specific objective of this thesis work is mainly focused on the following points.

- To identify the type and size of reactive power compensator devices of the selected wind farm as a case study.
- To design a voltage source converter based PV- solar system, as STATCOM termed as, PV-STATCOM at the main substation (PCC) of the wind farm.
- To minimize the steady state voltage variation, temporary over voltage problems, and to increases connectivity of wind farm to the grid.

1.5. Scope of the Study

This research is concerned with reactive power compensation and voltage support in the selected wind farm as base case study. In this study, the main substation (PCC) of the WF voltage is considered to be regulated with the use of PV-STATCOM. After PV-STATCOM generates the required active power to the grid, the reaming capacity is used to regulate the PCC voltage in both the daytime and nighttime. This regulation in voltage has been done by exchanging the reactive power between the grid (PCC) and the solar inverter.

Since, the PV-STATCOM is considered to be connected to the main substation of the WF the following components are not considered in this study

- Solar battery
- Solar battery controller
- Protecting devices of the in the wind farm

1.6. Methodology

Generally, the following main activities have been done throughout the whole work:

- Necessary primary and secondary data have been collected and analyzed.
- System design and simulation of the whole WECS has been done using MATLAB/PowerSim 2015b version software.

- The size of PV-STATCOM have been determined according to the total capacitive reactive power compensation requirement in the wind farm.
- The PV-STATCOM is designed and simulated using MATLAB R2015b version software.
- According to the WTGs' total energy consumption, auxiliary load consumption requirement in Adama-I WF substation and future expected loads at the neighboring of the selected wind farm have been determined.
- For steady state analysis of the selected system, the total capacity of the WTGs' and PV-STATCOM have been installed on the 33kVconnector transmission line and the output have been analyzed with power world simulator software version 18.0.
- Temporary over voltage of the study system, have been analyzed with MATLAB/ PowerSim software.
- Finally, result analysis and discussions have been done.

1.7. Adama-I Wind Farm Background

This work has been conducted at Adama-I WF, which is found in south east of Ethiopia around 4.7 km far from Adama/Nazret city. The Adama-I wind farm is found in Oromia National Regional State (ONRS), near Adama city, located about 95 km southeast of Addis Ababa. It has latitude of 80 36′ N, longitude 390 16′ E and an elevation of 1712 meters above sea level [6]. It is located in a strip of land stretching from northeast to southwest 400-600 m wide and 5 km long. The ground surface of the WF is covered with shallow grass, small shrubs and some gravel as shown in Fig.1.4

Fig.1.4 Adama-I wind farm simple topographic view

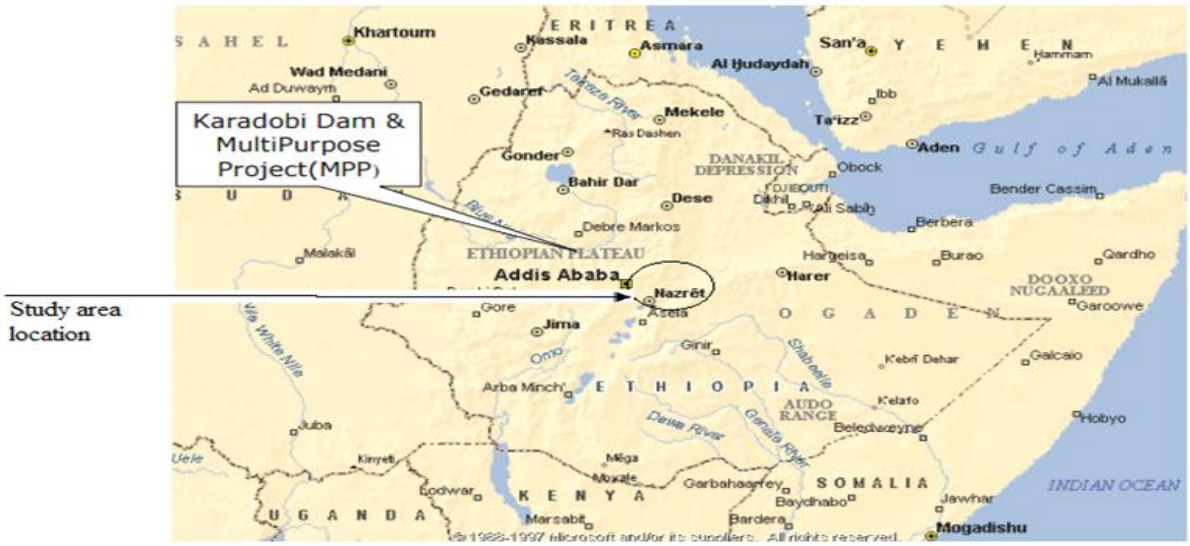

Fig.1.5. Study area location (Nazret/Adama) Map

The entire wind turbine on this farm has three blades full converter variable speed direct drive PMSGs mounted on the top of the wind tower with height of 65m. The WF has 34 turbines with 77 meter of rotor diameter. Each turbine has installed capacity of 1.5 MW with total power production of 51 MW and average annual energy production of 157GWh to the national grid through 132 kV step-up substations and an extension bay of Nazret -II substation connected 132kV transmission line and 33kV connector line. The annual average wind speed on the turbine is 9.56 m/s, the annual wind power density is 654.6 W/m^2 and the rated wind speed is 11 m/s [22]. The WF was started generating power and connected to national grid on March 31, 2012.

The study area is selected for the following reasons:

- Currently, in Adama-I WF MCR type SVC and capacitor banks are used as reactive power compensation/voltage regulation. However, capacitor banks are not fast enough in response to reactive power requirement. Moreover, MCR type SVC is expensive to use only as reactive power compensation and voltage regulation.
- The SLGF occurrences at the selected WF connector transmission line causes voltage rise at WF network and WTGs' are disconnecting from the national grid due to inability of the reactive power/voltage regulator devices.

1.8. Thesis Organization

This thesis work organized in to six chapters: this includes introduction, literature review, data collection and analysis, system modelling and analysis, results and discussions and finally conclusions, recommendations and future work.

The first chapter discusses the general background, statement of the problem, objectives, scope of the study methodologies and thesis organizations.

The theoretical backgrounds and review of literatures have been discussed in chapter two.

The third chapter deals with data collection and analysis.

Chapter-four focuses on modeling and analysis the wind energy conversion system, modelling and analysis of solar energy system as PV-STATCOM and sizing of the PV-STATCOM.

Results analysis and discussions of the selected wind energy conversion system, results analysis and discussions of the solar STATCOM and results analysis and discussions of the system under study have been done in chapter-five.

The thesis ends with chapter-six that is all about conclusion, recommendation and future work.

CHAPTER TWO

2. LITERATURE REVIEW

2.1. Introduction

Throughout the thesis work, different literatures in the area have been referred. In connection, books of relevant importance are disclosed and an internet browsed for updated information and further guidance in daily basis. In addition, the help option of the MATLAB for specific toolbox has been incorporated. The upcoming sections explain some of the review works conducted by various researchers in the area and found to be helpful for finalizing this thesis work.

2.2. Grid Connected Wind Farm

Generally, wind farms based on their grid connectivity are classified as grid connected and standalone wind farms. In this work, a grid connected Adama-I wind farm as shown in Fig.2.1 have been selected as a case study. Generally, this WF consists of wind turbine (blades, blade rotors, drive trains without gearbox, WTGs, generator side filters, rectifiers, inverter, grid side filter), wind turbine step-up unit transformers, WTG collecting and connector transmission line, wind turbine substation and the main grid transmission line. Where, wind turbine blades have connected to blade rotor, which, has fed to the generator shaft converts kinetic energy of the wind to mechanical energy, WTG convert the mechanical energy to an AC electric power from wind and then this power is filtered by generator side filter then rectified in to DC power by a rectifier. The DC power have been boosted by using DC-DC boost converter, then converted to AC power by the inverter. The output of inverter voltage is again filtered by grid side filter and stepped up to medium voltage level (33kV) with WTG unit transformer. Then the output of WTG unit transformer AC power /voltage is collected and transmitted to the wind turbine main substation. At the wind farm substation as shown in Fig. 2.1 the substation transformer is used to step up the 33kV line voltage to 132kV line voltage of the main grid, then the main grid transmission line transmits this power to the national grid.

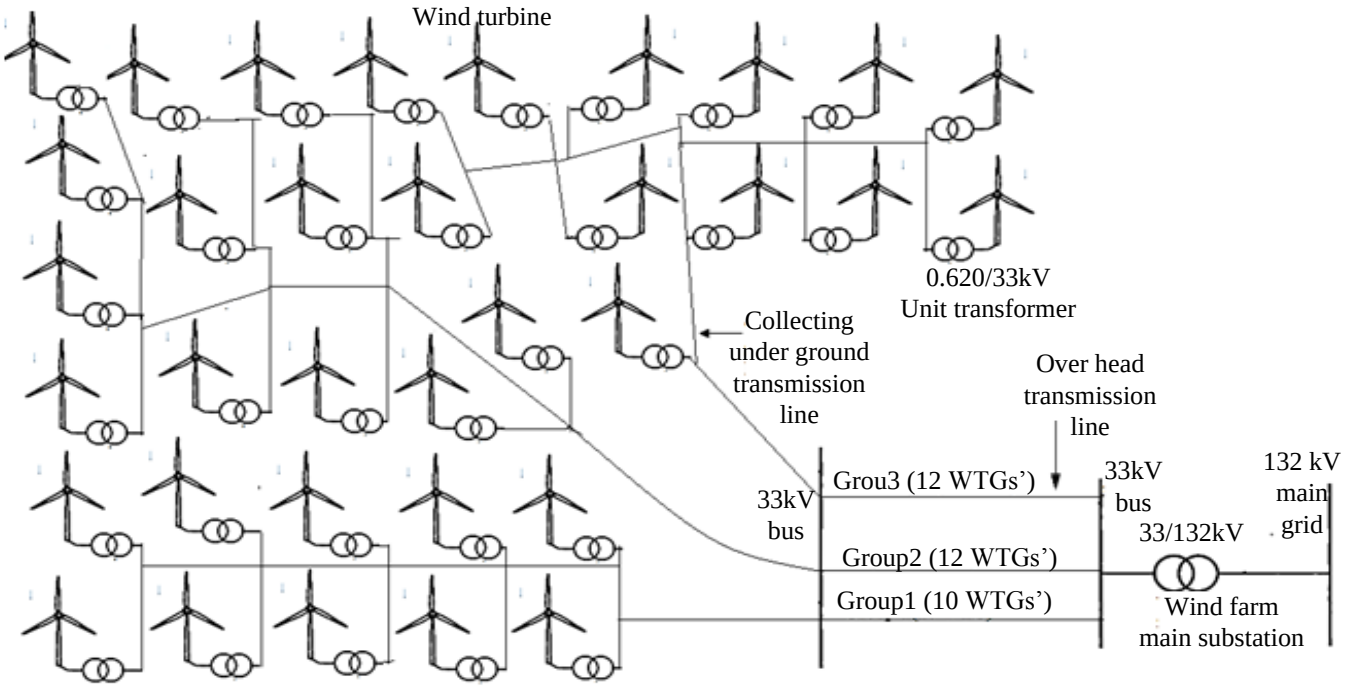

Fig. 2.1. Grid connected Adama-I wind farm simple lay out diagram

2.3. Elements of Grid Connected Wind Farm

In this topic, the main components of grid connected Adama-I wind farm have been described.

2.3.1. Wind Source

Wind is a huge source of renewable energy and it is generated by the atmospheric pressure differences, which arise from unequal heating of earth's surface by the sun [8] - [13].

2.3.2. Wind Turbine

A wind turbine is composed of several parts to achieve kinetic energy of the wind-to-electric energy conversion as shown in Fig. 2.2 [22]. Wind vane is a mechanical device attached to an elevated structure; rotates freely to show the direction of the wind and the anemometer is a gauge for recording the speed and direction of wind. The wind kinetic energy is converted to mechanical energy by the blades mounted on the rotor hub, which is installed on the main shaft, also known as the low speed (long blade length) shaft. The mechanical energy is transmitted through the drive train to the generator, which converts mechanical energy into electric energy. This conversion is usually assisted by a power converter system, which delivers the power from the generator to the grid.

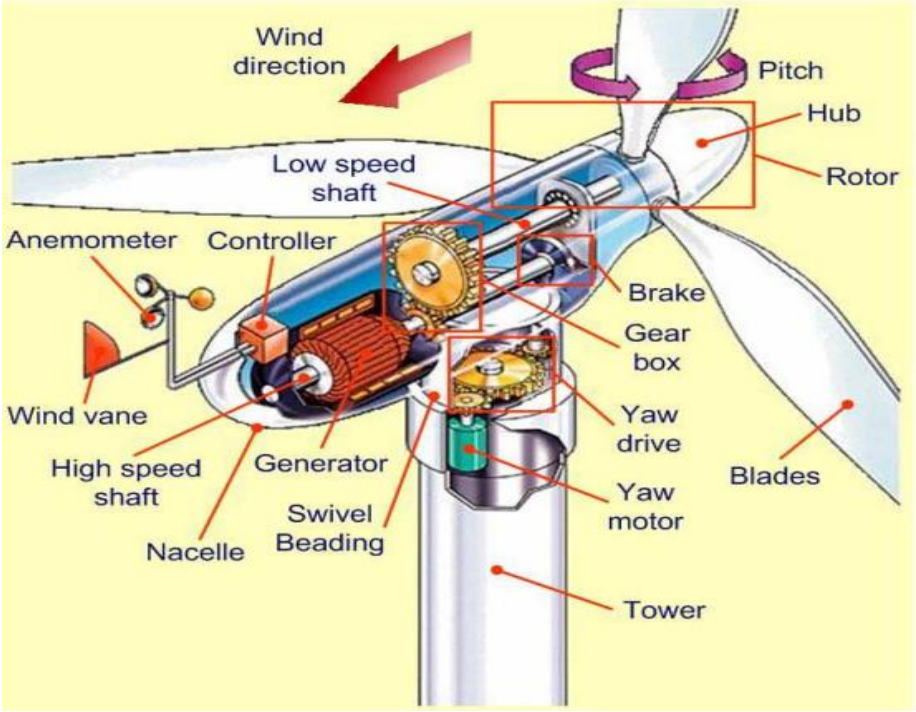

Fig. 2.2. .Major components of a typical horizontal axis, three-bladed, upwind wind turbine [22]

2.3.3. Wind Turbine Unit Transformer

This transformer is used to step up the 620V output of the WTGs' to 33kV transmission line. In Adama-I wind farm as shown in Fig.2.1, the unit transformer rating is 0.620/33kV.

2.3.4. Wind Turbine Transmission Line

Adama-I wind farm includes the collector and connector transmission lines as shown in Fig.2.1. A collector line collects individual WTG power output, which are located in different geographical locations as shown in Fig.1.4. Then the later transmission line connects the groups of the WTGs to wind farm main substation.

2.3.5. Wind Farm Substation

This station consists of the Supervisory Control and Data Acquisition (SCADA) system, harmonic filters, grounding transformer, step up transformers and different protecting devices. The main duty of the station is generally to control the stability operation of the wind farm and to boost up the incoming power from the WTGs. The substation transformer in Adama-I wind farm has 33/132kV rating. In addition to the main wind farm substation, WTGs' collector substation that is indicated as 33kV bus bar in Fig.2.1 is also found.

2.3.6. Main Grid Transmission Line:

This line connects Adama-I wind farm with national grid this line have 55MVA , 132KV rating.

2.4. Classification of Wind Farms

A wind farms are generally classified according to their location of installations as [9]:

(i) Onshore wind farm (ii) Offshore wind farm

In this research onshore Adama-I wind farm has been selected.

(i) Onshore wind farms: Onshore wind turbines are installed on land as shown in Fig.2.3 (a). Here, Wind speed is significantly reduced due to the obstacles in landscape, mountains, trees, and buildings. To get high wind speeds wind turbines need higher tower structure. Due to the higher tower structure and large rotor diameter, wind turbine sizes were limited to 1-3 MW [9]. As it is installed in the solid ground, standard concrete foundations cast on the site and there is unrestricted access to the site.

(a) Onshore Adama-I wind farm (b) Offshore wind farm [9]

Fig.2.3. Location view of onshore and offshore wind farms

(ii) Offshore wind farms: On the other hand, offshore wind turbines were located inside water bodies as shown in Fig.2.3 (b). Here due to absence of obstacles in the offshore, high wind speed is available very close to the water surface. Offshore wind turbines need lower tower structure for higher wind speeds. Due to the lower tower structure, wind turbine sizes up to 3-7 MW.

2.4.1. Classification of Wind Turbines

Wind turbines (either onshore or offshore installation) are generally classified based on:

(i). Orientation of their wind turbine blade rotor spin axis: According to the orientation axis of rotation of wind turbine blades rotor, wind turbines are classified as:

(a) Horizontal axis wind turbines (HAWT) (b) Vertical axis wind turbines (VAWT)

Since, today HAWT are most dominant they are also used in Adama-I WF.

(ii). Speed variation: According to the speed variation, wind turbines are classified as:

(a) Fixed Speed wind turbines (FSWT) (b) Variable speed wind turbines (VSWT)

In this study, variable speed Adama-I wind turbines have been selected as a base case study.

2.4.2. Direct Derive Synchronous Generator based Wind Turbines

It has been noted that Adama-I WTGs are operating with low speed direct derive (gearless) multipole PMSG. The elimination of the gearbox improves the efficiency of the system and reduces initial costs and maintenance. However, a low-speed generator has a substantially larger diameter to accommodate the large number of poles on the PMSG, which may lead to an increase in generator and installation costs [11]. Using vector control techniques, a bidirectional converter assures energy generation at nominal grid frequency and nominal grid voltage independently of the rotor speed.

Adama-I WECS systems include the main control systems as shown in Fig.2.4.

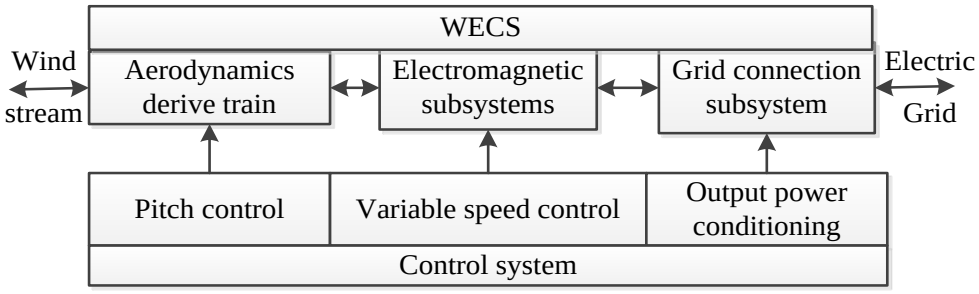

Fig. 2.4. Main control subsystems of Adama-I WECS

The first control subsystem affects the pitch angle following aerodynamic power limiting targets. The second implements the generator control, in order to obtain the variable-speed regime and the third controls the transfer of the full (or a fraction) of electric power to the electric grid, with effects on WECS output power quality. The control structures result from defining one or more of the above goals stated in relation to a certain mathematical model of WECS as described in chapter four. The controller determines the desired global dynamic behavior of the system, such that ensuring power regulation, energy maximization in partial load, mechanical loads alleviation and reduction of active power fluctuations.

There are three aerodynamic methods to control the capture of power for large wind turbines:

i. Passive stall,
ii. Active stall, and
iii. Pitch control

Since, Adama-I wind farm is used pitch angle control in this topic pitch control is described:

Pitch Control: When the wind speed exceeds the rated value, the pitch controller will reduce the angle of attack, turning the blades (pitching) gradually out of the wind. The pressure differences in front and on the back of the blade is reduced, leading to a reduction in the lifting force on the blade [4].The detailed pitch angle control is described in section 4.2.6.

2.5. Issues with Grid Integration of Wind Farms

The major issues encountered by wind farm integration to the grid includes but not limited to this only are steady state voltage variation, increased temporary over voltage, voltage flicker and harmonic components and restrictions on operation of existing grid protection [12], [13]. In this work steady state, voltage variation and temporary over voltage is considered as a case study.

2.5.3. Steady State Voltage Variation

Connecting wind farms towards grid through transmission system may create power flow fluctuations depending on load condition. Traditionally, a transmission line is designed to carry designed amount of power from the source (grid) end towards the load end, is likely to face increased/decreased voltage at the PCC of WTG due to this power fluctuation [12].

From Fig.2.7, the voltage drop over the impedance Z_L is:

$$V_1 - V_2 = \sqrt{3} \times I(R_L + X_L) \quad (2.1)$$

Where; V_1 is grid side voltage sources, V_2 is the PCC voltage of the wind power, R_L is line resistance and X_L is line reactance.

At the point of connection of the wind farm, there is also a local load. The short circuit power, S_{PCC}, in the wind power PCC is:

$$S_{PCC} = \frac{V_2^2}{Z_L^*} \quad (2.2)$$

Changes in wind power generation will cause changes in the current through the impedance Z_L. This current changes cause changes in the voltage V_2.

The voltage V_2 in the equation (2.2) is [12]:

$$v_2 = \left\{ -\frac{2\alpha_1 - v_1^2}{2} + \left[\left(\frac{2\alpha_1 - v_1^2}{3} \right)^2 - \left(\alpha_1^2 + \alpha_2^2 \right) \right]^{1/2} \right\}^{1/2} \quad (2.3)$$

Where;

$$\begin{Bmatrix} \alpha_1 = -R\left(P_W - P_{LD}\right) - X\left(Q_W - Q_{LD}\right) \\ \alpha_2 = -X\left(P_W - P_{LD}\right) + R\left(Q_W - Q_{LD}\right) \end{Bmatrix}$$

Equation (2.3) shows that the reactive power production in the wind farm, Q_W, has an impact on the voltage V_2. This impact is dependent on the local load and on the feeding grid impedance. From this expression, we can identify that the interconnection voltage will increase or decrease depending on the power flow created by the difference between load and generation at the PCC (Pw- P_{LD}), Qw- Q_{LD}), the line reactance X_L and the line resistance R_L.

In this work, the impact of WFs at the PCC voltage variation is analyzed with (Pw-P_{LD}) and (Qw-Q_{LD}).

The guidelines provided by IEEE standards (IEEE STD 1547-2003: IEEE standard for interconnecting wind farm resources with electric power systems) and CSA standards (CSA C22.3 No. 9-08: interconnection of wind resources and electricity supply systems) are widely implemented to specify the permissible steady-state voltage variation in medium voltage transmission line network. According to these standards, the steady state voltage limit of ±6 % of nominal value at the PCC terminal was permitted in Hydro China's technical interconnection requirements 2009. Appropriate reactive power compensation is required to maintain steady state voltage within permissible limits. The conventional mitigation measures for voltage issues is discussed in section 2.6.3 whereas, measures based on FACTS is discussed in Section 2.7.

2.5.4. Temporary over Voltage

In medium voltage networks, unbalanced faults, SLGF in the network as shown in Fig.2.5 causes temporary over voltages on the healthy phases of the network line [11], [12]. Over voltages between one phase and ground or between two phases are classified based on the shape of the voltage, percentage increase from nominal value and duration of application. Temporary

over voltages originating from switching or system faults (e.g. load rejection, unbalanced faults) or from nonlinearities (Ferro resonance effects, harmonics) are normally undamped or weakly damped [12].

In this study, SLGF have been considered as a base case study to observe the impact of temporary over voltages as shown in Fig. 2.5.

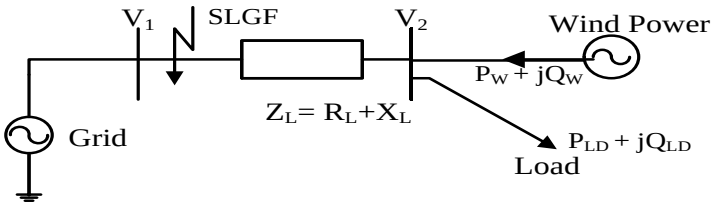

Fig. 2.5. Single line to ground fault (SLGF) at the end of transmission line

The temporary rises in voltage are specified by IEEE standards and CSA standards. Based on these requirements, hydro china's networks has specified that the temporary over voltage anywhere in the distribution network under no circumstances shall not exceed 130%.

2.5.5. Mitigation Measures for Voltage Issues

The main mitigation methods included in this study includes:

i. Voltage support and
ii. Reactive power compensation

i. Voltage support: The installation of reactive power compensator devices may be required to operate in voltage regulation mode, that is, to adjust its reactive power production or consumption in order to control voltage on the local network [11].

If the network voltage decreases to a level below a pre defined range, an installation of capacitive reactive power compensator devices may be required to supply reactive power to the network to raise the voltage level. Conversely, if the network voltage increases to a level above a pre defined upper limit, then the installation inductive reactive power compensator devices would be required to consume reactive power to bring the voltage back within acceptable limits [11].

ii. Reactive power compensation: The effect of applying reactive power compensation to manage the voltage-rise effect and hence allow an increase in penetration of wind generation is achieved by absorbing reactive power at the PCC. In this case, active power generation would be curtailed only when the reactive power absorbed is insufficient for maintaining the voltage within

permissible limits. To minimize losses and thus maintain high levels of efficiency, it is preferable that networks operate with voltage and current in phase that is, the power factor is unity.

In order to accomplish the reactive power control of the wind turbine either of the following methods can be used:

Reactive power control: The wind turbine is required to produce or absorb a constant specific amount of reactive power.

Automatic voltage regulation: The voltage in the wind turbine PCC is controlled. This implies that WF is ordered to produce or absorb an amount of reactive power.

In this work, reactive power compensation to control of the WTGs' is achieved indirectly by regulating the PCC voltage.

Shunt capacitors and inductors provide fixed compensation as shown in the Fig. 2.6. The variability of WECS requires a dynamic reactive power support make the conventional devices less effective in resolving voltage issues created. The FACTS (SVC, STATCOM etc…) devices, can provide continuously controlled reactive power output from inductive to capacitive region [14] as shown in Fig.2.6.

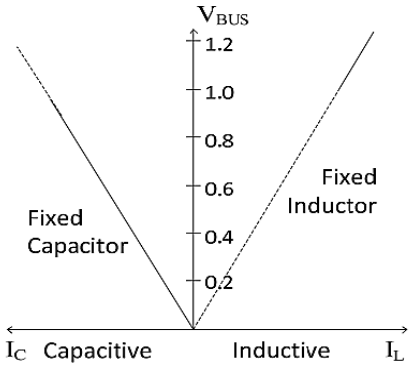

Fig. 2.6. Terminal characteristic of fixed Capacitor/Inductor

2.6. FACTS Controller based Mitigation Measures for Voltage Issues

The FACTS devices are defined as the AC transmission systems incorporating power electronics based and other static controllers to enhance controllability and increase power transfer capability [14], [15], [17]. Due to their fast response and dynamic reactive power support capability, FACTS controllers were most suitable to mitigate voltage fluctuation.

2.6.3. Static Synchronous Compensators (STATCOM)

The STATCOM is the family of FACTS devices, which regulates voltage at its terminal by controlling the amount of reactive power injected into or absorbed from the power system [14].

Operation principle of STATCOM: A single-line STATCOM power circuit is shown in Fig. 2.7 (a), where a VSC is connected to a utility bus through magnetic coupling (coupling transformer). In Fig. 2.7 (b), a STATCOM is seen as an adjustable voltage source behind a reactance meaning that capacitor banks and shunt reactors are not needed for reactive-power generation and absorption, thereby giving a STATCOM a compact design, or small footprint, as well as low noise and low magnetic impact.

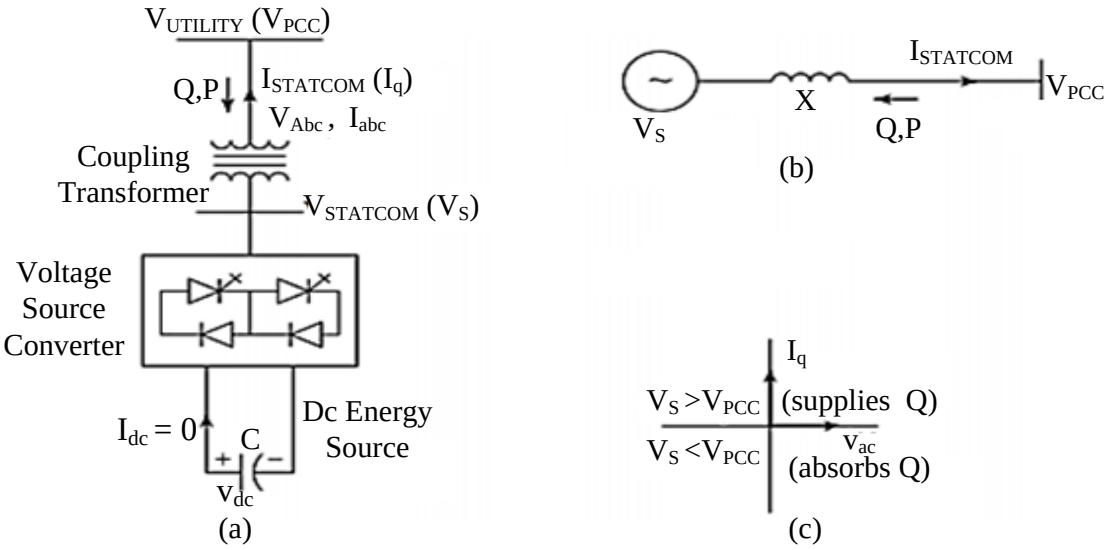

Fig. 2.7. The STATCOM principle of operation diagram: (a) a power circuit, (b) an equivalent circuit, (c) a power exchange [24]

Exchange of reactive power between the converter and the ac system (Vpcc) is controlled by varying amplitude of 3-phase output voltage, V_S., of the converter, as illustrated in Fig.2.7 (c).

From Fig.2.7 (a), the active and reactive power exchange between the utility (PCC) and STATCOM is given as:

$$P = \frac{(V_{PCC} \times V_S) \times \sin(\delta)}{X} \tag{2.4}$$

$$Q = \frac{V_{PCC} \times (V_{PCC} - V_S) \times \cos(\delta)}{X} \tag{2.5}$$

Where; V_{PCC} is line to line voltage of the utility source, V_S is line to line voltage output of STATCOM, X is reactance of interconnection transformer and filters and δ is phase angle of V_{PCC} with respect to V_S.

In steady state operation, the voltage V_S generated by the VSC is in phase with V_{PCC} (δ=0), so that only reactive power is flowing. If V_S is lower than V_{PCC}, Q is flowing from V_{PCC} to V_S (STATCOM is absorbing reactive power). On the reverse, if V_S is higher than V_{PCC}, Q is flowing from V_S to V_{PCC} (STATCOM is generating reactive power). Then the amount of reactive power is given by:

$$Q = \frac{v_{PCC} \times (v_{PCC} - v_S)}{X} \tag{2.6}$$

A capacitor connected on the DC side of the VSC acts as a DC voltage source. In steady state, the voltage V_S has to be phase shifted slightly behind V_{PCC} in order to compensate for transformer and VSC losses and to keep the capacitor charged. Any combination of real power generation or absorption with reactive generation or absorption is achievable if the STATCOM is equipped with an energy storage device of suitable capacity.

2.6.4. STATCOM Inverter Controller

As shown in Fig.2.8 the STATCOM controller is used either to regulate the voltage at the PCC or to regulate the reactive power flow. A PWM based typical PCC voltage regulation strategy of a STATCOM is described in Fig.2.8 where the controller is described with the use of d-q coordinate system signals [14], [15], [17], [25].

A phase-locked loop (PLL) synchronizes the positive-sequence component of three-phase primary voltage V_{ABC} of the STATCOM converter with V_{dq}. The output of the PLL (angle θ=ωt) is used to compute the d-axis and q-axis components of the AC three-phase voltage and current (labeled as V_{dq} or I_{dq} on the diagram) using park's transformation.

The output of the AC voltage (V_{PCC}), PI-2, is the reference current Iq-ref for the current regulator (I_q is current in quadrature with voltage which controls reactive power flow) by comparing it with q-axis measured current output. The output of the DC voltage, PI-1, is the reference current $I_{d\text{-}ref}$ for the current regulator (I_d is current in phase with voltage which controls active power flow) by comparing it with d-axis measured current output [15], [17], [24].

To maintain constant DC link voltage DC bus, is monitored and controlled through a controller PI-3 on direct axis current control loop which eventually defines the reference value I_{d_ref} for direct axis current control loop as shown in Fig.2.8. On the other hand, to regulate voltage at PCC through reactive power exchange, the PCC voltage is monitored and compared with PCC reference voltage, V_{PCC_ref}. The current signals are monitored from the PCC is then compared and passed through two PI controllers PI-3 and PI-4 to generate desired modulating signals m_d and m_q respectively.

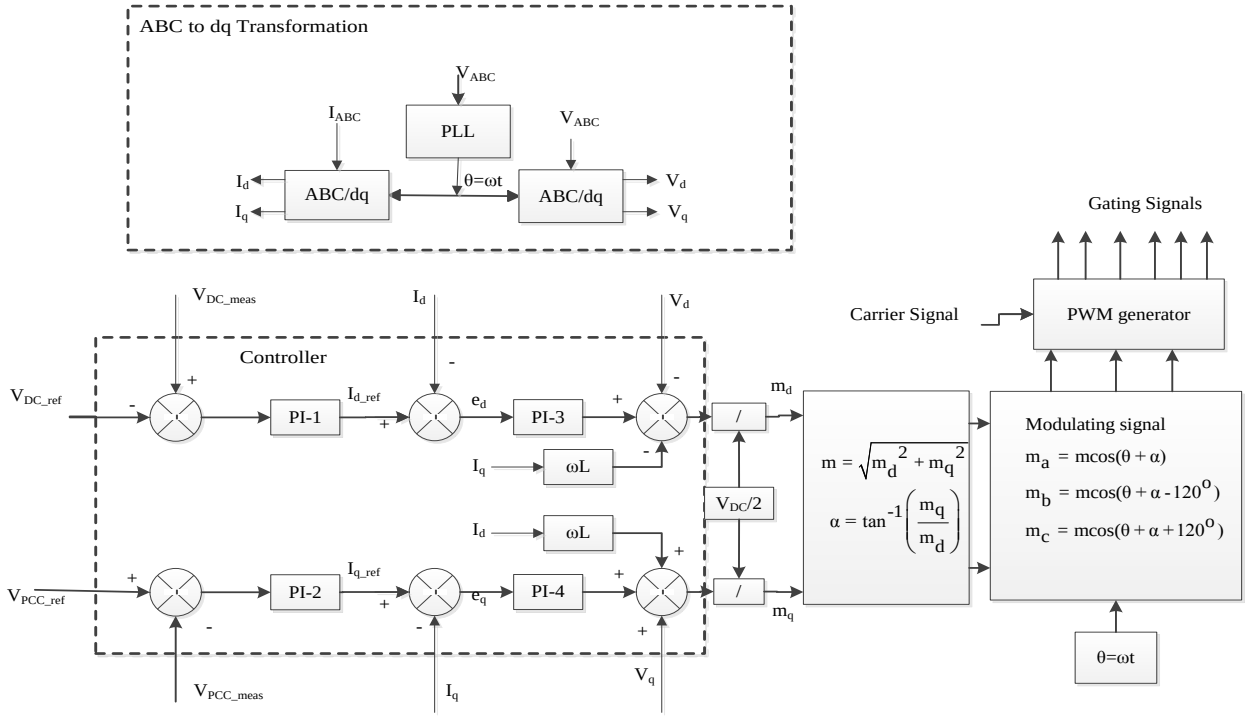

Fig. 2.8. Schematic diagram of generic conventional STATCOM controller [15], [24]

These modulating signals, m_d and m_q are converted back into three phase modulating signals as follows [14], [15], [24]:

$$m_a = m\cos(\theta+\alpha),\ m_b = m\cos(\theta+\alpha-120^o),\ m_c = m\cos(\theta+\alpha+120^o)$$

$$\text{Where; } m = \sqrt{m_d^{\,2} + m_q^{\,2}},\ \alpha = \tan^{-1}\left(\frac{m_q}{m_q}\right)$$

The direct axis and quadrature axis voltages act as disturbance signals in these control loops and a decoupling factor of ωL was included to decouple the two control loops where, ω is the angular frequency in rad/sec and L is the inductance at the output of the inverter.

For three-phase PWM converter, the AC voltage magnitude is given by:

$$V_{LL} = \frac{\sqrt{3} \times m_a \times V_{dc}}{2\sqrt{2}} \quad (2.7)$$

Where; V_{LL} is AC terminal voltage of three-phase converter, V_{dc} is DC link voltage of the converter; m_a is amplitude of modulating signal.

2.7. Power Converter Topologies for WECS and SECS

Power converters are used in different electric power generation conversion systems to convert an electrical energy from one form to another form. In variable-speed WECS, they are employed to control the speed/torque of the generator and the active/reactive power to the grid [4], [10], [12], [13]. In addition, in solar energy conversion systems (SECS), converters are used to control the DC link voltage output of the solar array/panel side and to control the grid side active/reactive power. The following power converters are widely used:

- Cascaded H-bridge converter
- Two-level voltage source converters
- Three-level neutral point clamping (NPC) converters

In this thesis work, two-level three-phase VSC/inverters have been used in both the WECS and PV-STATCOM as DC power to AC power converters.

2.7.3. Two-Level Voltage Source Converters

These converters are widely used in back-to-back full converter capacity based WECS and SECS. The two-level back-to-back VSC is shown in Fig. 2.9 (b). In grid, tied WECS 2-level 3-phase converter/inverter is as shown in Fig. 2.9 (a).

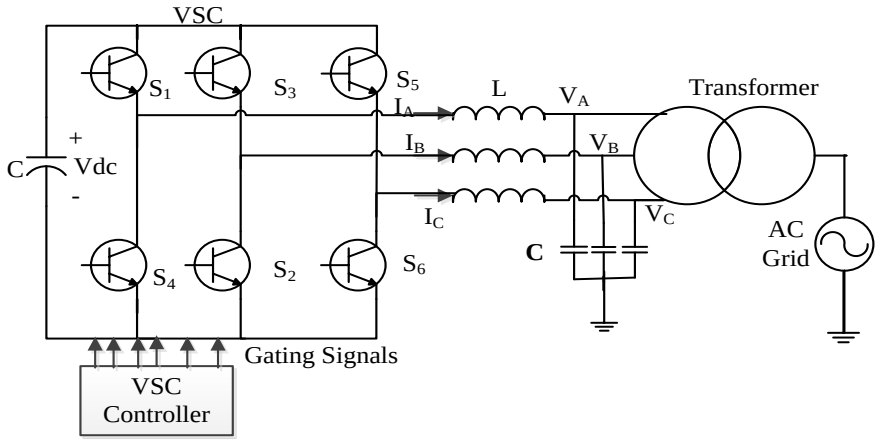

(a) 2-levele 3-phase Voltage source inverter/converter

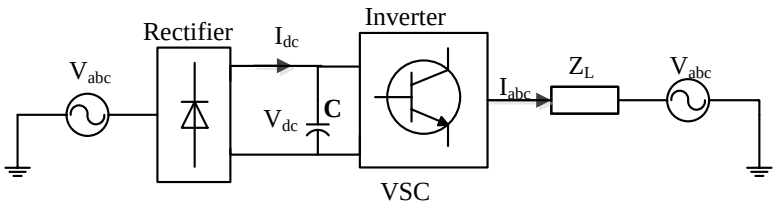

(b) 2 -level three - phase Back-to-Buck Voltage source converter

Fig. 2.9. Two - Level voltage source converter

2.7.4. Control of Power Converters

The most commonly used control methods for power converters are [4], [11]:

- Sinusoidal Pulse width modulation method (SPWM)
- Sinusoidal pulse width modulation (SPWM) technique with injection of third harmonic
- State Vector SPWM (SVPWM)

In this work, the SPWM controlled 2-level three-phase converter method has been used.

2.7.5. Sinusoidal Pulse Width Modulation (SPWM)

This method is the most common modulation technique and used in Adama-I WF. By using a triangular signal and comparing it with the reference signal (an image of the output voltage that is wanted at the output of the converter) as shown in Fig.2.10 is generated [4], [11], [13]. The block diagram of the SPWM scheme is shown in Fig.2.11 [11].

From Fig.2.13 (a), each switch is turned ON for 180°. The switches S1 and S4 produce the output voltage for phase A. The switching signals for the switches in the middle leg, S3 and S6 for phase B, and have delayed by 120° from those for S1 and S4 respectively for a positive sequence. Similarly, for the same phase sequence, the switching signals for switches S5 and S2 are delayed from the switching signals for S3 and S6 by 120°.It is called "six-step inverter" since there are six "steps" in the line to neutral (phase) voltage waveform [4],[11], [13].

The switching sequence is S1S2S3, S2S3S4, S3S4S5, S4S5S6, S5S6S1, S6S1S2, S1S2S3… for a positive sequence. The sequence is reversed to get the negative phase sequence.

Power inverter gating strategy: In SPWM inverter, three sinusoidal reference voltage waveforms at each phase is compared to the same triangular carrier as shown in Fig.2.10. The three -reference voltages are 120° apart. With this method, switch S1 is ON when triangular carrier is less than $V_{a\text{-reff}}$ and S4 is OFF. The output voltage V_{ag} is equal to V_{dc}. The same principles apply for the other legs of the converter. To summarize the principles are given as follows:

$V_{a,ref} > V_{tria}$	S_1 is ON
$V_{a,ref} < V_{tria}$	S_4 is ON
$V_{b,ref} > V_{tria}$	S_2 is ON
$V_{b,ref} < V_{tria}$	S_5 is ON
$V_{c,ref} > V_{tria}$	S_3 is ON
$V_{c,ref} < A_{tria}$	S_6 is ON

$$\begin{cases} v_{a,ref} = v_{ref}\sin(\omega t) \\ v_{b,ref} = v_{ref}\sin(\omega t - 120^0) \\ v_{c,ref} = v_{ref}\sin(\omega t + 120^0) \end{cases}$$

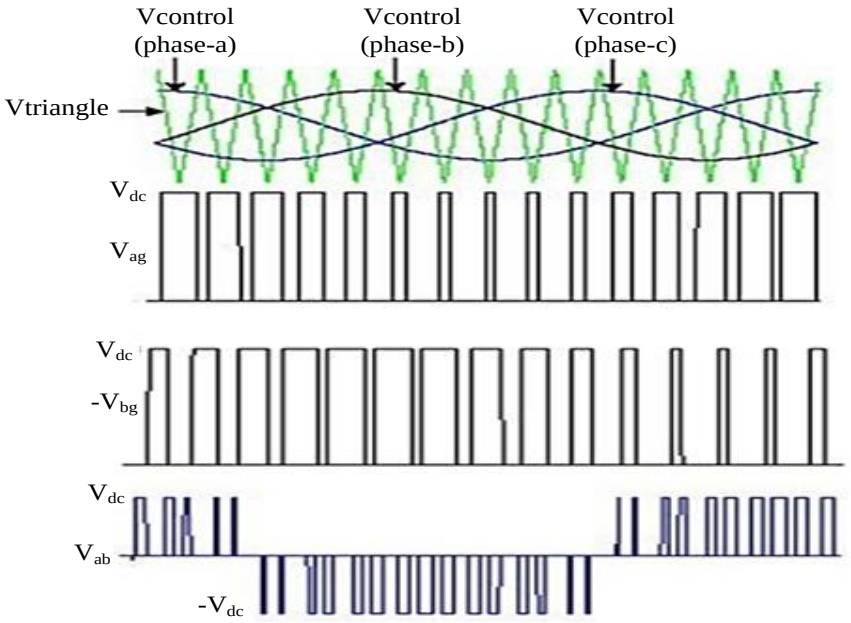

Fig. 2.10. Waveform of the sine triangle and the voltage reference comparison [1]

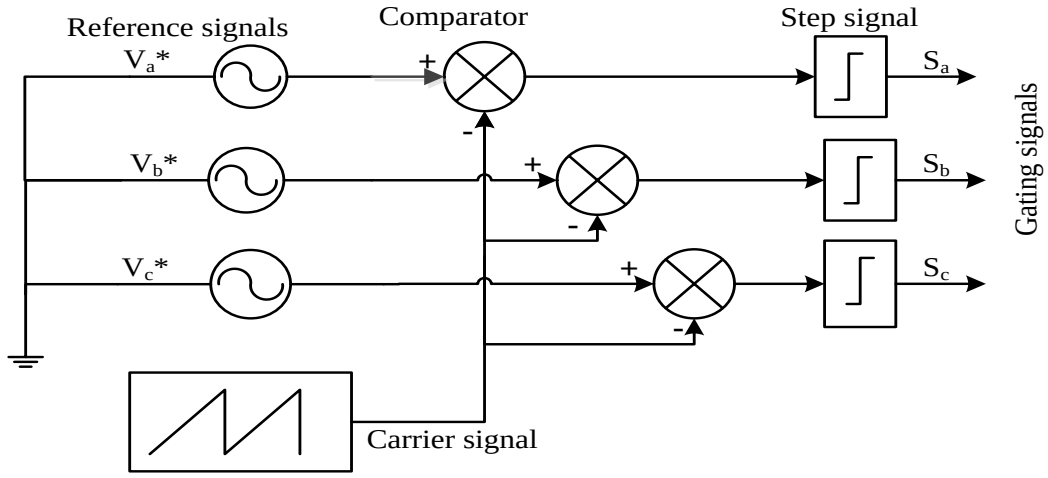

Fig. 2.11. Simplified block diagram of the SPWM scheme [11]

The relationships between the amplitudes and frequencies of the signals need the following indexes:

1. Amplitude modulation index (m_a): In SPWM as shown in Fig.2.10 the relationship between the amplitude of the reference signal and the triangular signal is expressed as:

$$m_a = \frac{\text{peak amplitude of } v_{tria}}{\text{amplitude of } v_{ref}} \quad (2.8)$$

Where; V_{tria} is the peak amplitude of the triangular carrier, V_{ref} is peak amplitude of the sinusoidal reference signal. Under ideal conditions, the relationship between modulation index, DC and AC voltage is given as:

$$v_{an,1} = m_a \frac{v_{dc}}{2}, \text{if } m_a \leq 1 \quad (2.9)$$

2. Frequency modulation index (m_f): The relationship between the frequency of the triangular signal and the reference signal is expressed as:

$$m_f = \frac{f_{tria}}{f_{ref}} \quad (2.10)$$

In general, in order to create a good quality output voltage, m_f should be a high number. However, since the imposed frequency of the triangular signal (f_{tri}) determines the switching frequency of the switches of the converter, this frequency should not be too high, in order not to produce high switching losses in the semiconductors.

2.8. Review of Literatures

Different researches had been written to solve voltage and reactive issues in wind farms: this includes:

Sunil Kumar J, Shalini J, Birtukan Teshome, Milkias Berhanu Tuka and Fikadu Wakijira, 2013 [27]. The title of this a journal paper is "Improvement of Active and Reactive Power at the Wind Based Renewable Energy Sources: A case study on ADAMA wind power plant". In this study, the wind capacitive reactive power compensator device have been suggested to be replaced with the dynamic reactive power compensator, STATCOM device.

Mr. Lakshman Naik Popavath, Dr. K. Palanisamy 2015, [28]. This a journal paper title is "A Dual Operation of PV-STATCOM as Active Power Filter and Active Power Injector in Grid Tie Wind -PV System PV-STATCOM based Mitigation Measures for Voltage Issues". In this, study the PV-STATCOM is utilized as STATCOM operation both in the nighttime and in daytime to filter both active power and reactive power the grid with connection of wind power.

.

Francisco D´ıaz Gonz´alez, Marcela Mart´ınez-Rojas, Andreas Sumper, Oriol Gomis-Bellmunt and Llu´ıs Trilla, 2014 [29]. This is a journal titled with “Strategies for Reactive Power Control in Wind Farms with STATCOM”. In this paper, a STATCOM is used to compensate to compensate the sudden reactive power requirement in grid connected wind farms.

Another research written by AC. Mahendra 2013 [30] with title of "Novel Control of PV Solar and Wind Farm Inverters as STATCOM for Increasing Connectivity of Distributed Generators". In his research, AC. Mahendr had used the PV-STATCOM to control the reactive power and to decease the voltage variations at the WTGs fed grid with direct reactive power control.

In this research as the structural and operational similarities between VSC based STATCOM and inverter based solar PV system, the PV-STATCOM has been used as dynamic voltage regulator.

CHAPTER THREE

3. DATA COLLECTION AND ANALYSIS

3.1. Introduction

To understand and obtain the advantages of PV-STATCOM by installing it at Adama-I wind farm, it is necessary to select an appropriate place and size of a PV-STATCOM. In this thesis work, the required data have been collected from Adama-I wind farm substation SCADA system which shows an average monthly wind speed, voltage (kV) (L-L rms), current (A), active power (MW) and reactive power (MVar) and the power factor of the WF for both 33kV and 132kV lines as shown in Fig.G2 of appendix G. The WTG unit transformer, the substation main transformer and the PMSG parameters have been taken from their nameplate data sheet. The wind turbine parameters have been taken from feasibility study manual [20], technical study manuals, from interviews of the wind farm operators and posters located on the buildings of the WF substation. In addition, parameters of the WTG collective transmission line has been taken from transmission line design calculation manual of the wind farm [20].

3.2. Wind Farm Transformers

In Adama-I, three types of transformers are found. This includes wind farm unit transformer, wind farm substation transformer and grounding transformer. The transformers are modeled as an ideal transformer between two system buses, i and j as shown in Fig. 3.1.

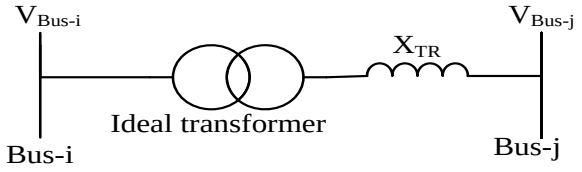

Fig. 3.1. Ideal transformer model with series reactance

3.2.1. Wind Turbine Unit Transformer

As described in section 2.1, this transformer is used to step up the output voltage of each WTG's. **P**arameters of the unit transformer taken from nameplate are given in table 3.1.

Table 3.1. WTG unit transformer parameters data sheet

Type	ZGS11-Z.F-1600/35
Rated power	1600KVA
Number of phase	3
Rated frequency	50Hz
Rated voltage	34.65±2×2.5%)/0.62 KV
Rated current	26.66/1489.94A
Impedance voltage	6.12%
Impedance p.u. value	4.0625

3.2.2. Wind Farm Main Substation Transformer

This transformer is used to step up the incoming 33kV from the transmission line to 132kV of the main grid. Its Parameters as taken from the nameplate are given in table 3.2.

Table 3.2. Main (substation) transformer parameter datasheet

Type	SFZ10-55000/132
Rated frequency	50Hz
Rated power	55000 KVA
Rated voltage	33/132 KV

3.3.3. Wind Farm Main Substation Grounding Transformer

This transformer is found in WF main substation to ground over currents mainly due to lightening effects. Its parameters as taken from the nameplate are given in table 3.3.

Table 3.3. Wind farm substation grounding transformer parameters data sheet

Rated capacity	12000KVAR
Rated voltage	33KV
Rated current	210 A
Rated frequency	50Hz
Rated reactance	272 Ohm
Number of phases	3

3.4. Wind Farm Transmission Line

The wind farm transmission line connects all WTGs' output power to the main (national) grid. In Adama-I wind farm, collector underground transmission line and connector overhead transmission (OHTL) lines are found as shown in Fig.2.1. In this study, only the connector overhead transmission line has been considered. The type line is all aluminum alloy conductors. The inductive reactance of the WTGs' group has been taken from Adama/Nazret wind power construction project technical manual [20] as given in table 3.4.

Table 3.4. Impedance values for Adama-I WTG 33kv connector line

Group connector line name	Inductive reactance value(p.u.)
Group 1(10 WTGs')	0.07115
Group 2(12 WTGs')	0.2250
Group 3(12 WTGs')	0.2250

This transmission line is represented by Π model as shown in Fig.3.2.

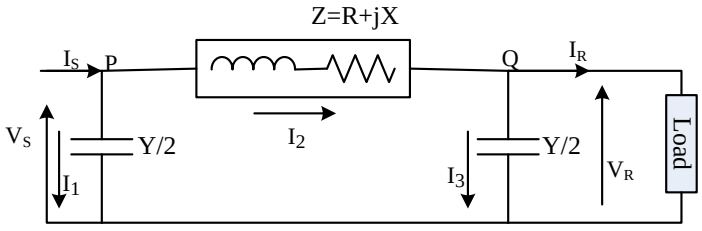

Fig. 3.2. Nominal network of medium voltage transmission line [25]

As shown in Fig.3.2 the Π network, the total lumped shunt admittance is divided into two equal halves, and each half with value $Y/2$ are placed at both the sending and the receiving end while the entire circuit impedance is between the two as shown in Fig.3.2 [25].

3.5. Reactive Power Compensator Devices in the Wind Farm

The main reactive power compensator devices capacity found at Adama -I wind farm includes 4.765MVar WTG side capacitor bank, 5.147MVar grid side of the WTG capacitor bank and 12 MVar MCR type SVC at the substation [20]. Generally, the range of reactive power compensation capacity of these devices is 2-to-10 MVar. In addition, the power factor of the wind farm is in the range of 0.95-to-0.999 [21].

3.6. Auxiliary Load

Auxiliary load includes the total power consumed at the Adama-I WF main substation and at WTGs. In this wind farm, 60kW total monthly average load (wind turbines consumption auxiliary load consumption) is connected. The average monthly load consumption ranges from 14.1kW-to-58.4kW excluding losses as shown in table 3.5.

Table 3.5. Monthly average auxiliary load consumption of Adama-I WF 2015/16

Month	Total Production (KWH)	WTG Consumption (kwh)	Auxiliary Consumption (kwh)	Total Consumption (kwh)	Max. Load (MW)	Av. Load Production (MW)
January	17422043	4931	6520	11451	51.18	24.20
February	18113326	12340	6800	19140	50.36	25.16
March	13,330,470	19166	7950	27116	51.02	18.24
April	7367184	35170	7310	42040	48.73	10.23
May	8,566,703	27,123	7,290	34,413	42.94	11.90
June	12,802,450	6,953	7,170	14,123	49.21	17.78
July	13587345	10334	6970	17304	50.37	18.87
August	8438540	22796	7110	29906	49.17	11.72
September	8902185	29467	6300	35767	49.17	12.36
October	19315440	5885	6300	12185	51.54	26.83
November	22255180	41847	6620	11467	51.94	30.91
December	21465521	4556	5620	10176	51.50	29.81
Total	171566387	220568	81960	265088	597.13	238.01

The data given in table 3.5 have been taken from the SCADA system of the wind farm. In this thesis, it has been considered that the wind farm will contribute a total 6.48 MW, 21 MVar peak load in the daytime hours and 3.38 MW, 12.07 MVar off-peak loads in the nighttime hours to the neighboring areas with inclusion of the total load being consumed in the WF substation and WTGs' side. The reactive power 21MVar during peak load and 12.07 off peak load have been considered to show that high power generated in the off peak load hours that causes voltage rise at the PCC of the WTGs' can be minimized with the use of more inductive loads in addition to the PV-STATCOM device.

3.7. Wind Speed Profile in the Wind Farm

Monthly average wind speed (m/s) of Adama-I wind farm, which has been determined from the SCADA system of the wind farm as shown in Fig.G1 of appendix G is given in table 3.6.

Table 3.6 Adama -I wind farm monthly average wind speed in 2015/16

R.no	Month	Wind speed (Vw) (m/s)
1	September	5.9
2	October	9.04
3	November	9.68
4	December	9.81
5	January	8.49
6	February	8.27
7	March	7.25
8	April	5.39
9	May	5.92
10	June	8.11
11	July	7.65
12	August	5.84

3.8. Wind Farm Main Grid

The main grid in Adama-I wind farm is 132 kV, 55MVA capacity grid. In this study, the grid has been represented as capable of supplying the required three-phase voltage source. The grid feeding the transmission line is represented by a voltage source behind equivalent source impedance as shown in Fig. 3.3.

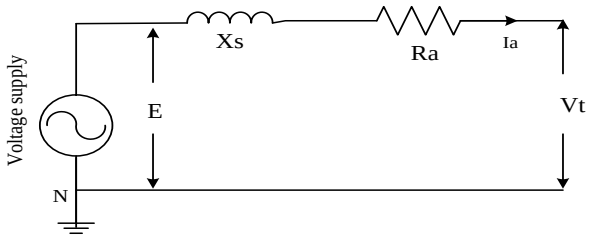

Fig. 3.3. Grid model as voltage source [17]

In Fig.3.3, Ra is armature resistance, E is no load voltage and Vt is voltage across the terminals of loaded machine. The voltage behind the reactance, E, is fixed whereas the terminal voltage Vt depends on the loading condition of the transmission line with parameters of Xs and Ra.

Table 3.7. Adama -I WF daily power generation lose due to SLGF over current and supply voltage block

Date	Name of Line / WTG	Tripping Time Hr : Min	Restoration Time Hr : Min	Total Outage Hr : Min	Loss of Load / Generation MW	Reasons
01/03/2007 E.C	G1	16:07	16:56	00:49	9.25	External voltage block
	G2	16:07	16:58	00:51	9.25	External voltage block
17/10/2007 E.C	Group 2	04:26	04:40	00:14		Over current
	Group 3	04:40	00:00			Over current
18/10/2008 E.C	G 3	00:00		00:00		Overcurrent
	line	11:30	15:55	04:25	2.69	Over current
23/10/2008 E.C	Line	03:45	04:28	00:43		Voltage lose from the system
27/10/2008 E.C	G 1	11:25	01:15	10:10	8.55	External voltage block
	G 2	11:28	01:15	10:13	8.58	External voltage block
12/04/2008 E.C	Line	15:09	17:06	01:57	33.03	Over current
	Line	15:09	17:06	01:57	33.03	Over current
15/04/2008 E.C	Line	04:34	07:49	03:15	32mw	Over current
27/04/2008 E.C	Line	16:15	17:48	01:33	26.82	Over current

From table 3.7 we can understand that the SLG fault at the transmission causes over currents that leads to disconnect the WTGs from the main grid. This leads to lose in power generation from the WTGs. Due to the external voltage supply voltage block from the main grid voltage is not supplied to the WTGS leads to power generation lose from the WTGs.

CHAPTER FOUR

4. SYSTEM MODELLING AND ANALYSIS

4.1. Introduction

In this chapter the modelling and analysis of the system under study which includes DD PMSG based Adama -I wind farm WTGs' connected to the main grid through 33kV, 4.7 km medium voltage transmission line and at the PCC of the WTGs' PV-STATCOM installation have been done as shown in Fig. 4.1.

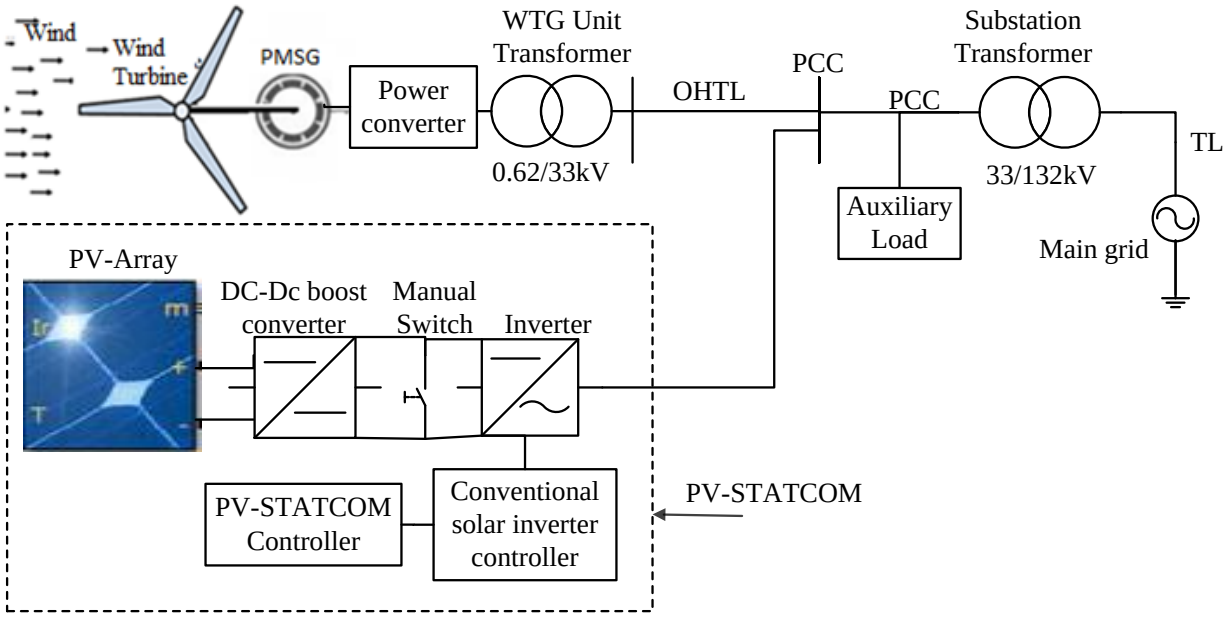

Fig. 4.1. Single line diagram of system under study

4.2. Modeling of PMSG Based Wind Turbine Energy Conversion System

In this topic, the mathematical analysis and modeling of the WTG have been done. As shown in Fig.4.2 the system consists of diode bridge rectifier, DC-DC boost converter with associated controllers, DC link capacitor, inverter with controllers, AC filter, unit transformer and AC grid.

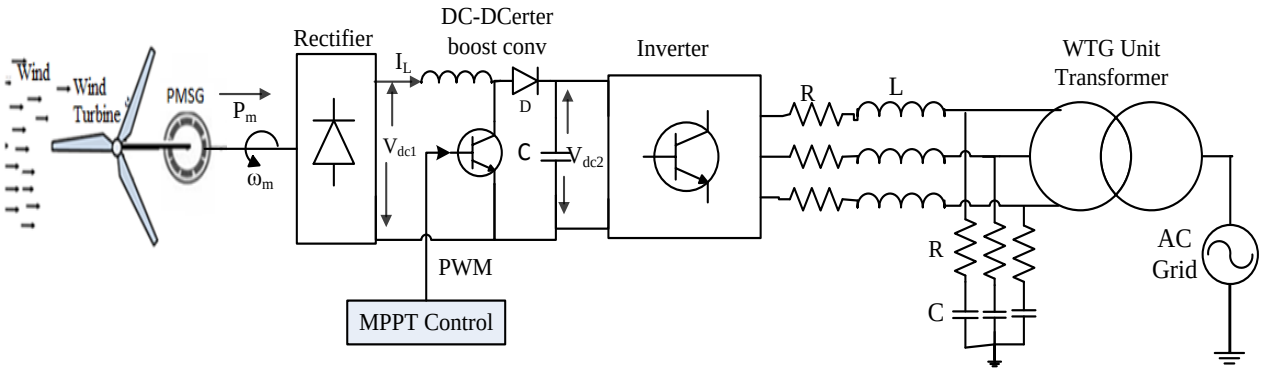

Fig. 4.2. Single line electrical diagram of 1.5MW Adama-I WTG

4.2.1. Modeling of Wind Turbine

Wind is the movement of air mass and it has kinetic energy. This kinetic energy is converted into mechanical energy using a wind turbine rotor with blades. This mechanical energy is converted to electrical energy using wind turbine generators.

Power in the Wind: Variation of wind velocity and direction above the ground level is necessary for energy conversion as described in equation (4.2).

The power expressed in equation (4.2) can only stand for the maximum potential power which is available when the wind with velocity, v_w, passes through the swept area of the wind turbine blade with length, r. In fact, only the wind turbine can capture a portion of this potentially available power. After influencing the rotor blades of the wind turbine, the velocity of the wind decreases, which means that when the wind passes through the wind turbine blades, there is still some kinetic power left in the wind. The relationship between the power that is captured by the wind turbine and the potential maximum power in the wind can be expressed as:

$$C_p = \frac{P_m}{P_w} \tag{4.1}$$

Where; P_m is the actual mechanical power captured by the wind turbine, and C_P is the power coefficient of the wind turbine. In most cases C_P =0.593 or 59.3% is Boltzmann's constant.

In this work the maximum power coefficient value is determined at zero pitch angle (β=0) as C_{Pmax}= 0.45. The actual wind power in the wind at any instant of time, $P_{w,}$ can be determined as:

$$P_w = \frac{1}{2}\rho\pi r^2 v_w^3 \tag{4.2}$$

Where; ρ is the air density kg/m^3, v_w is wind speed in m/s r is length of blade. The air density ρ at sea level and temperature of 15°c, air has a value of approximately 1.225 kg/m3.

4.2.2. Power Captured by the Wind Turbine

The rotor blades of the wind turbine capture only part of the available wind power:

$$P_m = \frac{1}{2}\rho\pi r^2 C_p(\lambda,\beta) v_w^3 \tag{4.3}$$

$$\begin{cases} C_p(\lambda,\beta) = c_1\left(\frac{c_2}{\lambda i} - c_3\beta - c_4\right)\exp\left(\frac{-c_5}{\lambda i}\right) \\ \text{Where;} \frac{1}{\lambda i} = \frac{1}{\lambda_{opt} + 0.08\beta} - \frac{0.035}{\beta^3 + 1} \\ \lambda_{opt} = \frac{\omega_r(\text{rad/s}) \times r(\text{m})}{v_w(\text{m/s})} \end{cases} \tag{4.4}$$

Where; β is the blade angle, which is indicated in Fig.4.4, and λ_{opt} is the optimal tip speed ratio of the wind turbine, ω_r is the angular speed of the wind turbine generator. The values of the coefficients (c_1-to-c_6) depend on the type of the wind turbine and given in table A3 of appendix A. The optimal value of the tip speed ratio (λ_{opt}) at rated wind speed of 11m/s and rated generator speed of 17.3 rpm is 6.14 in this work.

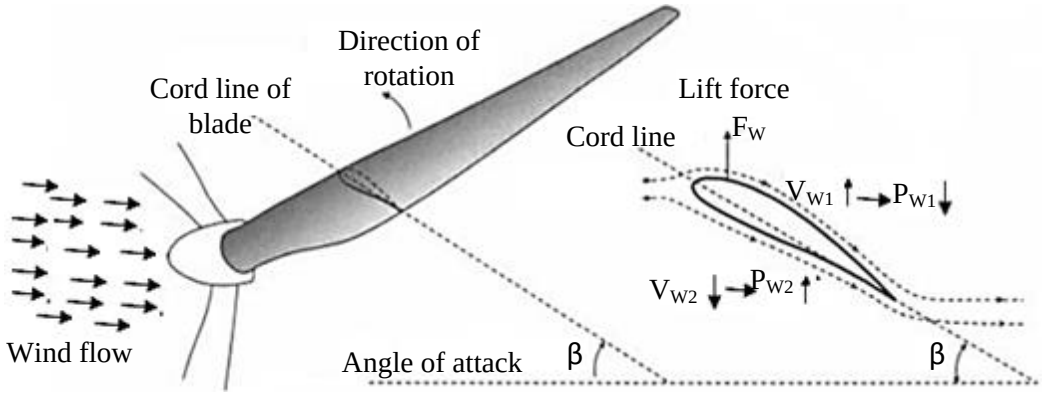

Fig. 4.3. Wind turbine blade aerodynamics and angle of attack [4]

Wind flow as shown in Fig.4.3 has the following speed stages.

Cut-in wind speed: Wind machines will not produce any more power below this wind speed. The cut in wind speed of Adama-I wind farm is 3m/s.

Cutout wind speed: Is highest wind speed at which wind turbines not being produced power rather should stop to protect from damage. In case of Adama-I WF cutout wind speed is 22 m/s.

Nominal or rated wind speed: Is wind speed at which the maximum power was derived and it determines the power curve. In Adama-I WF, the rated wind speed is 11m/s.

Mechanical torque of the WT blade rotor is determined as:

$$T_m = \frac{P_m}{\omega_m} \tag{4.5}$$

Where; ω_m is the rotational mechanical speed of the turbine blade rotor in (rad/s):

$$\omega_m = \frac{\omega_r}{p} \times \frac{2\pi}{60} \tag{4.6}$$

Where; p represents number of pole pairs of the wind turbine generator.

4.2.3. Drive Train Model

The power from the rotation of the wind turbine rotor transfers to the generator through the drive train, which is composed of hub with blades and the main shaft. The drive train of Adama-I wind turbine is modeled as two-mass model without gearbox as shown in Fig.4.4 [10], [16].

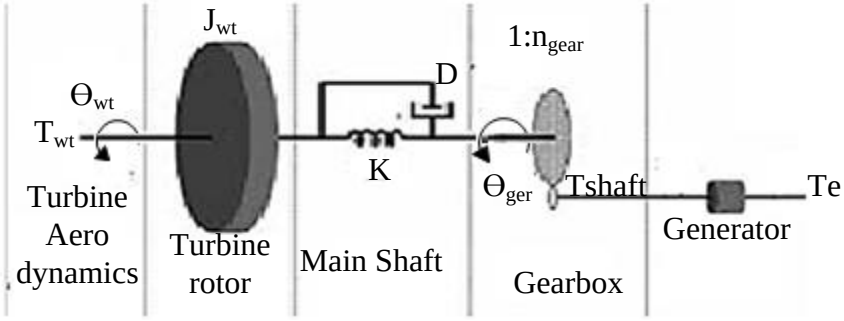

Fig. 4.4. Two-mass drive-train model [10]

The base angular speed difference between the two ends of turbine rotor and the main shaft is:

$$\omega_{base} = \omega_{rot} - \frac{\omega_{gen}}{n_{gear}} \tag{4.7}$$

Since; the WT is direct deriving (gearless) the gearbox ratio, n_{gear}=1, then equation (4.7) can be rewrite as:

$$\omega_{base} = \omega_{rot} - \omega_{gen} \tag{4.8}$$

The wind turbine rotor angular speed can be determined as [10]:

$$\begin{cases} J_{wt}\dfrac{d^2\theta_{wt}}{dt^2} = T_{wt} - T_{shaft} \;\; \text{but;} \dfrac{d\theta_{wt}}{dt} = \omega_{wt} \\ \dot{\omega}_{rot} = \dfrac{T_{wt} - T_{shaft}}{J_{rot}} \\ = D\omega_{base} + K\theta_{base} \end{cases} \tag{4.9}$$

Where; the subscript wt is the wind turbine rotor and the subscript, T (Nm) is the torque, J (K) is the moment of inertia, θ (rad) is the torsion angle, K (Nm/rad) is the stiffness coefficient and D (Nm /rad) is the damping coefficient.

4.2.4. Power and Torque Analysis of a PMSG

The electromagnetic torque developed by a PMSG of the WT is [4], [18]:

$$T_e = \frac{P_m}{\omega_m} = \frac{P_m}{\omega_r/\rho} = \frac{3}{2}\rho(\lambda_{ds} i_{qs} - \lambda_{qs} i_{ds}) \tag{4.10}$$

The rotor speed is governed by motion equation:

$$\omega_r = \frac{p}{JS}\left(T_e - T_m\right) \tag{4.11}$$

In addition, λ_{ds} and λ_{qs} are the d- and q-axis stator flux linkages, given by [4], [18]:

$$\begin{cases} \lambda_{ds} = -L_d i_{ds} + \lambda_r \\ \lambda_{qs} = -L_q i_{qs} \end{cases} \tag{4.12}$$

Substituting, equation (4.12) to equation (4.10), we get:

$$T_e = \frac{3}{2} p \times (\lambda_r i_{qs} - (L_d - L_q) i_{ds} i_{qs}) \tag{4.13}$$

For non-silent pole PMSG ($L_d = L_q$), therefore the electromagnetic torque is given by:

$$T_e = \frac{3}{2} p\, \lambda_r i_{qs} \quad \text{(Non-salient pole PMSG)} \tag{4.14}$$

4.2.5. Generator Side Converter (Rectifier) Modeling and Control

In Adama-I wind farm fully controlled converter direct derive PMSG based wind turbines with uncontrolled three-phase diode rectifier is used in the generator side as shown in Fig.4.5.

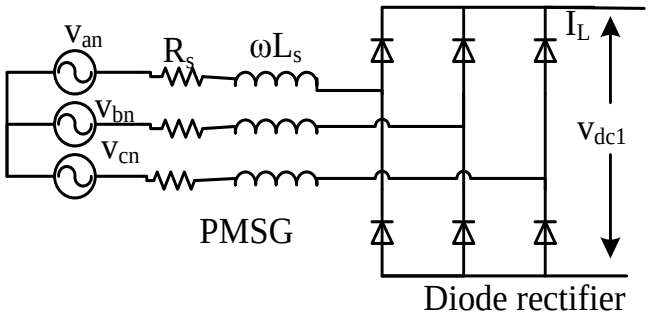

Fig. 4.5. PMSG with three-phase diode rectifier

The instantaneous phase voltages of PMSG, [17] [19] can be express as:

$$\begin{cases} v_{an} = V_m \sin(\omega t) \\ v_{bn} = V_m \sin(\omega t - 120^0) \\ v_{cn} = V_m \sin(\omega t + 120^0) \end{cases} \quad (4.15)$$

The average output voltage, v_{dc1}, (neglecting R_s and X_s) of the rectifier is [19]:

$$v_{dc1} = \frac{1}{\pi/3}\int_{\pi/3}^{2\pi/3} \sqrt{3} V_m \sin\omega t d\omega t = \frac{3V_{m(L-L)}}{\pi} \quad (4.16)$$

Where; Vm is peak value of phase voltage, $V_{m\,(L\text{-}L)}$ is line-to-line voltage of the PMSG output.

DC-DC Voltage Boost Converter Modeling and Control

The output of the three-phase rectifier (V_{dc1}) is fed to the input of the boost DC-DC converter to step up to the DC link voltage (V_{dc2}) to a suitable level for the proper operation of the inverter [4] as shown in Fig.4.6. The DC-DC boost converter is designed to regulate DC link voltage, which is the input to the inverter, under different wind speeds to extract maximum power.

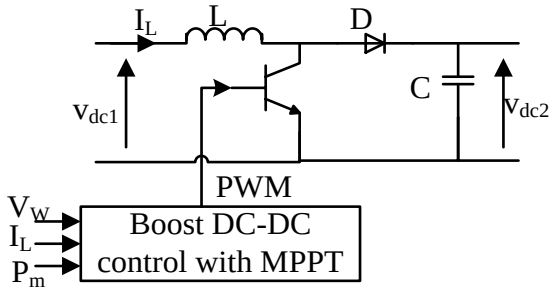

Fig.4.6. DC-DC boost converter control of Adama-I wind WTGs'

DC-DC Boost Converter Modeling

The input and output voltage relationship of the boost converter of Fig. 4.6, under an ideal condition is [4]:

$$v_{dc2} = \frac{v_{dc1}}{(1-D)} \tag{4.17}$$

Where; D = Ton/Ts and Ts =Ton + Toff, T indicates switching time, D is duty cycle.

The minimum inductance for continuous conduction of the boost converter can calculate as [4]:

$$L_{min} = \frac{D(1-D)^2}{2\,fs} \tag{4.18}$$

Where; fs =1/Ts which, is the switching frequency (Hz)

The inductance value for the boost converter should be higher than this value to ensure continuous conduction.

The capacitance, C is used to store energy output of the WTG:

$$C = \frac{D}{R \times f_s \times \frac{\Delta v_{dc2}}{v_{dc2}}} \tag{4.19}$$

Where; $R = v_{dc2}/I_{dc}$ which, is the output resistance.

4.2.6. DC-DC Voltage Boost Converter Control with MPPT

In PMSG based wind turbines, there are two distinctive characteristics [4]:

1. The rotor flux of the synchronous generator is produced by permanent magnets or rotor field winding, and, therefore, the generator does not require the rectifier to provide magnetization.
2. The output of DC voltage of the boost converter can regulate (increase) to a level required by the inverter. This is especially important at low wind speeds, when the output voltage of the diode rectifier is too low for the inverter to operate properly.

In the selected wind farm, the DC-DC boost converter is controlled based on collective pitch angle/rotor speed control method to extract maximum power as shown in Fig.4.7.

The PI controller parameters of Fig. 4.7 are found by trial and error method with similar considerations done in the PV-STATCOM. The values are given in table A3 of appendix A.

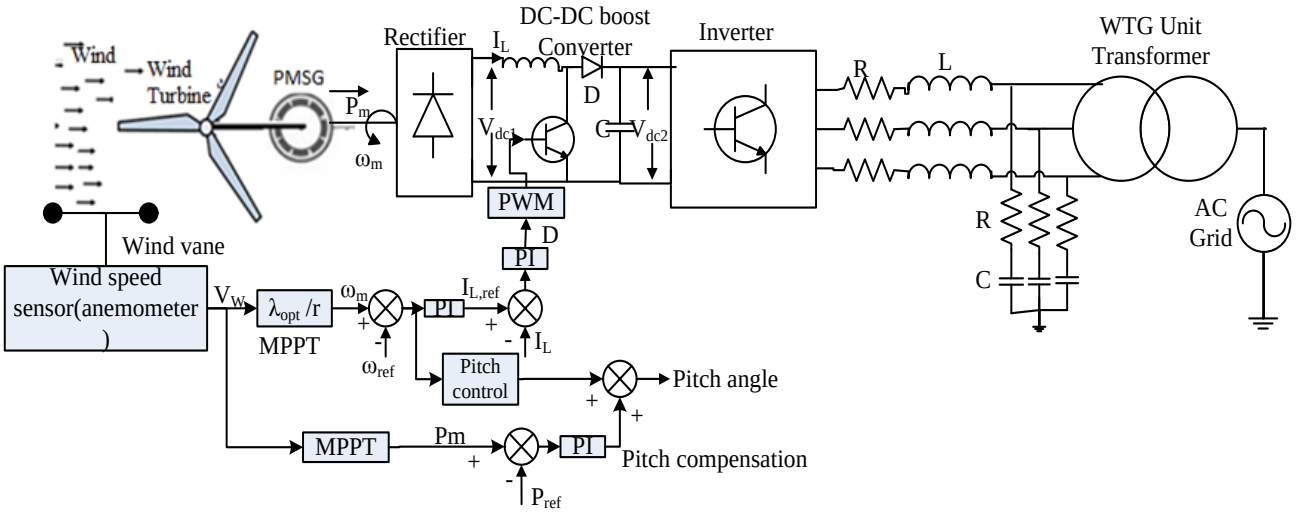

Fig. 4.7. Collective pitch angle/rotor speed control diagram of PMSG Adama-I WTGs

Tip Speed Ratio Based (TSP) MPPT for DC-DC Boost Converter Control

In this method, the maximum power operation of the wind turbine is achieved by keeping the tip speed ratio to its optimal value λ_{opt} at pitch angle, β zero value. As shown in Fig.4.7, the measured wind speed V_W is used to produce the blade rotor (generator) mechanical speed ω_m. By comparing the generator speed ω_m with sated reference speed ω_{ref} to generate the reference inductor current i_{Lref} of the boost converter and compared with the measured inductor current I_L of the DC boost converter, to generate the duty cycle D, which controls the ideal switch of the DC-DC boost converter to extract optimum power under fluctuating wind speeds. To reduce the error between reference inductor current i_{Lref} and measured inductor currents i_L is passed through PI controller. The mechanical speed of the WTG at MPPT extraction is given as:

$$\omega_m = \frac{\lambda_{opt}}{r} V_W = KV_W \qquad (4.20)$$

Pitch Angle Control Based MPPT for DC-DC Boost Converter Control

As described in sections 2.5.1 if the wind turbine operates beyond the rated wind speed without pitch control, the turbine will absorb more power from the wind than its capacity to withstand. Therefore, the control limits the power absorbed by the turbine from the wind to its capacity, even though much higher amount of power is available in the wind.

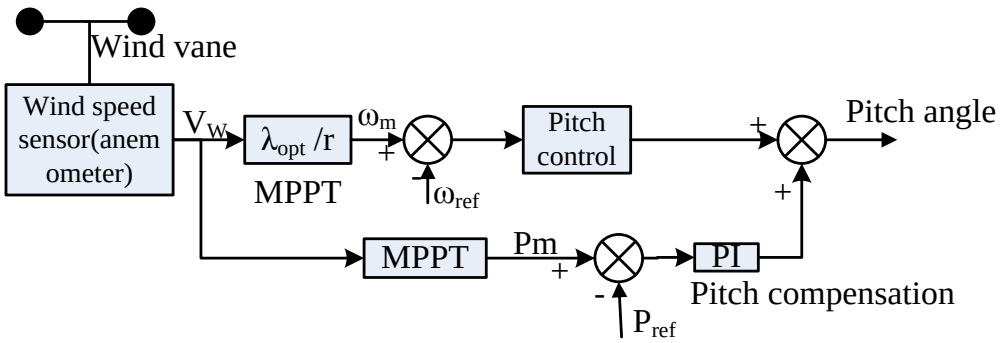

Fig. 4.8. DC-DC boost control diagram for pitch angle control of Adama-I wind turbine

By controlling the pitch angle, the optimal wind speed (λ_{opt}) at MPPT is determined as:

$$\lambda_{opt} = \frac{\omega_m \times r}{v_w} \tag{4.21}$$

The measured mechanical power output, Pm of the WTG at MPPT is:

$$P_m = 0.5\rho A C_{pmax} \left(\frac{r \times \omega_m}{\lambda_{opt}} \right)^3 \tag{4.22}$$

From equation (4.22), the pitch angle controller in Fig.4.8 controls the mechanical power output of the WTG by controlling the mechanical speed, $\omega_{m.}$ In lower wind speed conditions, the generated mechanical power, Pm, of the WTG is less than the actual reference mechanical power, P_{ref}. Here in the condition the pitch angle should be increased and compensated up to the maximum angle of attack to which the WT blade face to wind flow to gate more power.

4.2.7. Grid-Side Converter Control based on Voltage Oriented with decoupled Control

As the generator-side converter of the WTG controls the speed of the PMSG, the grid-side converter regulates the DC bus voltage while controlling the active power and reactive power injected into the grid. In this thesis, SPWM controlled 2-level three-phase grid-side converter/inverter is used as discussed in section 2.9.3.

The simplified system topology of the DD PMSG based Adama-I WECS is shown in Fig.4.9 where the currents, iag, ibg, and icg, are the three phase AC grid currents.

The active power and reactive power injected into grid is [4], [16]:

$$\begin{cases} P_g = 1.5(v_{dg} i_{dg} + v_{qg} i_{qg}) \\ Q_g = 1.5(v_{qg} i_{dg} - v_{dg} i_{qg}) \end{cases} \tag{4.23}$$

Where; Q_g grid side reactive power, P_g grid side active power, i_{dg} and i_{dq}, are the grid currents in dq -axes reference frame, v_{dg} and v_{qg}, are the grid voltages in dq -axes reference frame.

From equation (4.23), the d-axis and q -axis components of the grid currents and voltages are coupled in cross-product fashion in the reactive power term, which makes the active reactive power hard to control, and decreases the dynamic performance of the grid-side converter control.

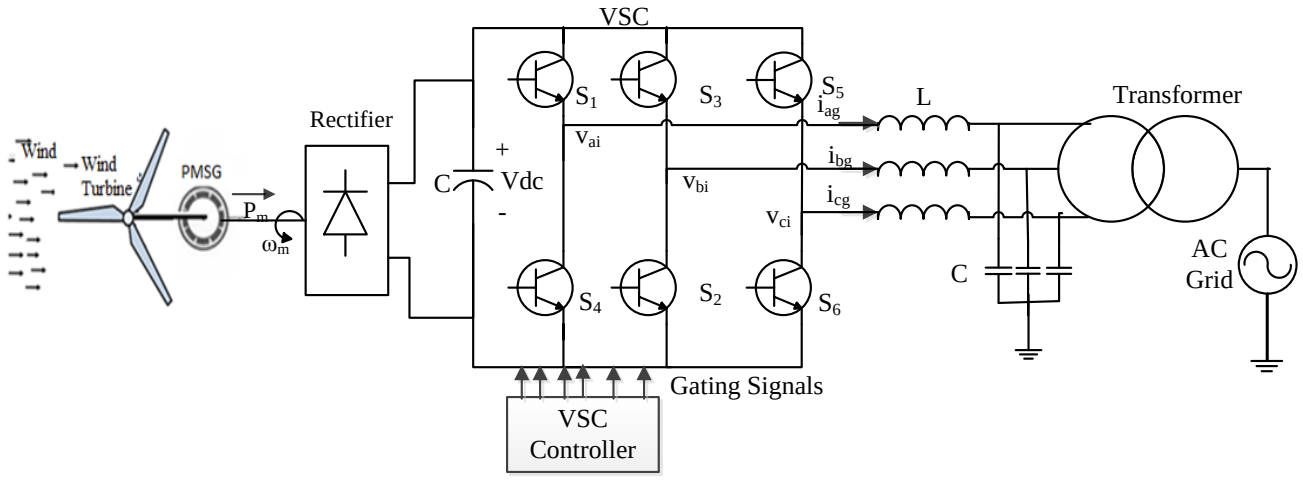

Fig. 4.9.Grid-connected WECS

To achieve the voltage oriented control (VOC) scheme, the d-axis of the synchronous frame is aligned with the grid voltage vector, therefore the d-axis grid voltage is equal to its magnitude (vdg = vg), and the resultant q-axis voltage vqg is then equal to zero ($vqg = \sqrt{vg^2 - vdg^2} = 0$).

With the application of the VOC approach i.e. vqg = 0, the expression of the active and reactive power of equation (4.23) can be reduced in to [4]:

$$Q_g = -\frac{3}{2} v_{dg} i_{qg} \tag{4.24}$$

The q-axis grid side reference current is obtained as [4]:

$$i_{qg}^* = \frac{Q_g^*}{-1.5 v_{dg}} \tag{4.25}$$

Neglecting losses in the inverter, the active power on the AC side of the inverter is equal to the DC-side:

$$P_g = \frac{3}{2} v_{dg} i_{dg} = v_{dc} i_{dc} \tag{4.26}$$

Where; vdc and idc are the voltage and current of the dc link respectively.

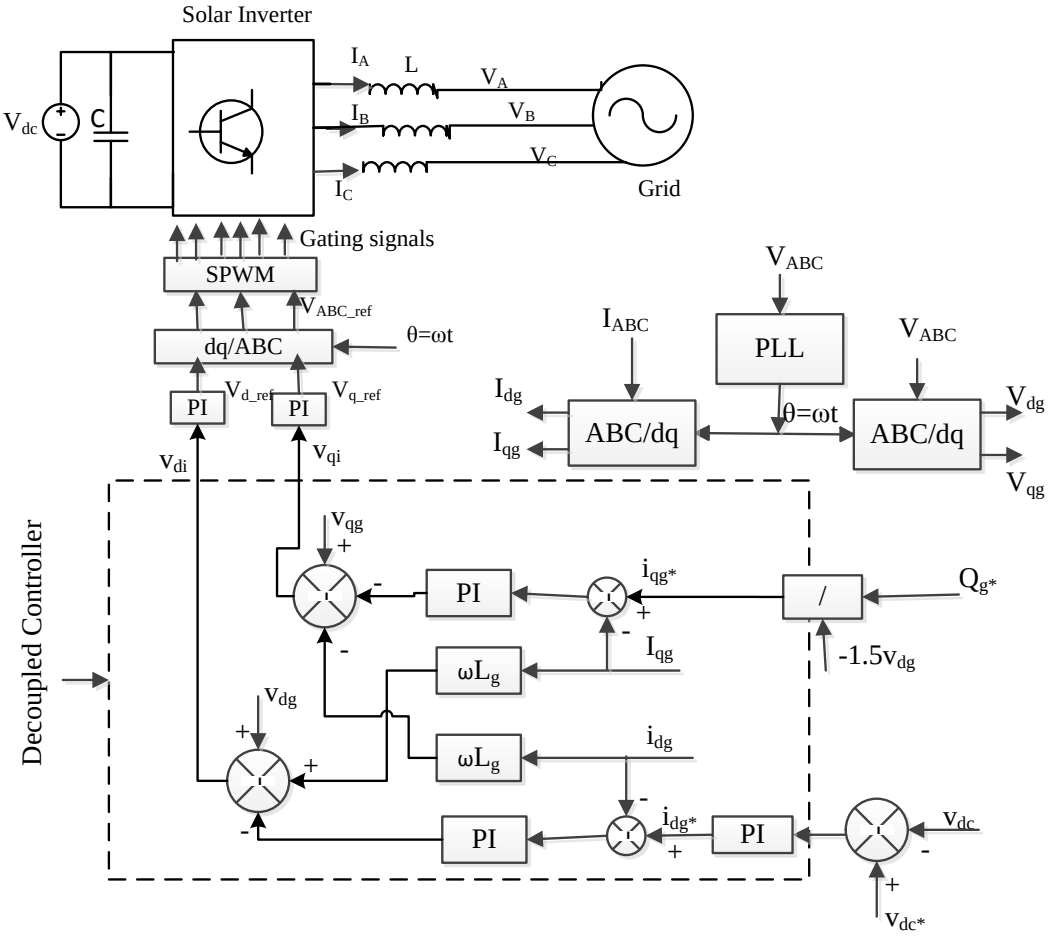

Fig. 4.10. Voltage-oriented with a decoupled controller

In Adama-I wind farm the grid side inverter of the WTG is controlled with VOC system. Even the system is simple in design and control system, it is not more stable in dynamic performance. To improve this stability voltage oriented with decoupled control system as shown in Fig. 4.10 has been used in this thesis.

Assuming that the controllers for the dq-axis currents in Fig.4.10 are of the PI type, the output of the decoupled controller is [4]:

$$\begin{cases} v_{di} = -\left(k_1 + k_2/s\right)(i_{dg}{}^{*} - i_{dg}) + \omega_g L_g i_{qg} + v_{dg} \\ v_{qi} = -\left(k_1 + k_2/s\right)(i_{qg}{}^{*} - i_{qg}) - \omega_g L_g i_{qg} + v_{qg} \end{cases} \tag{4.27}$$

Where; (k_1+k_2/s) is the transformation of the PI controller, ω_g is the speed of the synchronous reference frame, which is also the angular frequency of the grid, and ($\omega_g L_g i_{qg}$ and $\omega_g L_g i_{dg}$) are the induced speed voltages due to the transformation of the three-phase inductance, L_g from the stationary reference frame to the synchronous frame. Equation (4.27) indicates that the decoupled control makes the design of the PI controllers more convenient, and the system more easily stabilized.

4.2.8. AC Filter Model

An AC filter has been used both in the WECS and in the PV-STATCOM to minimize harmonic signal outputs of the voltage source converters/inverters. Different filter configurations can use at the inverter output which includes:

(a) L filter comprised of only series inductor

(b) L-C filter comprised of series inductor with a shunt capacitor and

(c) L-C-L filter comprised of two series inductors at either side of a shunt capacitor.

In this thesis work, RLC filter have been used as shown in Fig.4.11.The parameters of this filter are the filter inductance L, the filter capacitance C and the damping resistance R. The resistance of the filter inductor represents filter losses. The damping resistance can also neglect in the initial determination of the inductor and capacitor values.

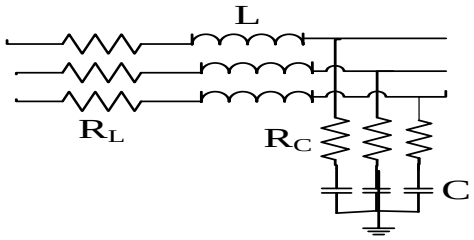

Fig. 4.11. LC filter circuit

The base power in inverter side (solar and wind inverters) or inverter side winding of the transformer (secondary side in this case) has been determined as:

$$P_{bas\_sec} = \frac{V_{nom\_sec}^{2}}{P_{nom}} \tag{4.28}$$

Where; P_{base_sec} is inverter coupling transformer secondary winding power, V_{nom_sec} is nominal voltage of the secondary winding (inverter side) of coupling transformer and P_{nom} is the nominal rated capacity (MVA) of the inverter. Hence, the RL parameters of the filter are determined as:

$$\begin{cases} R = R_{base} \times P_{bas\_sec} \\ L = \left(\dfrac{L_{base} \times P_{bas\_sec}}{2 \times \pi \times F_{nom}} \right) \end{cases} \quad (4.29)$$

Where; L_{base} and R_{base} parameters are the base values of the designed filter for the selected inverter type.

The RC parameters have been designed to dissipate active power (Pc) and compensate reactive power (Qc) respectively as:

$$\begin{cases} Qc(Var) = 0.1 \times Pnom \\ Pc(W) = Qc/100 \end{cases} \quad (4.30)$$

The choice of capacitor has been limited by the maximum allowable reactive power interchange between grid and inverters, and affects the power factor of the machine. This is usually kept to within 5% of the rated machine power [24].

Second order low pass filter: This filter is used in both the WECS and PV-STATCOM to alter the amplitude and phase characteristics of a signal (AC and DC) with respect to the required limit before their supplied to control system. The detailed analysis is given in appendix F.

4.3. Modeling and Sizing of PV-STATCOM

In this sub-topic, the detailed modeling of the solar inverters as STATCOM and the considerations made to size the PV system as STATCOM is analyzed.

4.3.1. Modeling of Grid Connected Conventional PV Solar System

In grid connected PV solar system, the PV solar array generates DC power based on solar irradiance, Ir and temperature, T as shown in Fig.4.12. A DC-DC boost converter is used to harvest maximum DC power at MPPT algorithm [1], [24].

A DC link capacitor is used to maintain the DC link voltage constant at the inverter DC terminal. The VSC/inverter transforms the DC power to AC power. The power quality at the output terminal of the inverter is maintained with the use of a filter. The output voltage level of the inverter is integrated with the network voltage by using a step up coupling transformer. The details of each components of the system have been described in the upcoming sections:

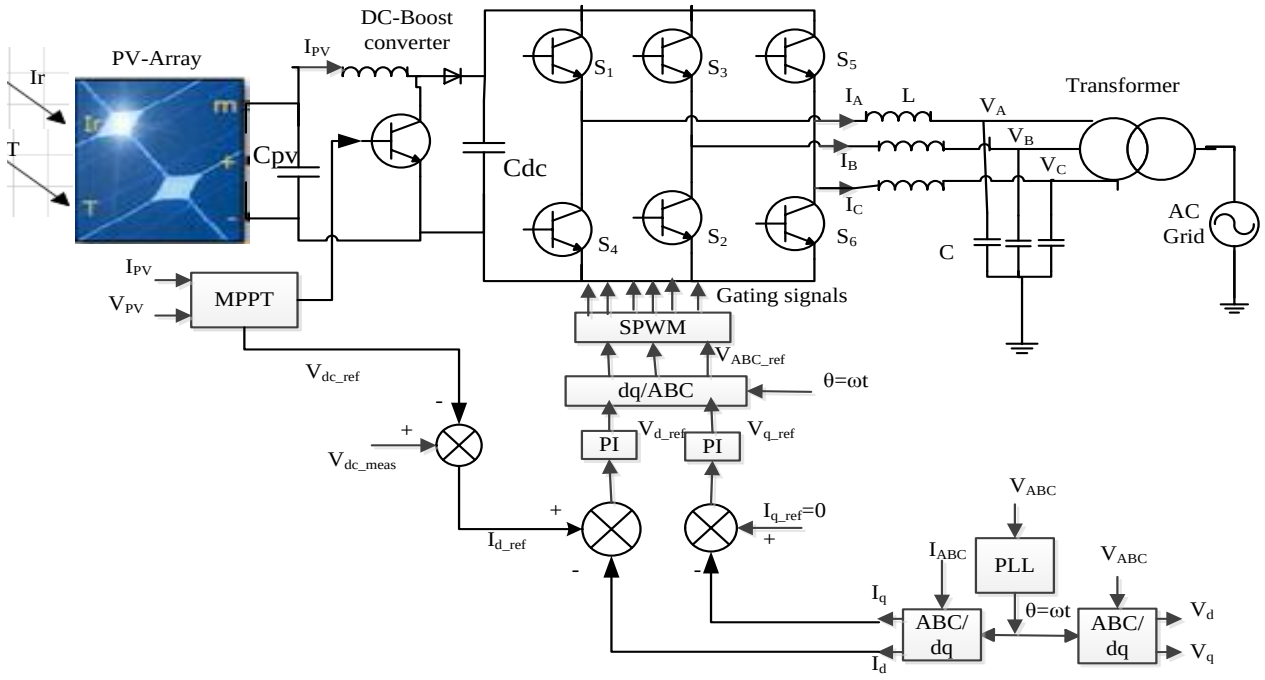

Fig. 4.12. Grid connected conventional PV system

Modeling of PV array: PV array is built of strings of modules connected in parallel, each string consisting of modules connected in series.

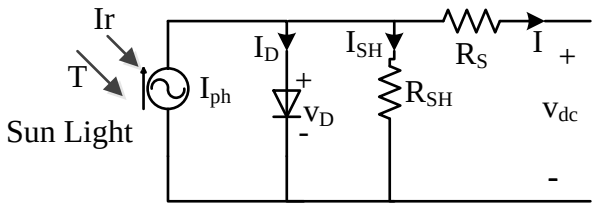

Fig. 4.13. PV array block electrical circuit

In this work, PV array has been taken from National Renewable Energy Laboratory (NREL) system advisor model (Jan. 2014) model of MATLAB/PowerSim software. PV array's single cell equivalent circuit and its solar light source (includes temperature T, and irradiance, Ir) is represented as shown in Fig.4.13.

The electrical characteristic of the PV array is generally represented by the I-V and P-V curves as shown in Fig.4.15. The irradiance (Ir) and temperature (T) input waveforms to the PV-array for simulation analysis is given as shown in Fig.4.14.

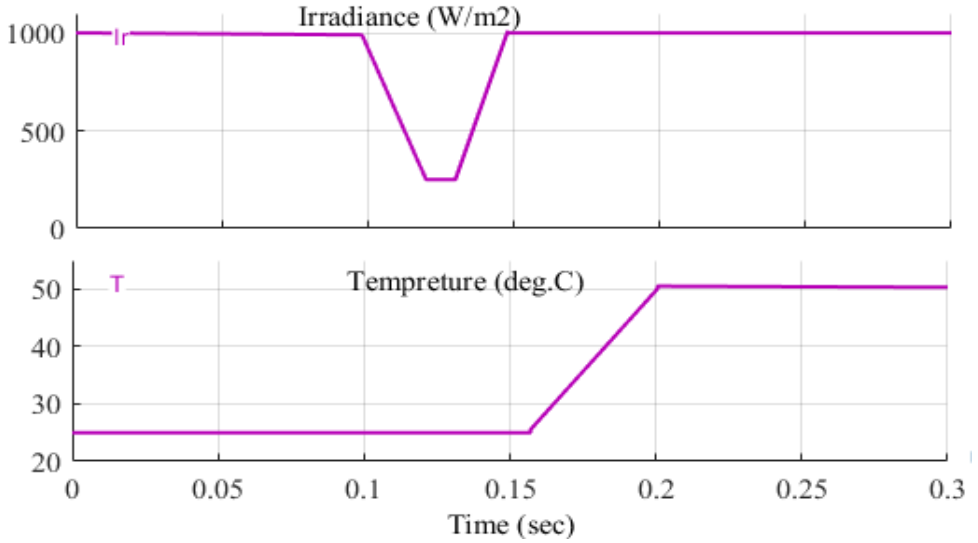

Fig. 4.14. PV-array input parameters (irradiance and temperature)

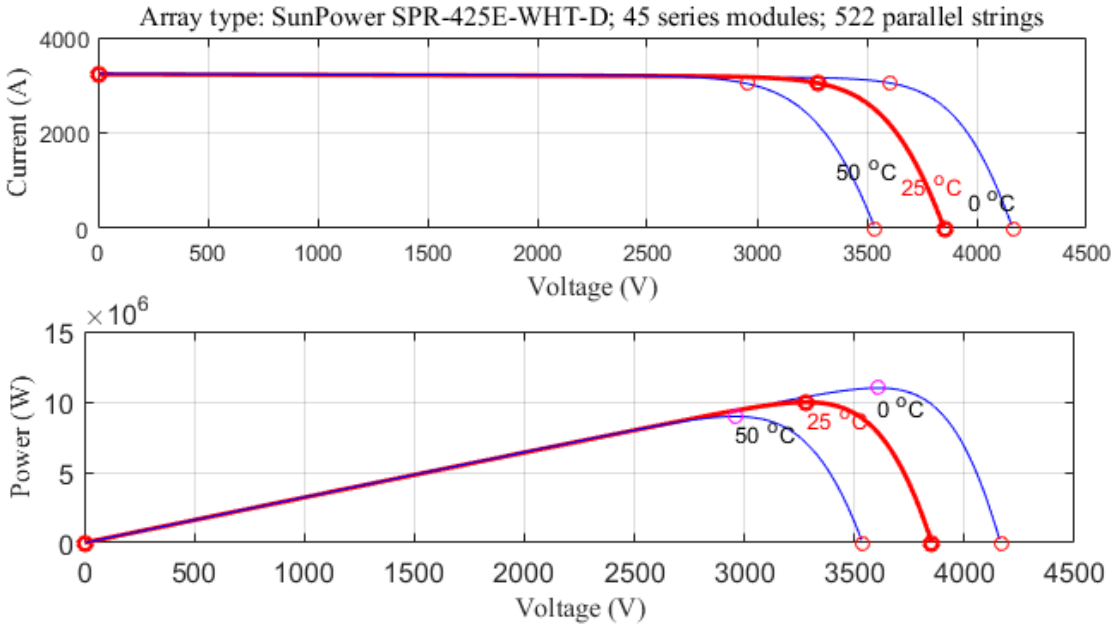

Fig. 4.15. I-V and P-V curves of the PV array for 1000 W/m^2 irradiance and temperature (0^0, 25^0 & 50^0) at MPPT

From Fig.4.13, we can derive the following equations:

$$I = I_{ph} - I_d \tag{4.31}$$

Where; I is the PV cell output current, Iph is photon produced by the cell and I_d is diode current.

By Shockley equation, the diode current I_d is given as:

$$I_d = I_0\left(e^{(v_d/V_T)} - 1\right) \tag{4.32}$$

Where; $V_T = kT/q \times nl \times Ncel$ is the PV voltage due to temperature T and V_d is diode voltage.

$$I = I_{ph} - I_0(e^{q\left(\frac{v+I.R_S}{\alpha kT}\right)} - \left(\frac{v + I.R_S}{R_{SH}}\right) \quad (4.33)$$

Where; I_0 is diode saturation current (A), nl is diode ideality factor, α number close to 1.0, k = Boltzman constant = 1.3806e-23 J.K-1, q is electron charge = 1.6022e-19 C, T is cell temperature (K), Ncell is number of cells connected in series in a module, R_S is series resistance and R_{SH} is shunt resistance.

The NREL system advisory model database has 10,000 modules, which are listed from main manufacturers, sorted in alphabetical order. In this research, Sun power SPR-425-WHT-D module has been selected from the NREL system to meet the required maximum power output of 425.007W for 10MW capacity of PV-STATCOM. This module is selected under standard test conditions (STC) (irradiance=1000 W/m^2, temperature = 0^{o}c, 25^{o}c & 50^{o}c).

The maximum power output, Pm of the module at MPPT, is determined as:

$$Pm = Vmp \times Imp \quad (4.34)$$

Where; Vmp and Imp are voltage and current values at MPPT respectively.

The total power output of the PV array with 522 parallel strings and 45 series-connected modules per string have been determined as:

$$P = N_P \times N_S \times Pm \quad (4.35)$$

$$P = 522 \times 45 \times 425 = 9983250\ W = 9.983MW$$

This power capacity of the PV-STATCOM has been selected depending on the total capacitive reactive power compensator requirement of Adama-I wind farm.

4.3.2. INC based MPPT for DC-DC Boost Solar Inverter Control

Due to high cost of PV cell, it is necessary to operate the PV array/cell at its MPPT [24]. Several MPPT algorithms have been proposed from time-to-time which includes the hill climbing method, incremental conductance (INC) method, constant voltage method, modified hill climbing method, β method, system oscillation method and the ripple correlation method, perturb and observe method, open and short circuit method, fuzzy logic and artificial neural network [24]. Since INC gives very fast response, this method has been selected in this work to track maximum power.

The INC method is working based on the principle that the derivative of the PV array power curve is zero at MPPT, i.e. the slope of the power curve is zero (dp/dV=0) [24]. The slope of power curve is positive on the left of the MPP and negative on the right [1], [24] as shown in Fig.4.15 of the P-V-curve.

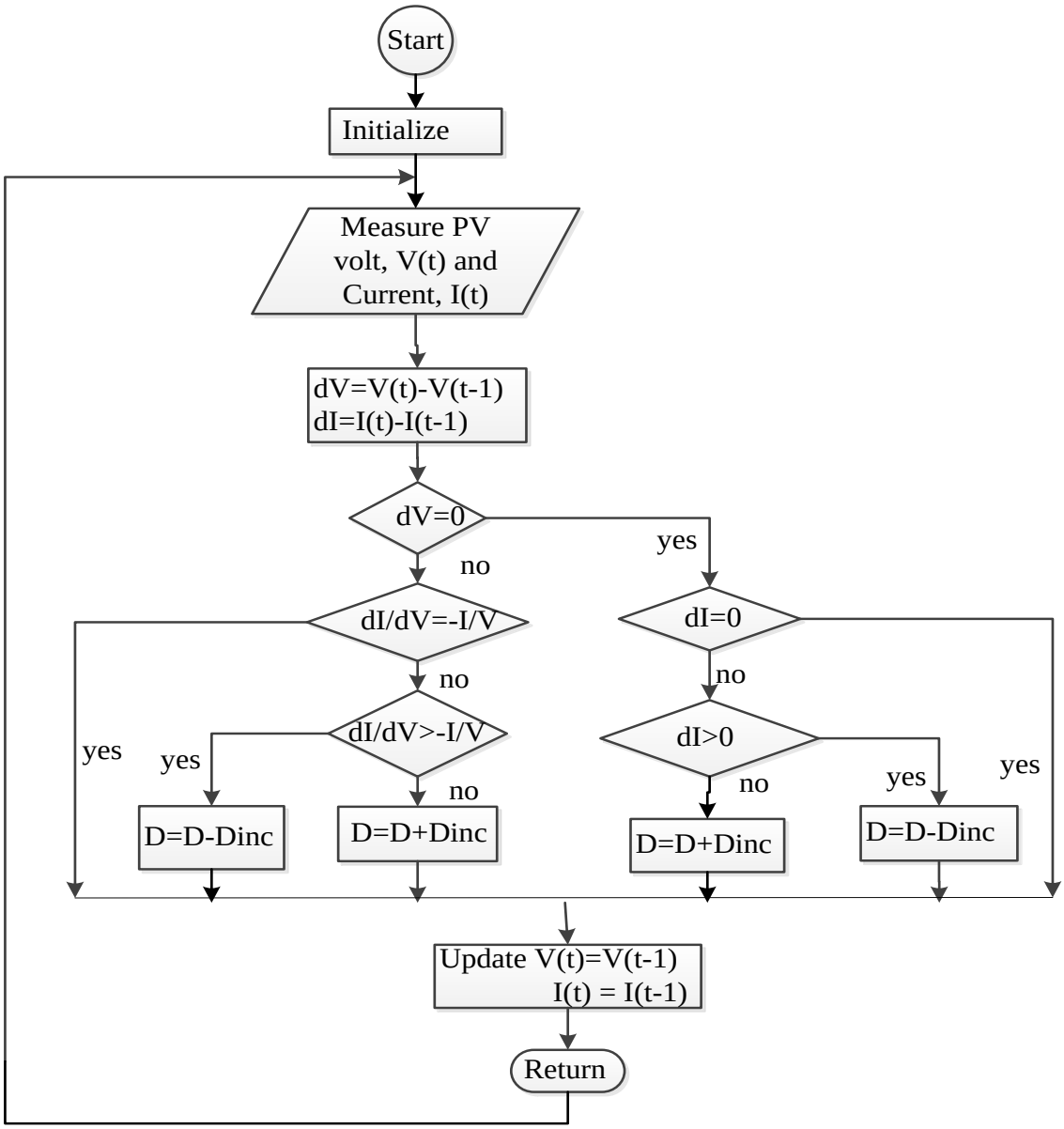

Fig. 4.16. Incremental conductance algorithm flow chart *A*

In this method, the PV model operates at MPPT when the voltage reference V_{dcref} is reached. As shown in Fig.4.16, the algorithm for the INC starts by measuring the voltage and current of the PV array. Then, it calculates the difference from the previous measurement and determines the

power. The difference of voltage and current should perform at each step. When there is a variation of the irradiation or the temperature, the current changes (dI) and then the MPPT. The algorithm decrements (D=D-Dinc) or increments (D=D+Dinc) the duty cycle which controls the DC-DC converter voltage and tracks the new MPP again.

Modeling of the dc-dc voltage boost solar converter: Appropriate capacitor and inductor selection is required to boost the PV array power output.

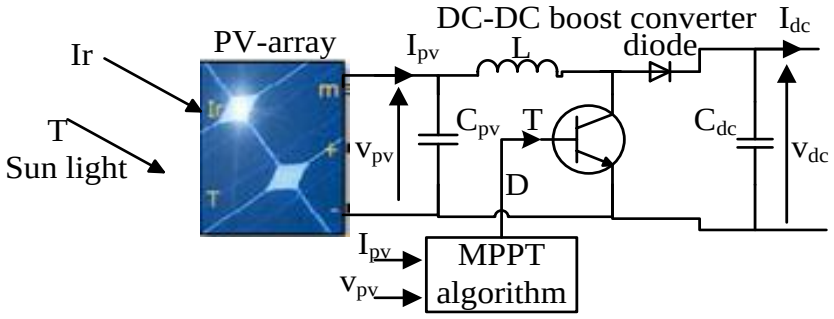

Fig. 4.17. MPPT with DC-DC voltage boost converter

Selection of the inductor: In PV system, the boost converter functions in the discontinuous and continuous modes of conduction. The inductor value is calculated as:

$$L \geq \frac{v_{dc} \times D(1-D)}{f_s \left| \Delta I_{L,ripple} \right|} \tag{4.36}$$

Where; D is duty cycle of the switch, f_s is switching frequency, v_{dc} is maximum of the dc component of the output voltage, $\Delta I_{L,\,ripple}$ is ripple current of the inductor.

Power decoupling capacitor selection: The power decoupling capacitor C_{pv} is the capacitor linked in parallel near the PV array:

$$C_{PV} \geq \frac{I_m \times D^2}{0.02(1-D) f_s v_{pv\_mpp}} \tag{4.37}$$

Where; I_m is output current at maximum output power, V_{pv_mpp} is PV output voltage at MPP.

The DC boost capacitor converter is installed in parallel with the load and stores generated energy from the PV system:

$$C_{DC} \geq \frac{v_{load} \times D}{f_s \times \Delta v_{load} \times R_{load}} \tag{4.38}$$

Where; v_{load} is output voltage of the boost converter and ΔV_{load} is output ripple voltage.

The DC boost capacitor converter helps to reduce the voltage ripple and provides energy storage for a short period and for a rapid change of the PV voltage [1], [24].

The value of the DC-DC converter parameters is given in table B2 of appendix B.

4.3.3. Conventional PV Inverter Controller

PV solar array is required to inject power to the grid at close to unity power factor according to several PV array inter-connection standards as shown in Fig 4.12.

With additional new control system, the conventional PV inverter control method is similar to the conventional STATCOM control system. Except in the case of conventional PV inverter the DC reference voltage, $V_{DC\text{-}ref}$ is the output voltage of the PV array at MPPT and the q-axis reference current, i_{q_ref} is considered to zero ($i_{q\_ref} = 0$) value (unity power factor principle).

For three phase voltage (v_a, v_b, v_c) and current (i_a, i_b, i_c) measured at grid side of the inverter, the d-q components voltage (v_d, v_q) and current (i_d, i_q) respectively are found through Park's transformation.

The real power, P and the reactive power, Q outputs in d-q co-ordinate system is given as [1]:

$$\begin{cases} P = \frac{3}{2}\left[v_d i_d + v_q i_q \right] \\ Q = \frac{3}{2}\left[v_q i_d - v_d i_q \right] \end{cases} \tag{4.39}$$

To achieve the vector control scheme, the d-axis of the synchronous frame is aligned with the grid voltage vector, therefore the d-axis grid voltage is equal to its magnitude ($v_d = v_g$), and the resultant q-axis voltage v_q is then equal to zero ($v_q = 0$).

Then expressions the active and reactive power of equation (4.39) can be reduced to :

$$\begin{cases} P = \frac{3}{2}\left[v_d i_d \right] \\ Q = \frac{3}{2}\left[-v_d i_q \right] \end{cases} \tag{4.40}$$

Filter model for solar inverter: This filter is used to remove the voltage and current harmonic outputs of the solar inverter. The parameter selection and operation analysis of these solar inverters were similar to the above wind farm inverters described in section 4.2.8 except their capacity. The value of the solar filter is described in table B2 of appendix B.

4.3.4. Modeling of Solar Inverter as Conventional VSC based STATCOM

PV array inverter setup is analogous to the design of conventional STATCOM. From Fig.4.18, it is clear to understand how PV inverter setup can utilize as STATCOM.

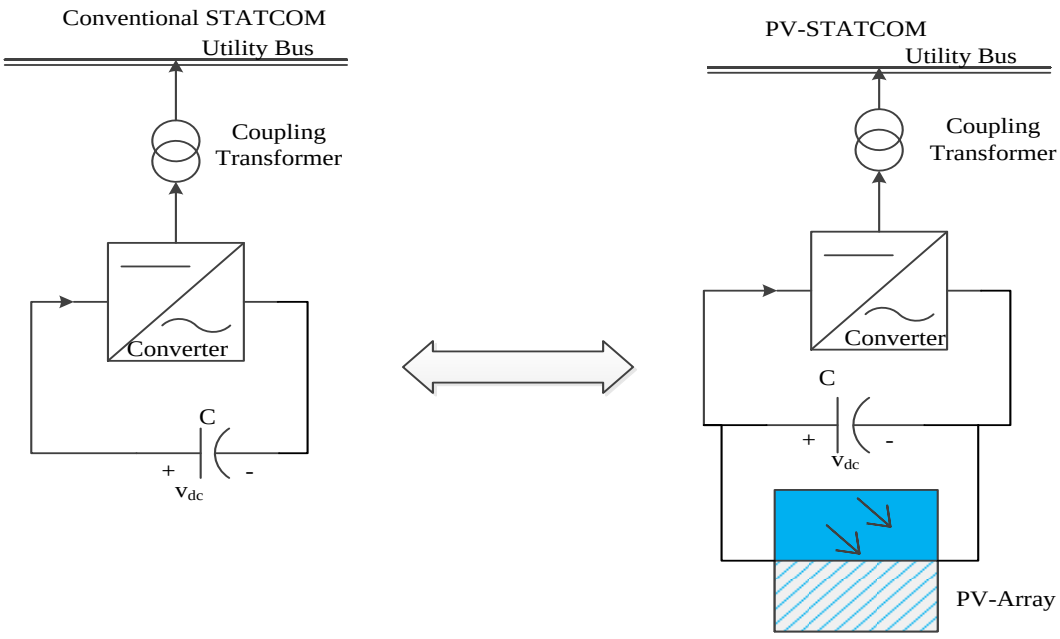

Fig. 4.18. Conventional STATCOM versus PV - STATCOM comparison diagram

The main advantage that helps in utilization of PV inverter as STATCOM is having a DC output voltage from a PV array which is used as capacitor link in a conventional STATCOM as shown in Fig.4.18. In addition, the solar inverter design is made to operate as converter in conventional STATCOM arrangement. Therefore, PV array along with inverter has been conveniently used as STATCOM for the assumed system.

4.3.4.1. Modes of operation of PV array based STATCOM

The operation of the proposed PV-STATCOM can divide into three modes:

i. Daytime excess power mode
ii. Daytime mode
iii. Nighttime mode

i. Daytime excess power mode: In this mode, the output voltage of the PV array drives the boost converter based STATCOM for compensating the source as well as charges the battery

(capacitor). Assume the inverter capacity, S is the rated peak power capacity of the PV array and with the active power P then the reactive power Q, capability is:

$$Q = \sqrt{S^2 - P^2} \tag{4.41}$$

According equation (4.41) after the PV- array generates the required active power the remained capacity is used for reactive power compensation.

ii. **Day time mode:** When continuous compensation is required, if the PV output voltage is equal to the requirement of the boost converter input, the PV array can directly connect to the boost converter so as to step-up the voltage and match the dc link voltage of the three-leg VSC. In this mode, the battery is not charged.

iii. **Nighttime mode (active power, P = 0):** In this mode, PV array output is idle and only the battery (capacitor) supplies the boost converter. In this condition, the whole capacity of the solar inverter can use for reactive power compensation. Thus, the reactive power supplied is equal to the rating power of the solar inverter (Q = S).

4.3.5. PV- STATCOM Controller Modeling for Reactive Power Compensation

Since the inverter based solar panels and the VSC based STATCOM devices are similar in structural operation and functionality as shown in Fig.4.18, these solar inverter have been used as STATCOM functionality with the addition of new control method termed as PV-STATCOM.

In this thesis work, PV-STATCOM has been used as an automatic voltage regulator at PCC (main substation) of the selected wind farm. As shown in Fig.4.19, only the V_{DC_ref} of the conventional STATCOM have been replaced with MPPT controlled V_{DC_ref} voltage output of the solar array but, the control system and its' other components are not changed. In the PCC voltage regulation mode of operation of the PV-STATCOM, the PCC voltage is regulated through reactive power exchange between the PV inverter and the grid (PCC). In this system, the q-axis reference current, I_{q_ref} controls the reactive power exchange between the PV-STATCOM and the grid (PCC). The measured signal, V_{PCC}, at the PCC is compared with reference value V_{PCC_ref} and is passed through PI-2, to generate I_{q_ref}. The rest of the controller settings remain similar to the conventional STATCOM controller of Fig 2.19. The amount of reactive power flow from the inverter to the grid depends on set point voltage at PCC.

The PI parameters of the PCC voltage controller tuned by systematic hit and trial method to achieve the fastest step response, least settling time, and a maximum overshoot of 10% & 15%. The procedures of the hit and trial method for selecting the parameters for all four PI controllers have been described in table D1 of appendix-D.

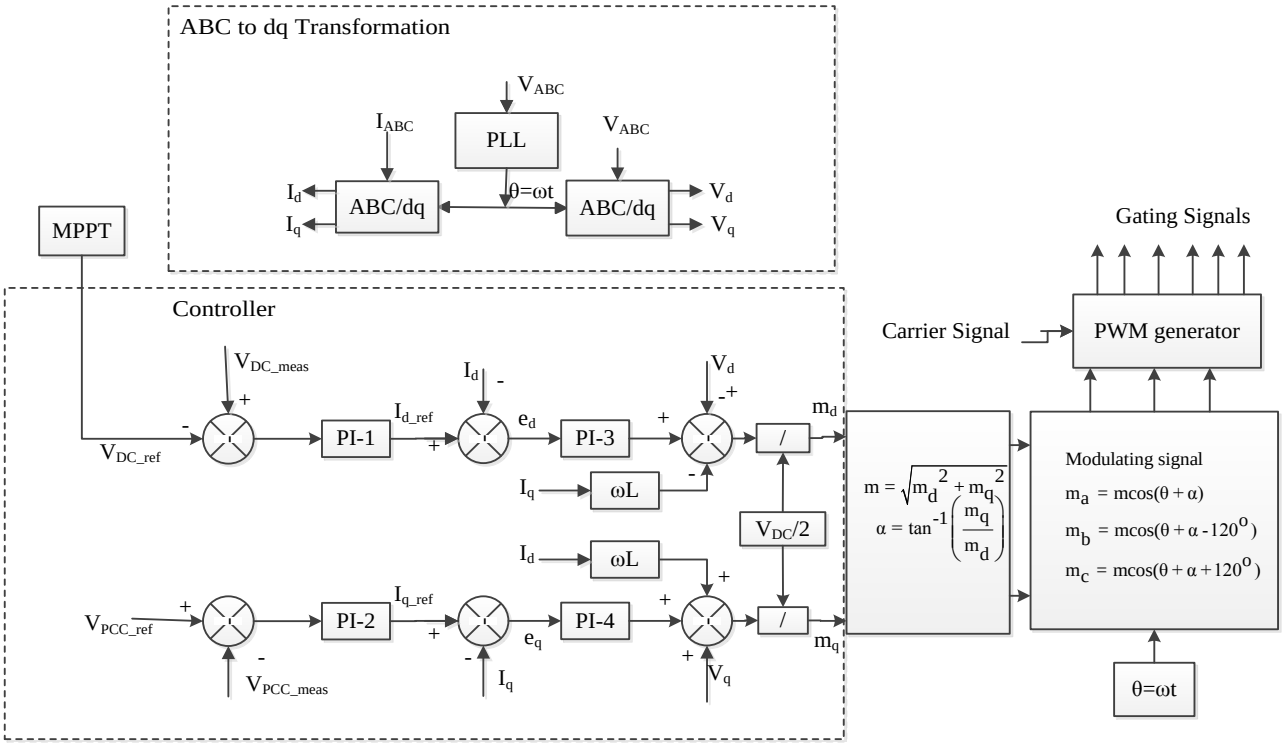

Fig.4.19. PCC voltage control schematic diagram of solar controller as PV-STATCOM

The direct axis and quadrature axis voltages act as disturbance signals in these control loops and a decoupling factor of ωL have been included to decouple the two control loops where, ω is the angular frequency in rad/sec and L is the inductance at the output of the inverter. The values of ω and L are given in appendix-E.

4.3.6. Sizing of the PV-STATCOM

The size of the PV-STATCOM has been determined depending on the total capacity of the capacitive reactive power compensator devices that is installed in the wind farm. This includes 4.765 MVar machine side capacitor bank and 5.147 MVar grid side capacitor bank.

The size of the PV-STATCOM = 4.765 MVar + 5.147 MVar = 9.912 MVar

This is the total requirement of reactive power of the selected wind farm and 10MW capacity solar inverter has been selected to operate as STATCOM for reactive power compensator.

CHAPTER FIVE

5. RESULTS AND DISCUSSIONS

5.1. Introduction

This chapter briefly describes about the steady state voltage variation and temporary over voltage of the system under study based on the simulation results. Power world simulator and MATLAB software has been merely used to carry out the analysis of a system's performance at steady state voltage variation and temporary over voltage conditions to enable in obtaining some important pieces of information respectively. Aiming on the achievement of the aforementioned points, the system under study has been modeled in MATLAB/PowerSim software as shown in Fig. 5.1.

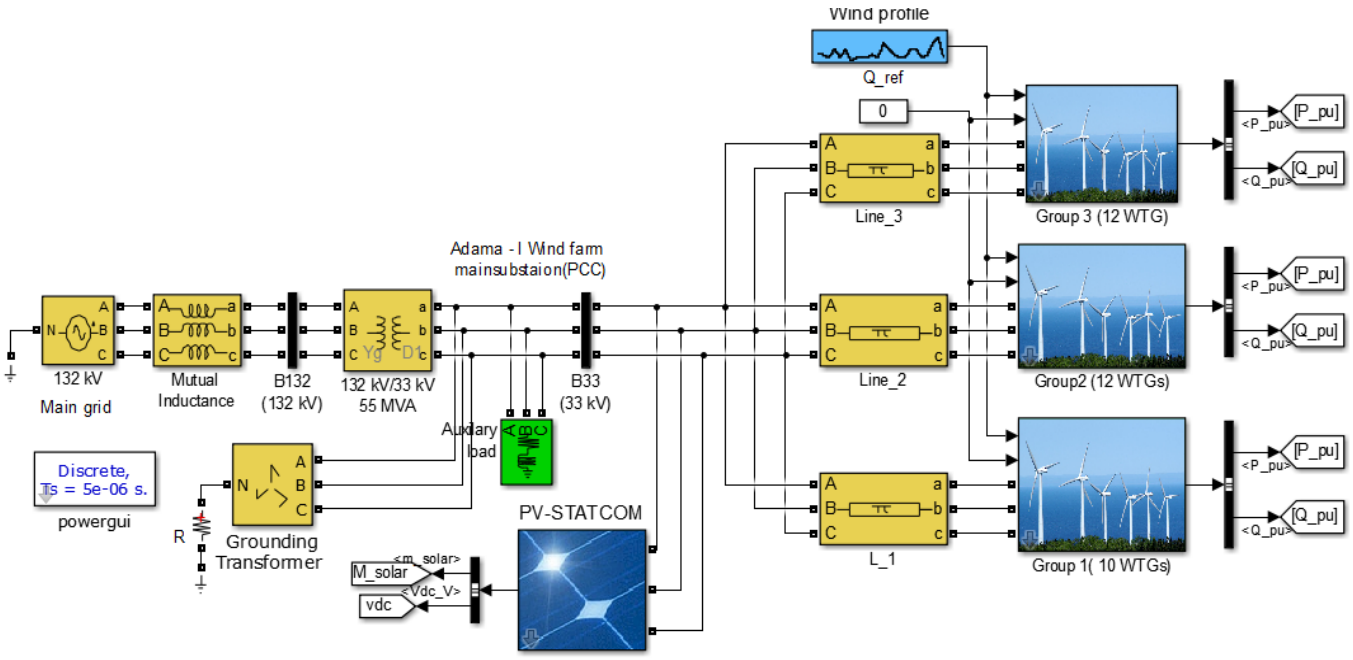

Fig. 5.1. The overall system model in Matlab/PowerSim

5.2. Simulation Results

As shown in Fig.5.1, the system under study includes PMSG based WTGs' and the PV-STATCOM. In the subsequent sections, the simulation results of PMSG based WTGs' and the PV-STATCOM is analyzed and discussed.

5.2.1. PMSG Based WTG

For the whole of the selected wind farm WTGs' (34 in number) and its control systems, simulation based on the modeling as depicted in previous sections have been carried out using

the dedicated MATLAB/PowerSim software as shown Fig.5.1 with disconnection of PV-STATCOM and the results are shown and discussed here by.

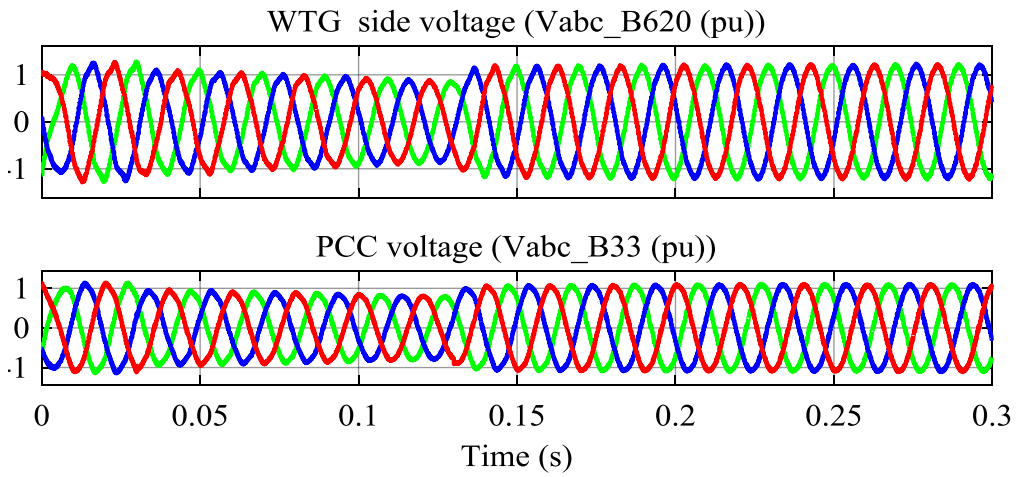

Fig. 5.2. WTG side bus (B620V) and PCC bus (B33kV) output voltage waveforms

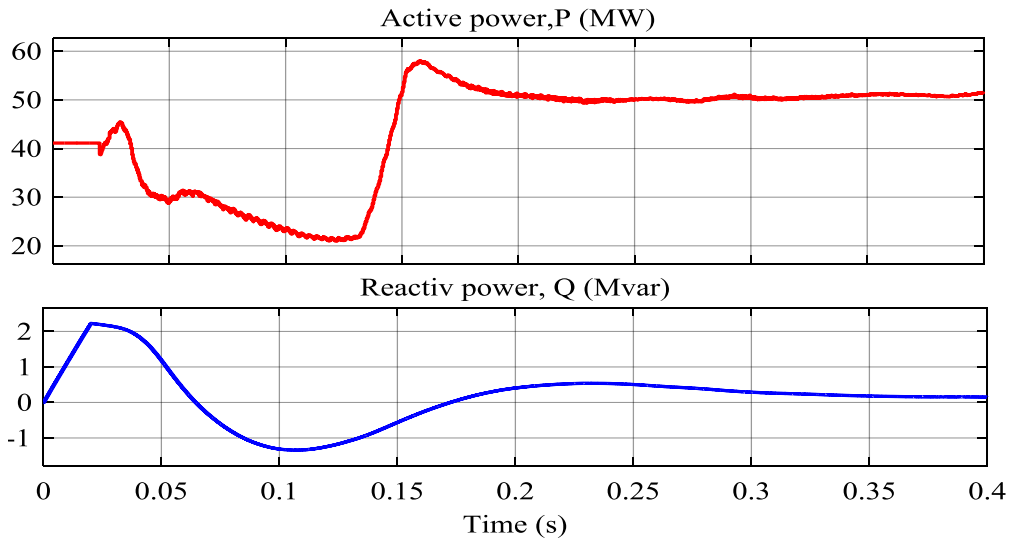

Fig.5.3. Active power (MW) and reactive power (MVar) outputs of the WTGs'

Discussions

The WTGs' side (B620) and PCC (B33) voltage (p.u) waveforms under normal operating conditions are determined as shown in Fig.5.2. These voltages have been considered as a base case study for the temporary over voltage study analysis.

From Fig.5.3, the simulation have been done to generate an active power output of 51MW, which is Adama-I wind farm WTGs' total capacity and the reactive power to be nearly zero with a power factor consideration between 0.95 and 0.99. The simulation results displayed in Fig. 5.3

shows the conformity of power factor with that of the rated value used WF. From Fig.5.3 the PMSG based WTG reactive power, Q(MVar) have positive and negative values, which indicates the generator is consuming and generating reactive power.

5.2.2. The PV-STATCOM

The PV-STATCOM has been done by disconnecting the PMSG wind turbine and its' 33kV connector transmission line from the system of Fig.5.1.

Discussions

Using the same operation principles as that of the conventional STATCOM controller implemented at grid side of the solar inverter, the simulation have been carried out and hence the results of the PV-STATCOM is illustrated in the upcoming figures.

As we see from Fig.5.5, the active power output magnitude of the solar inverter is smaller as compared to the reactive power output of the solar inverter. This indicates that the solar inverter is acting as conventional STATCOM as described insection 2.7.2. Fig.5.4 shows three phase voltage of the solar system.

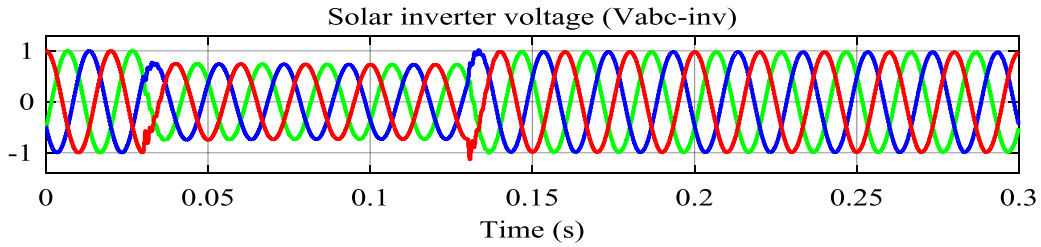

Fig. 5.4. Grid connected PV-STATCOM three phase output voltage (p.u) during daytime

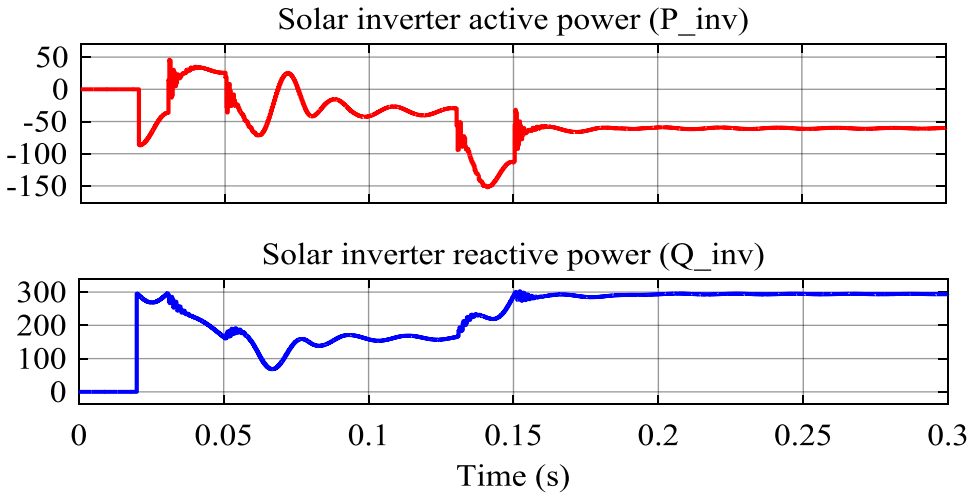

Fig. 5.5. Active (kW) and reactive power (kVar) outputs of PV-STATCOM without sunlight

Throughout the whole simulation results analysis of PV-STATCOM, during nighttime the solar array and its DC-DC, boost voltage converter has been disconnected from DC link capacitor of the solar inverter. However, in the case of daytime in the absence of sun radiation, only the solar array inputs (irradiance and temperature) is set to zero value.

5.3. System Model for Steady State Analysis

The steady state network status namely bus voltage magnitude, active and reactive power flows, and transmission line ampacity (capacity) are evaluated using load flow studies in power world software with the use of 4-bus system as shown in Fig.5.6. The steady state power flow results using power world software is given in appendix C.

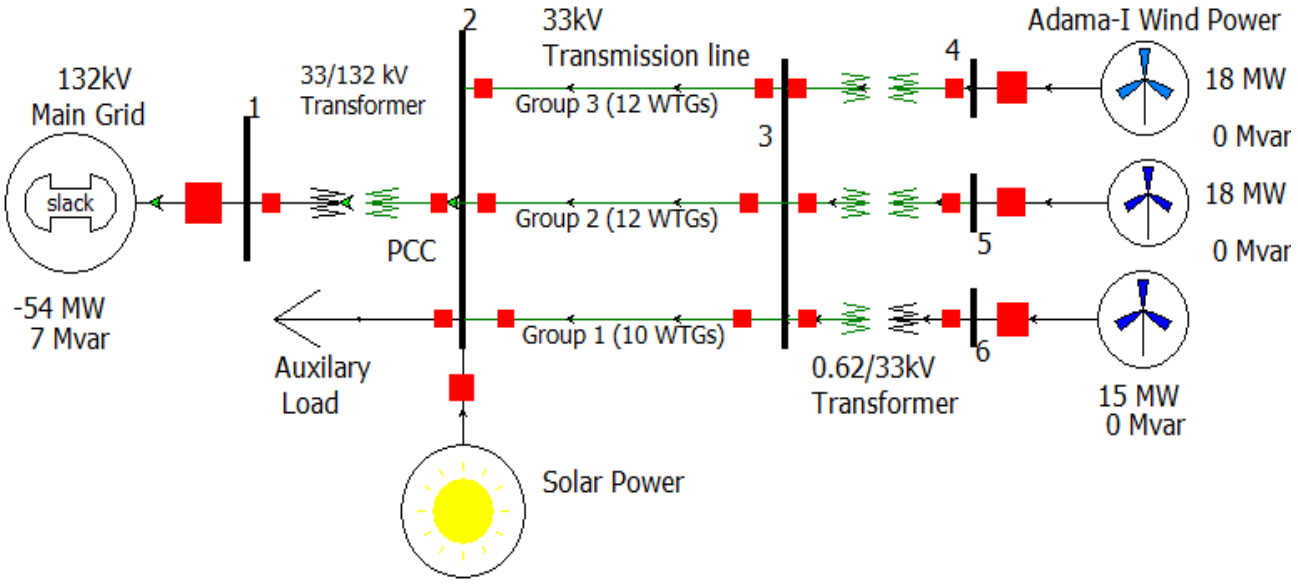

Fig. 5.6. System model for steady state voltage analysis using power world software

5.3.1. Base Case Study

The model in Fig.5.6 is analyzed as a case study for two cases. The first case relates with the daytime in which the solar inverter generates 10MW active power. Once the active power generation is over, the remaining capacity of the solar inverter is used for reactive power generation.

Second, in the nighttime case in which the solar inverter full capacity is used for reactive power compensation (Q=10MVar & P=0). With the sending end main grid voltage set to 1.0 p.u, the steady state voltage results have been obtained without voltage regulation (reactive power compensation) for both the peak-load and off-peak load conditions. Peak loads (P_{LD} = 6.48 MW

and reactive power, Q_{LD} = 21MVar have been used for daytime. Off-peak loads of active power, P_{LD} = 3.38 MW and reactive power, Q_{LD} =12.07 MVar have been used for nighttime hours.

Load selection have been done to show the effect of more inductive load (e.g. Induction motors) demand at PCC of WTGs'. In addition, this inductive load is considered again to limit the steady state voltage rise at the PCC. Bus voltage magnitudes for daytime and nighttime loading conditions are given in Table 5.1.

Table 5.1. Steady state voltage analysis at various nodes of the system for daytime and nighttime

Daytime(peak load) P_{LD} = 6.48 MW, Q_{LD} = 21 Mvar		Night time (off peak load) P_{LD} = 3.38 MW, Q_{LD} = 12.07.Mvar	
Bus. No	Voltage (p.u)	Bus. No	Voltage (p.u)
1	1.0000	1	1.0000
2	0.9407	2	0.9655
3	0.9408	3	0.9663
4	0.9423	4	0.9679

Discussion

In table 5.1, the wind farm main substation voltage (V_{PCC}) of bus-2 is observed 0.9407 p.u at daytime and 0.9655 at nighttime. This shows that inductive load connection at the PCC can reduce the steady state voltage-rise (power loss) caused by power flow variation. The voltages at all the buses in the network are within the permissible limits of ± 6 % of rated values, which fulfills the Hydro chain's network requirements.

From table 5.1, we can observe that the variation of inductive load (Q_{LD}) and active power load (P_{LD}) during off-peak load and peak load causes steady state voltage variation at the PCC of the wind power and other buses of the network even if it is in the required limit.

5.3.2. Impact of Wind Farm Integration on Steady State Voltage Variation

The base case study system is now modified with addition of 10 MW solar powers to the existing wind power as shown in Fig.5.6. Integration of WF through transmission line reduces the amount of power flow from the supply end to the receiving end or cause reverse power flow depending on the amount of loading in the network.

Steady state voltage at four buses in the network: Vbus1, Vbus2, Vbus3 and Vbus4 are evaluated with varying wind power (P_W). The current flow through the line is measured in terms of line current from the source terminal (I_{line}). Both voltage limits as per the Hydro china's

specifications and line flow limits based on the conductor ampacity of transmission line were considered for evaluating the impact of wind farm integration to grid during steady state operation. To observe the effect of wind farm integration on grid, no reactive power compensation is considered except the purely active power injection for both the wind turbine and solar array.

Daytime Analysis

A peak load of 6.48 MW active powers and 21 Mvar of reactive power is been considered for three conditions of solar array output: Case 1 with 0% (0.0 MW), Case 2 with 50% (5MW) and Case 3 with 100% (10 MW).

Table 5.2. Case 1: 0% Solar array output, P_{SA} = 0.0 MW, Q_{SA} = 0.0 Mvar

P_{WF}	10	15	20	25	30	35	40	45	50	52
V_{bus1}	1.0000	1.0000	1.0000	1.0000	1.0000	1.0000	1.0000	1.0000	1.0000	1.0000
V_{bus2}	0.9570	0.9565	0.9552	0.9541	0.9521	0.9499	0.9474	0.9444	0.9409	**0.9395**
V_{bus3}	0.9586	0.9581	0.9571	0.9556	0.9535	0.9512	0.9485	0.9453	0.9417	0.9401
V_{bus4}	0.9607	0.9603	0.9592	0.9578	0.9554	0.9530	0.9502	0.9469	0.9431	0.9416
I_{Line} (AMP)	198.22	283.99	371.72	461.23	551.95	643.87	736.85	830.97	926.36	964.15

Table 5.3. Case 2: 50% Solar array output, P_{SA} = 5MW, Q_{SA} = 0.0 Mvar

P_{WF}	10	15	20	25	30	35	40	45	48	49	50
V_{bus1}	1.000	1.000	1.000	1.000	1.000	1.000	1.00	1.00	1.00	1.00	1.00
V_{bus2}	0.9567	0.9561	0.9549	0.9533	0.9511	0.9487	0.9459	0.9427	0.9406	**0.9398**	**0.9390**
V_{bus3}	0.9583	0.9577	0.9565	0.9548	0.9524	0.9499	0.9470	0.9436	0.9414	0.9406	**0.9398**
V_{bus4}	0.9603	0.9598	0.9586	0.9548	0.9543	0.9518	0.9488	0.9452	0.9429	0.9421	0.9412
I_{Line} (AMP)	199.12	284.08	371.93	438.05	552.51	644.67	737.94	832.42	889.70	908.94	928.22

Table 5.4. Case 3: 100% Solar array output, P_{SA} =10 MW, Q_{SA} = 0.0 Mvar

P_{WF}	10	15	20	25	30	35	40	47	50
V_{bus1}	1.0000	1.0000	1.0000	1.0000	1.0000	1.0000	1.0000	1.00	1.00
V_{bus2}	0.9564	0.9555	0.9541	0.9523	0.9499	0.9473	0.9443	**0.9394**	**0.9369**
V_{bus3}	0.9579	0.9571	0.9557	0.9538	0.9512	0.9485	0.9454	0.9403	**0.9376**
V_{bus4}	0.9600	0.9592	0.9578	0.9559	0.9531	0.9504	0.9471	0.9419	0.9391
I_{Line} (AMP)	198.54	284.24	372.22	462.05	553.18	645.61	739.20	872.33	930.32

The steady state bus voltages at all buses of the system for the three cases of the solar array output conditions is given in tables 5.2 - to -5.4. For Case1 wind farm output power can go up to 51 MW without violating any voltage limits. The maximum wind power that can incorporate into the grid without violating limits in the grid is 48 MW for Case2. For Case3 only 40 MW of wind power can integrate into the grid, without violating the voltage limit.

Discussions

The results in table 5.2-to-5.4 shows that the effect of the wind farms on steady state voltage variation due to more reactive current consuming loads (inductive) loads. As described in section 2.6.1 in this study, ($P_{WF} >> P_{LD}$) and ($Q_{WF} << Q_{LD}$) have been considered at the main substation (PCC) of the WTGs'. In the earlier condition, the steady state voltage rises due to reverse power flow occurred and in the latter case, more inductive load has been considered to reduce the steady state voltage rise. The decrease in voltage is due to the addition of more reactive load and this decreases reactive power loss in the line with higher wind power.

Nighttime Analysis

An off-peak load of 3.38 MW active powers and 12.07 Mvar reactive powers has been considered for nighttime analysis. The voltage magnitude at various buses in the system for nighttime loading condition is presented in table 5.5. It is observed that a wind power more than 50 MW should be integrated into the network during nighttime without violating the voltage limit for all buses using full capacity of the PV-STATCOM as reactive power compensation.

Table 5.5. Case 3: 0% solar array output, P_{SA} =0 MW, Q_{SA} = 10 Mvar

P_{WF}	10	15	20	25	30	35	40	45	50
V_{bus1}	1.0000	1.0000	1.0000	1.0000	1.0000	1.0000	1.0000	1.0000	1.0000
V_{bus2}	1.0079	1.0075	1.0065	1.0053	1.0037	1.0019	0.9997	0.9971	0.9939
V_{bus3}	1.0096	1.0092	1.0082	1.0069	1.0053	1.0033	1.0009	0.9983	0.9949
V_{bus4}	1.0117	1.0114	1.0104	1.0091	1.0074	1.0053	1.0029	1.0001	0.9966
$I_{Line(AMP)}$	192.96	272.31	354.85	439.27	524.92	611.56	699.12	787.60	877.27

Discussions

As shown in table 5.5, the variation in voltage for nighttime with the increasing of wind farm integration is explained. This demonstrates that during nighttime, wind farms generate more

power and the PV solar array is idle. Therefore, using proper PV-STATCOM we can increase wind farm connectivity with appropriate reactive power compensation with all bus voltage limit ± 6% of nominal value.

From tables 5.4 - to -5.5 it is observed that in the daytime, it is possible to increase wind farm connectivity by adding solar power in the absence of wind power source or in low wind speed by keeping the node voltages limits. In the nighttime, we can generate more power from the wind farm; since no power is generated from the solar array in the nighttime, full capacity of the solar inverter is used for WF PCC voltage regulation.

5.3.3. Steady State Voltage Control Using PV-STATCOM

In section 5.3.2, the wind farm integration is limited by steady-state voltage drop due to more addition of reactive load (Q_{LD}) than the active load (P_{LD}). This selection considered to reduce the steady voltage rise during high wind speed and save wind power. Such a variation in voltage can also be reduced by reactive power compensation PV-STATCOM, in the network.

Daytime Analysis

For Case1 (P_{SA} = 0.0 MW) during daytime loading, the voltages for all the buses are within limits up to 50 MW wind farm injection without reactive power compensation. With the appropriate reactive power compensation, the wind power injection can be increased up to 52.0 MW while maintaining the conductor ampacity of 961.80 ampere as shown in table 5.6.

For Case2 (P_{SA} = 5MW) up to 48 MW of wind power can be injected into the network with all the voltages staying within limits without compensation. With appropriate reactive power compensation, the wind farm injection can be increase up to 50 MW while maintaining the conductor ampacity and voltages at all buses within limits as shown in table 5.7.

Table 5.6. Steady state voltages with reactive power compensation during daytime

Case 1: 0% solar array output, P_{SA} = 0.0 MW

P_{WF}	10	15	20	25	30	35	40	45	50	52
V_{bus1}	1.0000	1.0000	1.0000	1.0000	1.0000	1.0000	1.0000	1.0000	1.0000	1.0000
V_{bus2}	0.9570	0.9565	0.9552	0.9541	0.9521	0.9499	0.9474	0.9444	0.9409	0.9424
V_{bus3}	0.9586	0.9581	0.9571	0.9556	0.9535	0.9512	0.9485	0.9453	0.9417	0.9431
V_{bus4}	0.9607	0.9603	0.9592	0.9578	0.9554	0.9530	0.9502	0.9469	0.9431	0.9445
I_{Line} (AMP)	198.22	283.99	371.72	461.23	551.95	643.87	736.85	830.97	926.36	961.80
Q_{SA}(MVar)									0.00	1.0

Table 5.7. Steady state voltages with reactive power compensation during daytime

Case 2: 50% solar array output, P_{SA}= 5 MW

P_{WF}	10	15	20	25	30	35	40	45	48	49	50
V_{bus1}	1.000	1.000	1.000	1.000	1.000	1.000	1.00	1.000	1.000	1.00	1.00
V_{bus2}	0.9567	0.9561	0.9549	0.9533	0.9511	0.9487	0.9459	0.9427	0.9406	0.9414	0.9421
V_{bus3}	0.9583	0.9577	0.9565	0.9548	0.9524	0.9499	0.9470	0.9436	0.9414	0.9422	0.9429
V_{bus4}	0.9603	0.9598	0.9586	0.9548	0.9543	0.9518	0.9488	0.9452	0.9429	0.9438	0.9444
I_{Line} (AMP)	199.12	284.08	371.93	438.05	552.51	644.67	737.94	832.42	889.70	907.42	925.19
Q_{SA}(MVar)										0.5	1

Similarly for Case 3 (P_{SA} = 10 MW) during daytime loading, only up to 40 MW output power of the wind farm output can be injected into the network with all the voltages remaining within limits without reactive power compensation. With appropriate reactive power compensation, the wind power injection can be increased up to 50 MW while maintaining the conductor ampacity and voltages at all buses within limits as shown in table 5.8. Thus, maximum reactive power, Q_{SA} = 1.25 MVar is needed for regulating the steady state voltage within acceptable limits.

Table 5.8. Steady state voltages with reactive power compensation during daytime
Case 3: 100% solar array output, PSA= 10 MW

P_{WF}	10	15	20	25	30	35	40	47	50
V_{bus1}	1.0000	1.0000	1.0000	1.0000	1.0000	1.0000	1.0000	1.0000	1.00
V_{bus2}	0.9564	0.9555	0.9541	0.9523	0.9499	0.9473	0.9443	0.9408	0.9407
V_{bus3}	0.9579	0.9571	0.9557	0.9538	0.9512	0.9485	0.9454	0.9417	0.9415
V_{bus4}	0.9600	0.9592	0.9578	0.9559	0.9531	0.9504	0.9471	0.9432	0.9429
I_{Line} (AMP)	198.54	284.24	372.22	462.05	553.18	645.61	739.20	870.98	926.54
Q_{SA}(MVar)							0.00	0.5	1.25

Nighttime Analysis

For nighttime loading, wind farm integration without reactive power compensation is within its expected node voltage limit as shown in table 5.5. In which all the bus voltages are between 0.94 to 1.06 p.u limit. However, with reactive power compensation at the PCC terminal using PV-STATCOM can increase wind farm connectivity above 50 MW while maintaining the steady-state voltages within required limits and conductor ampacity. From tables 5.2 –to-5.8 the

transmission line ampacity is improved. As the node/bus voltage of the PCC drops the below the required limit the current flow through the line is increased, shows that line temperature and resistivity of the conductor is increased and as the bus voltage is within its required limit the temperature and resistivity of the line decreases.

5.4. System Model for Temporary over Voltage Analysis

As discussed in section 2.6.2, most of the temporary over voltage in wind farms are caused by short duration faults on the grid side network or on the WTGs' side.

In this work, a single line to ground fault (SLGF) have been considered at the end of the 33kV transmission line for 0.1 second time duration as shown in Fig.5.7.

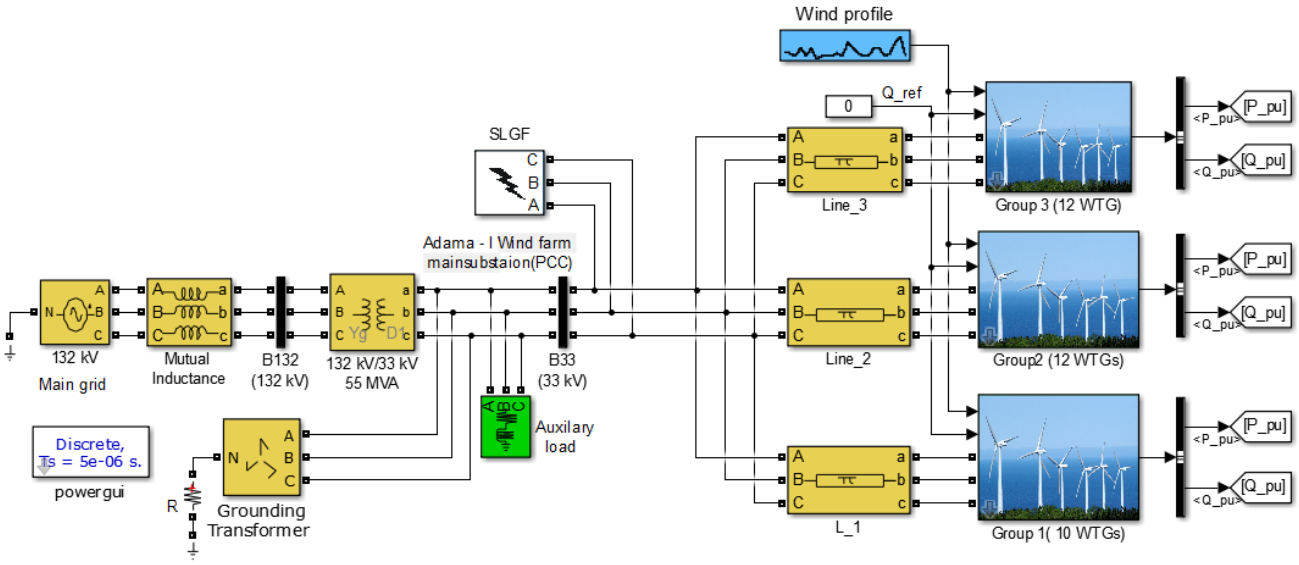

Fig.5.7. Single line to ground fault application at 33kV line of WTGs'

5.4.1. Base Case Study

The phase voltage observed for SLGF occurrence of the PCC of the wind farm and at the WTGs is shown in Fig. 5.8. Both these values are considered the voltage rise magnitude due to SLGF within the permissible limit of 130% of the nominal voltage for Hydro china's network.

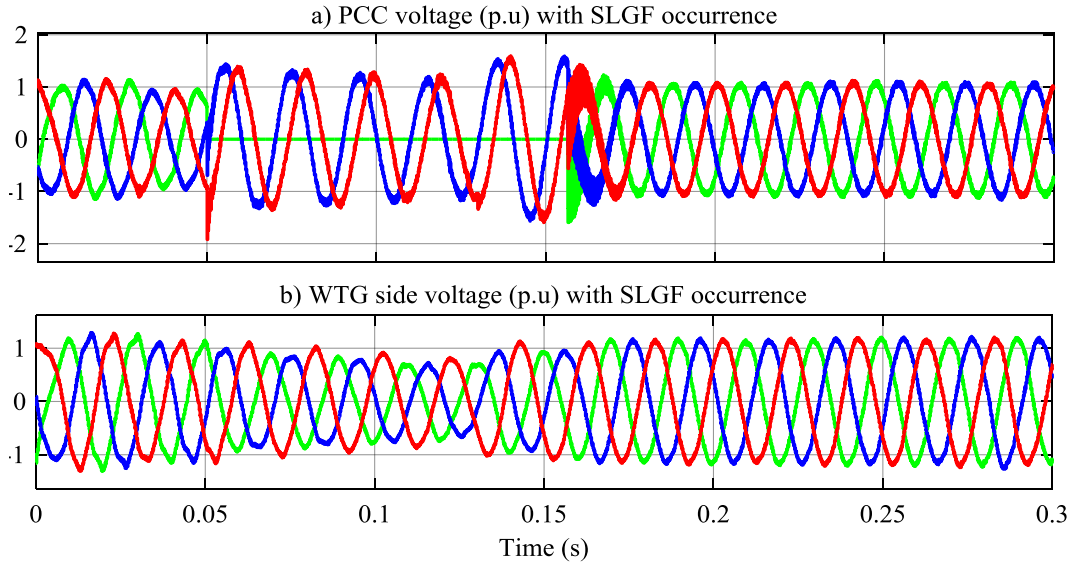

Fig. 5.8. WTG side bus (B620V) and PCC bus (B33kV) output voltage waveforms under SLGF

From Fig.5.8 (a) when SLGF is occurred at the end of the transmission line near to the PCC of the WTGs' PCC single line phase voltage is to zero value for 0.1 second and this leads to overloading to the normally running phases. In addition, as shown in Fig. 5.8(b), this fault disturbs the WTGs' side voltage. If the WTGs' are unable to withstand to this voltage disturbance, they can be disconnect from main grid. However, this is uneconomical.

5.4.2. Temporary over Voltage Control using PV-STATCOM

As in base case scenario presented in section 5.4.1, a SLGF for 0.1-second time duration is applied at the receiving end (PCC) of the transmission line without PV-STATCM. Here, PV-STATCOM is considered at the wind farm main substation (PCC) to examine the effect of PV-STATCOM on the temporary over voltages in the study system for daytime and nighttime.

In daytime analysis the remaining capacity of the VSC based solar inverter have been used for reactive power compensation after required active power generated. Three phase voltages at PCC of WF with SLGF for 0% solar array power (P_{SA}=0) is shown in Fig.5.9 (a). For sunny time hours the three phase voltages at PCC of WF is shown in Fig.5.9 (b).

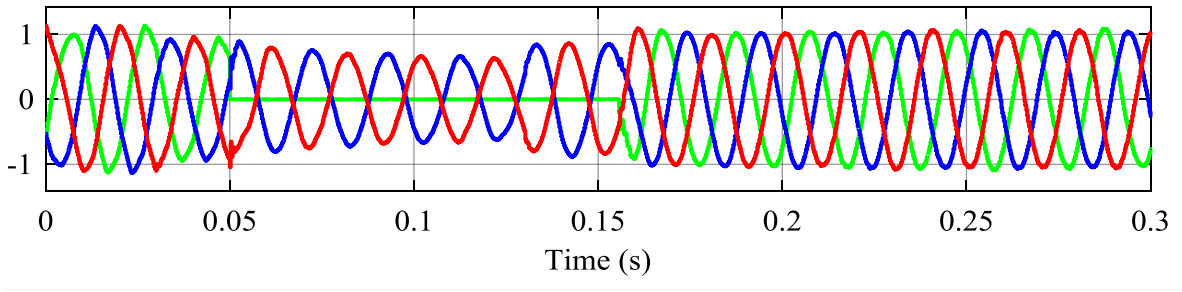

a) PCC Phase voltages with PV-STATCOM (without sun radiation) and with SLGF occurrences

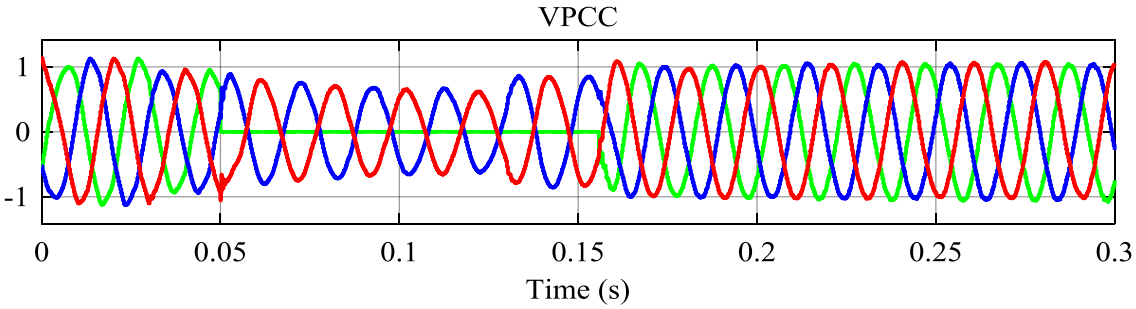

b) Three phase PCC voltage with PV-STATCOM (with sunny time) and SLGF occurrence

Fig.5.9. PCC voltage waveforms with the application of PV-STATCOM and SLGF

Discussions

As shown from the above Fig 5.9 (a and b) the magnitude of the PCC loaded phase voltage have been improved and limited within 1p.u value in magnitude with the installation of PV-STATCOM at the PCC of the WTGs'. However, without the use of this device in the case of fault occurrence, the phase voltage magnitude violates the required limit 1p.u as shown in Fig.5.8 (a).

Generally, the effect of the PV-STATCOM installation at the PCC of the WTGs' to compensate the reactive power is summarized in table 5.9.

Table 5.9. Power profile of the study system with and without PV-STATCOM & SLGF

Conditions	Time	Proposed power output of solar array, P_{SA}(MW)	Obtained actual power output of solar array, P_{SA}(MW)	Solar inverter side power profile		WTG side power Profile	
				P_inv (MW)	Q_inv (MVar)	P_WTG (MW)	Q_WTG (MVar)
Without fault and	Daytime	0 %(P_{SA}=0)	-0.000	-0.1268	0.8365	50.82	0.31
		5 %(P_{SA}=5)	0.42	-0.1496	0.7964	52.20	0.25

with PV-STATCOM		100 %(P_{SA}=10)	8.29	5.8448	-5.8164	52.71	0.20
	Nighttime	P_{SA}=0	0.000	-0.1476	0.9172	51.60	0.17
With fault and with PV-STATCOM	Daytime	0 %(P_{SA}=0)	-0.000	-0.1464	0.7855	66.44	0.41
		5 %(P_{SA}=5)	1.28	0.0608	0.8335	64.56	0.47
		100 %(P_{SA}=10)	8.79	6.6925	-5.5095	64.9	0.38
	Nighttime	0	0.000	-0.1457	0.8311	66.59	0.40
With Fault and without PV-STATCOM	Daytime loadings	0.00	0.00	0.00	0.00	58.94	0.29
	Nighttime loadings	0.00	0.00	0.00	0.00	50.98	0.12
Without both STATCOM and fault	Daytime loadings	0.00	0.00	0.00	0.00	50.54	0.29
	Nighttime loadings	0.00	0.00	0.00	0.00	51.25	0.23

The parameter of table 5.9, have been determined from MATLAB output measurements at 0.3-second simulation duration time.

From table 5.9, the proposed active power output of the solar array is match greater than the actual obtained active power output of the solar array. In addition, the reactive power output magnitude of the solar inverter is greater than the active power output of the solar inverter because, the solar inverter controller have been designed to act as a conventional STATCOM control principle i.e. as described in section 2.7.1 based on the following equations:

$$P = \frac{(v_{PCC} \times v_{inv}) \times \sin(\delta)}{X} \tag{5.1}$$

$$Q = \frac{v_{PCC} \times (v_{PCC} - v_{inv}) \times \cos(\delta)}{X} \tag{5.2}$$

In steady state operation, the solar inverter voltage, V_{inv} is in phase with Vpcc (δ=0), so that only reactive power is flowing:

$$Q = \frac{v_{PCC} \times (v_{PCC} - v_{inv})}{X} \tag{5.3}$$

A WTG side reactive power (Q_WTGs') have been controlled nearly at unity power factor for all cases but the WTG active power (P_WTGs') output is increased above the designed 51MW in the presence of SLGF. This shows fault occurrence at the transmission line leads WTGs' to be loaded. If the WTGs' are unable to withstand such overloads they may disconnect from the main grid, this is the worst case.

From table 5.9, the reactive power of the WTG (Q_WTG) in the night time is less than in the daytime, this indicates that the PV-STATCOM is more efficient in the nighttime than daytime to regulate the reactive power.

5.5. Economic Benefit Analysis of the PV-STATCOM

From the steady state analysis of section 5.3.2, in the daytime at PV array power of 0% (P_{SA}=0) the WTGs' has been forced to generate power up to 50MW (50MW < 51MW). At PV solar array power output of 5% (P_{SA}=5MW) the WTGs' has been forced to generate 48MW (48MW<51MW) and at PV array power of 100% (P_{SA}=10MW) the WTGs' have been forced to generate power up to 40MW (40MW < 51MW) to meet the required voltage limit. These shows us in the case of low wind speed conditions the solar array can compensate the required power which have being generated by WTGs. With the use of 10MW PV array considered to act as STATCOM, we can save an additional cost to generate 5MW to 11MW wind power and, we can decrease the number of WTGs' from 3 to 7 installation at the WF. Here using proper PV-STATCOM to keep node voltages to the required limit, we can connect 5MW and11 MW an additional wind power during the daytime and nighttime respectively.

As deduced in this work PV-STATCOM have a dual advantage than conventional SVC/STATCOM which are limited in size and limited application i.e. is conventional SVC/ATATCOM are only used as reactive power/voltage regulators, but the PV-STATCOM are used both as reactive power regulators/voltage and as active power regulators.

CHAPTER SIX

6. CONCLUSSION, RECOMMENDATION AND FUTURE WORK

In this section, the general conclusion of the research work, recommendations and directions for further work is described.

6.1. Conclusion

Reactive power compensation and voltage support in wind farms have been successfully achieved with installation of PV-STATCOM at the wind farm main substation (PCC). To identify the size of the PV-STATCOM, the size of static reactive power compensator capacitor devices have been considered in the selected wind farm. Moreover, to determine the auxiliary load, the average monthly power consumptions of the wind turbine generators, load consumptions of the wind farm substation and the expected future load supply of the WF to the neighboring areas is considered. For the three groups of WTGs' with capacity, the PV-STATCOM and auxiliary load are get installed in 3km, 33kV overhead WF transmission line for simulation and the expected results are obtained.

Steady state voltage variation analysis have been checked with 4-bus network using power world simulator software and MATLAB software have been used for the temporary over voltage system analysis & study system modelling. From results, it has been observed that PV-STATCOM is able to improve the connectivity of the WTGs' by regulating both the active and reactive power.

For temporary over voltage analysis, SLGF have been considered near PCC of WF transmission line and simulation resulted the use of PV-STATCOM have been minimized the temporary voltage rise.

Generally, PV-STATCOM has a dual advantage over STATCOM/SVC devices. The STATCOM/SVC are mostly limited to reactive power regulation or voltage regulation but the PV-STATCOM can regulate voltage, reactive power and active power of the WTGs' network. Moreover, "STATCOM/SVC controller is more expensive than the PV-STATCOM controller." Hence, we can generally increase WF generators connectivity and minimize the unnecessary costs on STATCOM/SVC by using the PV-STATCOM.

6.2. Recommendations

In Adama-I wind farm, capacitors and MCR type SVC are currently used as reactive power compensators. However, as it is known capacitors are not fast (dynamic) enough to regulate the reactive power. In connection, even the MCR type SVC is more expensive to use them only as reactive power regulators. Thus, the PV-STATCOM can minimize the aforementioned problems with an additional active power regulation if used at the main substation (PCC) of the wind farm. Thus, the researcher recommends its use in the WF so to achieve added benefits with reduced costs.

In Ethiopia, most of the national grid is supplied with hydropower plants and Adama-I WTGs' are consuming more active power from the grid to start their operation. But, Since, hydro power plants are water source dependents and there frequently happens a limitation of water source especially in dry seasons, the national grid may not supply enough power to the WTGs' under such a circumstance. Moreover, as of like the Adama-I wind farm where the PMSG based WTGs' are used and hence this kind of generators are not self-starting, an additional need of power to start the operation is required which is not economical option. Therefore, the use of PV-STATCOM can supply both active and reactive power to WTGs' and hence the power demand from the grid can be compensated.

Finally, the researcher strongly suggests the EEP to re-think for the use of MCR type SVC versus PV-STATCOM use for improved performance.

6.3. Future Work

The work carried out through the thesis is leading the researcher to put the following main important areas as future directions for further investigations.

- With the addition 12Mvar capacity of MCR type SVC to the existing capacity of the PV-STATCOM, the total reactive power compensation requirement of Adama-I WF can be replaced by PV-STATCOM and detailed economic benefits of this device can be made.
- The study can further be tested and proved with laboratory experimentation if opportunities are found whereby the factory test, practical, and simulation results are compared and hence very concrete practical conclusions are drawn.

- With the additional applications of Fuzzy Logic Controller (FLC) to the selected study system, the wind farm network can be made smart-micro grid.
- The study can be implemented in any type of wind farms of the same kind of generator having its specific parameters and thus anyone who is interested in the area can use it for further investigations in a wind power industry.
- The study can also be preceded with power quality issues like harmonics analysis, low voltage ride through capability (LVRT), and with various kinds of fault scenarios from either grid side or generator itself.
- Lastly, but least stability of the system under dynamic conditions and other related works can be pursued.

REFERENCES

[1]. Alroza Khaligh and Omar G. Onar, "Energy Harvesting Solar, Wind, and Ocean Energy Conversion Systems," CRC Press Taylor & Francis Group LLC, Boca Raton London, New York, 2010

[2]. Erich Hau, "Wind Turbines, Fundamentals, Technologies, Application, Economics," PTP-Berlin Protage-TEX-production GmbH and Springer-Verlag Berlin Heidelberg, Germany, 2nd edition, 2006

[3]. "Global status report-REN21," http://www.ren21.net/Portals/0/documents/Resources/GSR/2014/GSR2014_full%20report_low%20res.pdf, [online], June 12, 2014

[4]. BinWu, Yongqiang Lang, Navid Zargari and Samir Kouro, "Power Conversion and Control of Wind Energy Systems," IEEE-John Wiley & Sons, Inc. January 2011

[5]. Hydro China Corporation, "Master Plan Report of Wind and Solar Energy in the Federal Democratic Republic of Ethiopia (Final Version)," [unpublished], July 2001

[6]. "NASA's Surface Solar Energy: Data Set provides monthly average solar and wind radiation data, for everywhere on earth at," http://eosweb.larc.nasa.gov/sse/, [online], 2012

[7]. "Global Forecast: Solar Installation Capacity to Top 57 GW." http://www.renewableenergyworld.com/articles/2015/10/global-forecast-solar-installations-to-grow-by-25-30-percent-in-2015.html, [online], October 2, 2015

[8]. S.M. Muyeen, Junji Tamura and Toshiaki Murata, "Stability Augmentation of a Grid-connected Wind Farm" Green Energy and Technology ISSN 1865-3529, Springer-Verlag London Limited, London, Britain, 2009.

[9]. "E. ON Offshore Wind Energy Fact book /E. ON Climate & Renewables" http://www.eon.com/en/about-us/structure/company-finder/e-dot-on-renewables.html, [online], August 24, 2016.

[10]. Iulian Munteanu, Antoneta Iuliana Bratcu ,Nicolaos-Antonio Cutululis and Emil Ceangă, "Optimal Control of Wind Energy Systems," Advances in Industrial Control series ISSN 1430-9491, British Library Cataloguing Number: 2007942442,London,British, 2008

[11]. Gonzalo Abad, Jesu´sLo´pez, Miguel A. Rodrı´guez, Luis Marroyo and Grzegorz Iwansk, "Doubly Fed Induction Machine Modeling and Control for Wind Energy Generation" IEEE Inc, John Wiley & Sons, Inc., Hoboken, New Jersey, Canada, 2001

[12]. Thomas Ackermann, "Wind Power in Power Systems," John Wiley & Sons, Ltd, the Atrium, Southern Gate, Chichester, West Sussex PO19 8SQ, England, 2005

[13]. M. Muyeen, Ahmed Al-Durra and Hany M. Hasanien, "Modelling And Control Aspects Of Wind Power Systems," http://dx.doi.org/10.5772/55090, [online] March 20, 2013

[14]. Xiao-Ping Zhang, Christian Rehtanz and Bikash Pal, "Flexible AC Transmission Systems modeling and Control," ISBN: 3-540-30606-4, Springer, Berlin, 2012

[15]. N. G. Hingorani and L. Gyugyi, "Understanding FACTS; Concepts and Technology of Flexible AC Transmission Systems," IEEE ® Press book, 2000

[16]. Djamila Rekioua, University de Bejaia and Algeria, "Wind Power Electric Systems Modeling, Simulation and Control" 2014935979, Springer Ltd, London Heidelberg New York Dordrecht, 2014

[17]. Kalyan K. Sen and Mey Ling Sen, "Introduction to Facts Controllers Theory, Modeling, and Applications," ISBN 978-0-470-47875-2, John Wiley & Sons, Inc., Hoboken, New Jersey, Canada, 2009

[18]. P.Kundur, " Power System Stability and Control," ISBN 0-07-035958-X. McGraw-Hill, Inc., New York San Francisco Washington, D.C. Auckland Bogota, 1994

[19]. Bin Wu, "High-Power Converters and Ac Drives," ISBN-13 978-0-471-7317-9, John Wiley & Sons, Inc., Hoboken, New Jersey, Canada, 2006

[20]. "Adama/Nazret Wind Power Construction Project," (Construct no.33.20/12/09), Adama-I wind farm substation, Adama/Nazret, Ethiopia [unpublished]

[21]. "Hydrochina-Cgcoc Jv Adama wind farm project, "Technical Description, Fields Electric Installation and Connection Technology, System Structure and SCADA System Setup Manual," Adama-I wind farm substation, Adama/Nazret, Ethiopia, 17/12/2011 [unpublished]

[22]. "Modelling and Control Design of Pitch-Controlled Variable Speed Wind Turbines," www.intechopen.com, [online], August 5, 2016

[23]. "Passive Filters and Transfer Functions." https://www.google.com.et/search?site=&source=hp&q=Passive+Filters+and+Transfer+Functions , [online], January 12, 2017

[24]. "Chapter 3: Modelling Of PV Solar Farm as STATCOM." http://shodhganga.inflibnet.ac.in/bitstream/10603/32802/12/12_chapter%203.pdf, [online], Jolly 9, 2016

[25]. "Electrical Power Transmission System and Network." http://www.electrical4u.com/medium-transmission-line/, [online], December 15,2016

[26]. Rajiv K. Varma and Ehsan Siavashi, "Lab Validation of PV Solar Inverter Control as STATCOM (PV-STATCOM)",The University of Western Ontario London, CANADA, 2016

[27]. Sunil Kumar J, Shalini J, Birtukan Teshome, Milkias Berhanu Tuka and Fikadu Wakijira, "Improvement of Active and Reactive Power at the Wind Based Renewable Energy Sources: A case study on ADAMA wind power plant, Adama, Ethiopia,2013

[28]. Mr. Lakshman Naik Popavath, Dr. K. Palanisamy "A Dual Operation of PV-STATCOM as Active Power Filter and Active Power Injector in Grid Tie Wind- PV System" . VIT-University, Vellore, India, 2015

[29]. Shah Arifur Rahman, "Novel Controls of Photovoltaic (PV) Solar Farms Shah Arifur Rahman". University of Western Ontario, Canada, 2013

[30]. Francisco D´ıaz Gonz´alez, Marcela Mart´ınez-Rojas, Andreas Sumper, Oriol Gomis-Bellmunt and Llu´ıs Trilla, "Strategies for Reactive Power Control in Wind Farms with STATCOM". Catalonia, Spain, 2014

APPENDICES

Appendix A: Paramaetere list for the PMSG based Adama-I WTG

Table A 1. Wind turbine data set

WTG Version	GW 1.5/77
Wind turbine nominal power (MW)	1.5
Number of wind turbines	34
Wind turbine inertia constant (H(s))	4.32
Rotor diameter (m)	77
Wind turbine rotor radius(m)	37.3
Tower height(m)	65
Cut-in wind speed	3 m/s
Rated wind speed	11m/s
Optimal speed ratio (λ_{opt})	6.14
Maximum Power coefficient ($C_{p,max}$)	0.45
Cut-out wind speed	22 m/s
Swept area	4649m^2
Number of blades	3
Power control	Collective pitch control/rotor speed control

Table A 2. Generator data set

Generator Type	PMSG, 1.5 MW, 620 V, 12.7 Hz, multi - pole (non-salient pole)
Rated Mechanical Power	1.5MW
Rated Apparent Power	1.6 MVA
Generator inertia	35000(J(kg.m^2))
Rated Power Factor	0. 97
Speed Range	9-17.3 rpm
Rated speed	17.3rpm
Shaft stiffness (pu)	0.3
Number of Pole Pairs	44

Rated Rotor Flux Linkage	1.48
Stator Winding Resistance	0.006Ω
d axis Synchronous Inductance	0.395mH
q axis Synchronous Inductance	0.395mH
Rated current	680 A
Static friction	0.01
Viscous damping	1.5

Table A 3. The parameters determination and control system of the WTG in MATLAB Simulink

Data type		Value
Generator data	Nominal frequency (Fnom)	50Hz
	Rated generator mechanical power (Pmec1)	1.5e6 W
	Number of wind turbines (Nb_wt)	34
	Rated nominal apparent power (S)	1.5e6 VA
	Nominal line to line rated voltage (Vnom_L_L)	690 rms
	Grid side converter nominal voltage (Vnom)	620 V
	Total Adama one wind farm power output (MW)	Pnom = S×Nb_wt
	Rated voltage of PMSG	Vnom_gen = Vnom_L_L
Converters data	DC-voltage inductance and resistance of single WTG: L_R_Boost=[0.001 25e-3]	L_Boost=L_R_Boost (1)/Nb_wt
		R_Boost=L_R_Boost (2)/Nb_wt
	Quality factor of a filter	Q_filter =100
	DC_link capacitor of WTGs'	C_DClink=C_DClink1× Nb_wt
Controller data	Corner frequency of the L_C filter Hz	Freq_filter=10000
	Damping factor of the filter	Zeta_filter=0.707
	DC bus voltage regulator gains [Kp Ki]:	[1.1 27.5]
	Grid-side converter current regulator gains [Kp Ki]:	[1 50]
	Speed regulator gains [Kp Ki]	[5 1]
	Boost inductor current regulator gains [Kp Ki]	[0.025 100]

	Pitch compensation gains [Kp Ki]:	[1.5 6]
	Mod_index_max	1.1
	Iq_ref limit time constant	0.3
	Current regulator output limit	1.1
	Var regulator output higher limit	1.1
	Var regulator output lower limit	0.9
	Boost converter frequency (Freq_sawtooth)	2000 Hz
	Inverter PWM frequency	3000Hz
	Sample time to compute snubber resistance (Ts_snub)	50e-6 second
	Coefficients of power characteristics:[c1 c2 c3 c4 c5]	[0.6450 116 0.4 5 21]
AC filter	WTG grid side converter choke of single WTG: LR_choke = [0.003 0.3]	L_RL=L_choke(1) ×Vnom^2/Pnom/ (2×pi×Fnom)
		R_RL=R_choke(2) ×Vnom^2/Pnom
	Capacitor value (C_var_filter = Pnom×0.1)for the WTGs'	C_var_Filter =C_var_filter×Nb_wt

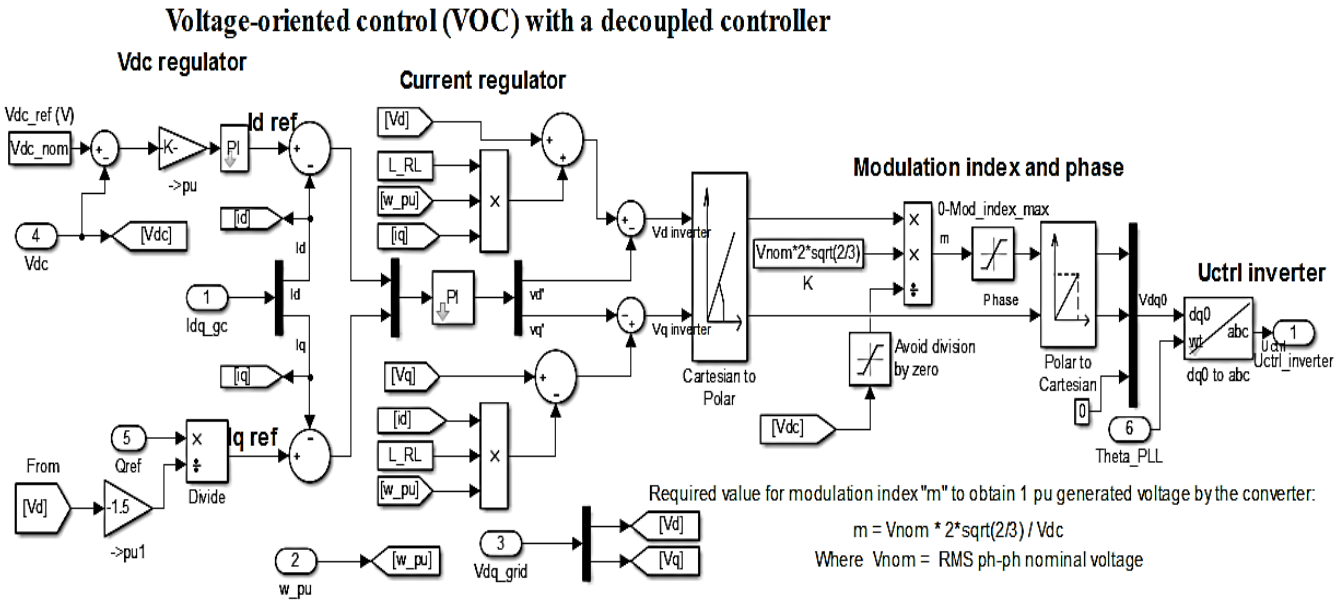

Fig.A1. MATLAB simulation VOC with a decoupled controller of WTG

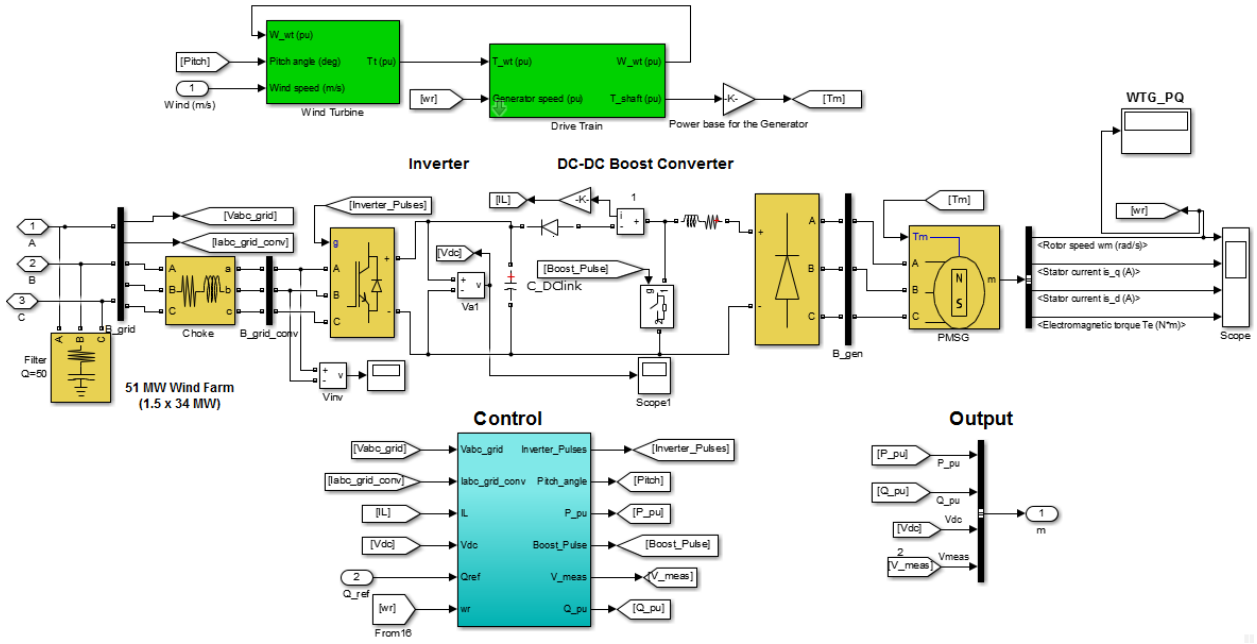

Fig. A 2. Masked sub-system under Adama one wind farm of Fig.5.1

Appendix B: Parameters and components of Grid connected solar array

The power parameters determinations of the grid connected PV-array in the above table B.2 is determined from the standard datasheet of NREL.

Table B1. PV array /module parameters from Sun power SPR-425E-WHT-D datasheet

Data		Value
Module type		Sun power SPR-425E-WHT-D
Sun irradiance (w/m^2)		1000
Cell temperature(Deg.c)		0,25,50
Array data	Number of Parallel strings	522
	Number of Series connected modules per strings	45
Module data	Power at MPPT(Pm)	425.007 W
	Voltage at MPPT(Vmp)	72.9 V
	Current at MPPT (Imp)	5.83A
	Number of Cells per module (Ncel)	128
	Open circuit voltage (Voc)	85.6 V
	Short circuit current (Isc)	6.18A
	Light generated current (IL)	6.1907A
	Diode saturation current (IO)	5.6723e-11 A
	Diode identity	1.0248

	Shunt resistance (R_{sh})	825.5551 Ohm
	Series resistance (R_s)	0.38594 Ohm
	Temperature coefficient of Voc(%/deg.C)	-0.326
	Temperature coefficient of Isc (%/deg.C))	0.019304

Table B 2. Parameters of grid connected PV-array

Parameter			Value
Control time	System frequency		50Hz
	SimPower Systems sample time (s): Ts_Power =1/ (40 ×Fnom)/100		5×10^-6 (s)
	Inverter Control system sample time (s): Ts_Control =10×Ts_Power=		50×10^-6 (s)
Power parameters	Inverter nominal 3-phase power (MVA)		10
	Nominal inverter primary line-to-line voltage (Vrms)		33 (kV)
	Nominal inverter secondary line-to-line voltage (Vrms)		400 (V)
	Nominal DC link voltage		6kV
Transformer parameters	Transformer total leakage (pu)		0.06
	Nominal transformer primary (grid side) line-to-line voltage (Vrms)		33 (kV)
	Total leakage inductance (pu) in primary(grid side)		0.003
	Total resistance(Pu) in primary winding (grid side)		0.00012
	Nominal secondary primary (inverter side) line-to-line voltage (Vrms)		400 (V)
	Total leakage inductance(H) in secondary (inverter side)		0.00012
	Total resistance (ohm) in secondary (inverter side)		0.003
	Magnetization resistance (pu);		500
	Magnetization inductance (pu);		500
Filter parameters	Choke impedance [R (mΩ), L (μH)]		[2, 250]
	Pbase_sec=Vnom_sec^2/Pnom=260^2/10e6		0.00676 (W)
	RL(choke)	R =RLchoke(1)×Pbase_sec	13.52 (μΩ)
		L (2) =RLchoke(2) ×Pbase_sec/(2×pi×Fnom)	10×10^-9 (H)
	Capacitor	Capacitive reactive power (Var)=0.1×Pnom	1Mvar
		Pc=Qc/100: Active power (W)	1MVar/100
DC-DC boosts parameters:	PV-link capacitor, Cpv		1000 (μF)
	Boost inductance [L(mH) , R(Ω)]		[5 , 0.005]
	Boost capacitance, Cdc		12000 (μF)
	PWM Switching frequency		5 kHz

PWM	Carrier frequency (Hz), Fc	40 × Fnom

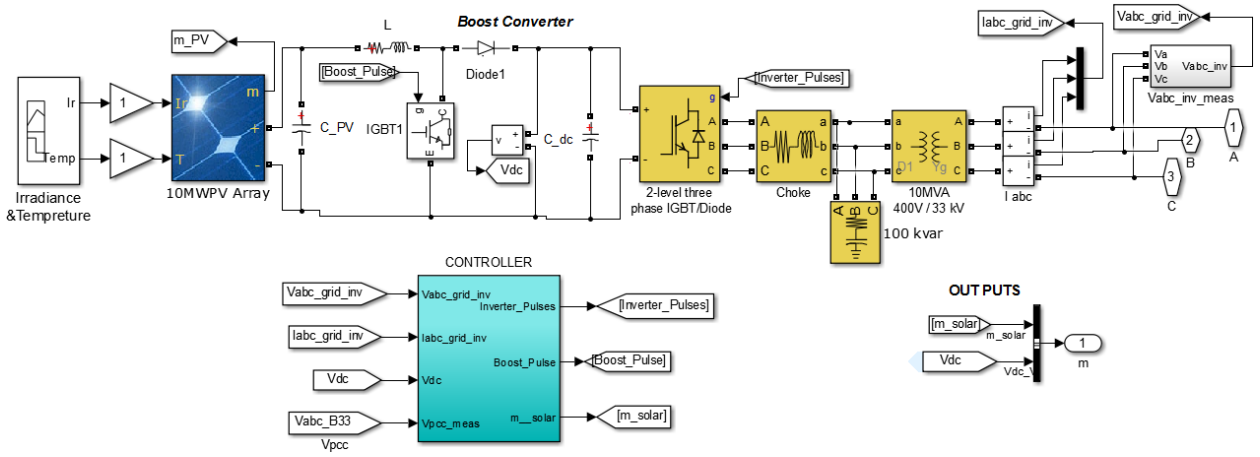

Fig.B1. Sub systems under the masked sub system of PV-STATCOM Matlab of Fig 5.5

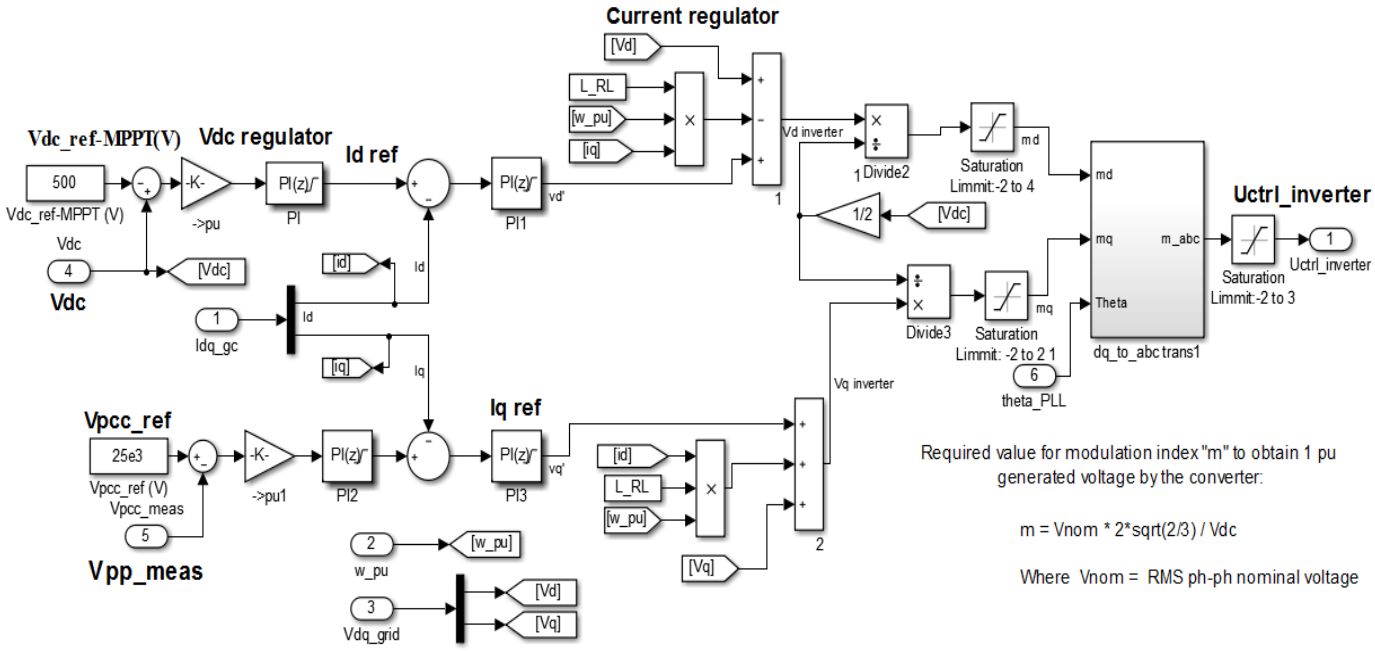

Fig.B2. PV-STATCOM control system model with MATLAB

Appendix C: Steady state bus power flow

Table C1. The steady state power flow analysis during daytime with P_{WF} =51MW and P_{SA} =10MW

Bus Power Flows

Records Geo Set Columns f(x) Options

Bus Flows

BUS	1	1		132.0	MW	Mvar	MVA	% GIC	Amps	1.0000	0.00	1 1
GENERATOR	1				-53.76	29.65R	61.4			0.0		
TO	2	2	1		-53.76	29.65	61.4	0		0.0N	1.0000TA	0.0
BUS	2	2		33.0	MW	Mvar	MVA	% GIC	Amps	0.9363	8.33	1 1
GENERATOR	1				10.00	0.00N	10.0			0.0		
LOAD	1				6.48	21.07	22.0					
TO	1	1	1		54.07	-20.63	57.9	0		0.0N	1.0000NT	0.0
TO	3	3	1		-50.55	-0.44	50.5	0		0.0		
BUS	3	3		33.0	MW	Mvar	MVA	% GIC	Amps	0.9369	8.44	1 1
TO	2	2	1		50.58	0.06	50.6	0		0.0		
TO	4	4	1		-50.58	-0.06	50.6	0		0.0N	1.0000TA	0.0
BUS	4	4		0.6	MW	Mvar	MVA	% GIC	Amps	0.9414	8.70	1 1
GENERATOR	1				51.00	0.00N	51.0			0.0		
TO	3	3	1		51.00	-0.00	51.0	0		0.0N	1.0000NT	0.0

Table C2. Nighttime power flow list using power world software PWF =51MW and PSA =0MW

Bus Power Flows

Records Geo Set Columns f(x) Options

Bus Flows

BUS	1	1		132.0	MW	Mvar	MVA	% GIC	Amps	1.0000	0.00	1 1
GENERATOR	1				-46.91	6.64R	47.4			0.0		
TO	2	2	1		-46.91	6.64	47.4	0		0.0N	1.0000TA	0.0
BUS	2	2		33.0	MW	Mvar	MVA	% GIC	Amps	0.9908	6.84	1 1
GENERATOR	1				0.00	10.00N	10.0			0.0		
LOAD	1				3.38	12.07	12.5					
TO	1	1	1		47.17	-1.51	47.2	0		0.0N	1.0000NT	0.0
TO	3	3	1		-50.55	-0.56	50.6	0		0.0		
BUS	3	3		33.0	MW	Mvar	MVA	% GIC	Amps	0.9914	6.94	1 1
TO	2	2	1		50.58	0.12	50.6	0		0.0		
TO	4	4	1		-50.58	-0.12	50.6	0		0.0N	1.0000TA	0.0
BUS	4	4		0.6	MW	Mvar	MVA	% GIC	Amps	0.9957	7.17	1 1
GENERATOR	1				51.00	0.00N	51.0			0.0		
TO	3	3	1		51.00	-0.00	51.0	0		0.0N	1.0000NT	0.0

Appendix D: PV-STATCOM control parameters

The proportional and integral gains have been determined in a systematic hit and trial manner with the objective to obtain a minimum settling time, a quick rise time, and a peak overshoot

less than 10% in the PCC bus voltage as shown in table D1.

Table D1. Proportional and integral (PI) parameters values for PV-STATCOM

Parameters	PI			
	PI-1	PI-2	PI-3	PI-4
Kp	7	10	0.3	0.3
Ki	800	66.67	20	20

Appendix E: For 10 MW grids connected solar array total solar inverter coupling inductor calculation:

At the high voltage side of the transformer, side of the transformer:

$$V_{base} = V_{phpeak} = 33kV \times \frac{\sqrt{2}}{\sqrt{3}} = 57.09kV; P_{base} = 10MW$$

$$I_{base} = \frac{2}{3} \times \frac{P_{base}}{V_{base}} = 0.117kA$$

At the low voltage side of the transformer:

$$V_{base} = V_{phpeak} = 0.26kV \times \frac{\sqrt{2}}{\sqrt{3}} = 0.4498kV; P_{base} = 10MW$$

$$I_{base} = \frac{2}{3} \times \frac{P_{base}}{V_{base}} = 14.89kA$$

$$Z_{base} = \frac{V_{base}}{I_{base}} = \frac{0.4498kV}{14.89kA} = 0.03\Omega \text{ and}$$

$$\omega_{base} = \omega_{actual} = 2 \times \pi \times f = 314 \text{rad/sec for} 50Hz$$

$$\text{Hence}, L_{base} = \frac{Z_{base}}{\omega_{base}} = \frac{0.03}{314} = 95.5 \times 10^{-6} H$$

The leakage reactance of the 100 MVA, 0.26/33 kV, 3-phase transformer is 6%.

Hence, % Z× $\sqrt{3}$= 0.06× $\sqrt{3}$=0.1039pu. The actual impedance has determined as:

$$Z_{actual} = Z_{pu} \times Z_{base} = 0.1039 \times 0.03 = 0.003\Omega$$

$$\text{The total inductance is given by}: L_T = \frac{0.003}{314} = 9.55\mu H$$

$$\text{Then}, L = L_1 + L_T = (500 + 9550) \times 10^{-9} = 10.05\mu H = 0.105pu$$

$$\omega = \frac{\omega_{actual}}{\omega_{base}} = 1pu, \quad \text{hence}, \omega L = 0.105pu$$

The base value of the DC side has based on the base value at low voltage side of the transformer, as the low voltage side is the inverter output side.

Hence, $V_{dc,\,base} = 2\times V_{base} = 2\times 0.4498 = 0.8996$kVat switching frequency, fsw =5 kHz

Appendix F: Second order low pass filter design analysis

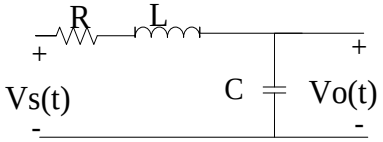

Fig.F1.Second order low pass filter equivalent circuit

Using voltage division principle, the output voltage was determined as:

$$Vo(t) = \frac{Zc}{Zc + ZL + ZR} \times Vs(t) = \frac{1/j\omega C}{1/j\omega C + j\omega L + R} \times Vs(t) \qquad (F.1)$$

Setting, $\omega_0 = 1/\sqrt{LC}$ and $2\varsigma\,\omega_0 = R/L$, where; ω_0, is the natural frequency and ς, is the damping ratio yields:

$$H(j\omega) = \frac{V_0(t)}{Vs(t)} = \frac{\omega_0^{\,2}}{(j\omega)^2 + j\omega 2\varsigma\omega_0 + \omega 0^2} = \frac{\omega_0^{\,2}}{-\omega^2 + j\omega 2\varsigma\omega_0 + \omega_0^{\,2}}$$

The magnitude of the complex transfer function is given as:

$$\left|H(j\omega)\right| = \sqrt{\frac{\omega_0^{\,2}}{(\omega_0^{\,2} - \omega^2)^2 - (\omega 2\varsigma\omega_0)^2}} = \frac{\omega_0}{\sqrt{(\omega_0^{\,2} - \omega^2)^2 - (\omega 2\varsigma\omega_0)^2}} \qquad (F.2)$$

The phase of H (jω), φ, is:

$$\varphi = -\tan^{-1}\left(\frac{\omega 2\varsigma\omega_0}{\omega_0^{\,2} - \omega^2}\right) \qquad (F.3)$$

There are two terms associated with this circuit, the quality factor Q of the circuit and the damping factor ratio (zeta), ς of the circuit. Their relationship is given as:

$$Q = \frac{1}{R}\sqrt{\frac{L}{C}} = \frac{1}{2\varsigma}$$

The damping ratio Zeta (Q = 1/ (2*Zeta)): Zeta = 0.707, the damping ratio (Zeta) has typically a value between 0 and 1.

Appendix G: Adama -I wind farm SCADA system diagrams.

Fig.G1.Active power (kW) and wind speed (m/s) profile of Adama one SCADA system.

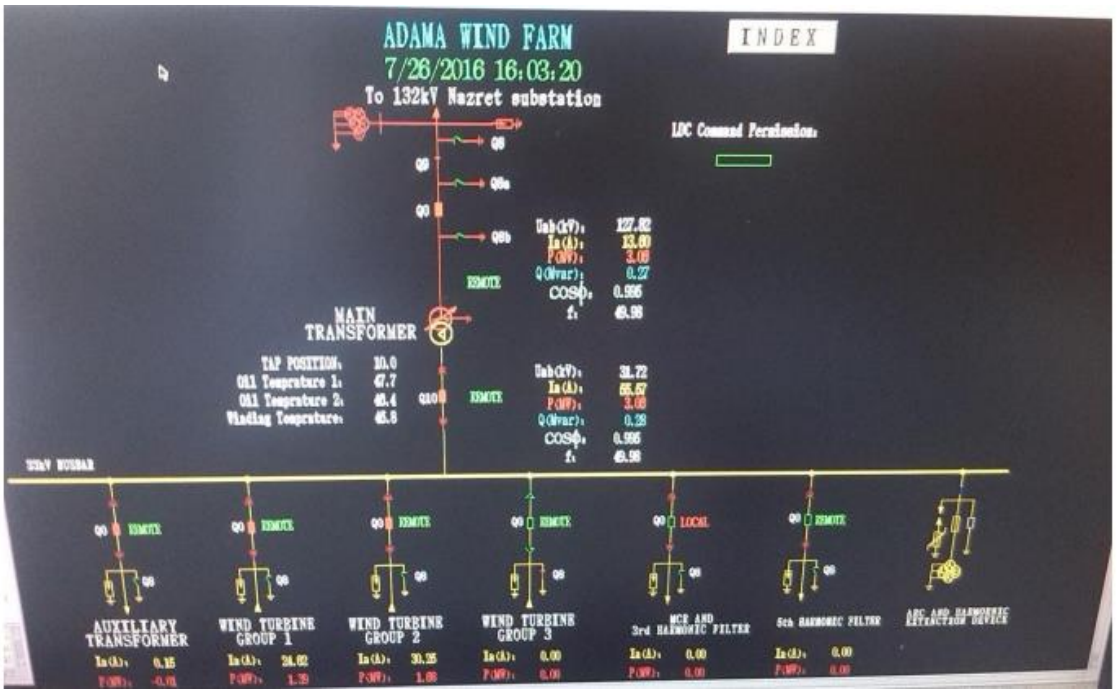

Fig.G2.33kV bus bar in Adama-I wind farm SCADA system